ARO 19982.6-GS

(2)

FOUR-WAVELENGTH LIDAR EVALUATION OF PARTICLE CHARACTERISTICS AND AEROSOL DENSITIES

Final Report

June 1985

Prepared by:

Edward E. Uthe
John M. Livingston
Stephen A. DeLatour
Norman B. Nielsen
Atmospheric Science Center

Prepared for:

U.S. Army Research Office
P.O. Box 12211
Research Triangle Park, NC 27709
Attn: Dr. Walter Flood
Director, Geosciences Division

Contract DAAG29-82-K-0191
SRI Project 4980

Approved:

Warren B. Johnson, Director
Atmospheric Science Center

David D. Elliott, Vice President
Research and Analysis Division

SRI International
333 Ravenswood Avenue
Menlo Park, California 94025
(415) 326-6200
TWX: 910-373-2046
Telex: 334-486

THE FINDINGS IN THIS REPORT ARE NOT TO BE CONSTRUED AS AN OFFICIAL DEPARTMENT OF THE ARMY POSITION, UNLESS SO DESIGNATED BY OTHER AUTHORIZED DOCUMENTS.

UNCLASSIFIED

SECURITY CLASSIFICATION OF THIS PAGE (When Data Entered)

REPORT DOCUMENTATION PAGE	READ INSTRUCTIONS BEFORE COMPLETING FORM
1. REPORT NUMBER: ARO 19982.6-GS	2. GOVT ACCESSION NO.: AD-A158 500
	3. RECIPIENT'S CATALOG NUMBER:
4. TITLE (and Subtitle): FOUR-WAVELENGTH LIDAR EVALUATION OF PARTICLE CHARACTERISTICS AND AEROSOL DENSITIES	5. TYPE OF REPORT & PERIOD COVERED: 27 Sep 82 - 30 Apr 85 Final Report
	6. PERFORMING ORG. REPORT NUMBER: SRI Project 4860
7. AUTHOR(s): Edward E. Uthe, John M. Livingston, Stephen A. DeLateur, Norman B. Nielsen	8. CONTRACT OR GRANT NUMBER(s): DAAG29-32-K-0191
9. PERFORMING ORGANIZATION NAME AND ADDRESS: SRI International, 333 Ravenswood Avenue, Menlo Park, CA 94025	10. PROGRAM ELEMENT, PROJECT, TASK AREA & WORK UNIT NUMBERS:
11. CONTROLLING OFFICE NAME AND ADDRESS: U. S. Army Research Office, Post Office Box 12211, Research Triangle Park, NC 27709	12. REPORT DATE: June 1985
	13. NUMBER OF PAGES: 95
14. MONITORING AGENCY NAME & ADDRESS(if different from Controlling Office)	15. SECURITY CLASS. (of this report): Unclassified
	15a. DECLASSIFICATION/DOWNGRADING SCHEDULE:

16. DISTRIBUTION STATEMENT (of this Report)

Approved for public release; distribution unlimited.

17. DISTRIBUTION STATEMENT (of the abstract entered in Block 20, if different from Report)

NA

18. SUPPLEMENTARY NOTES

The view, opinions, and/or findings contained in this report are those of the author(s) and should not be construed as an official Department of the Army position, policy, or decision, unless so designated by other documentation.

19. KEY WORDS (Continue on reverse side if necessary and identify by block number)

LIDAR
MULTIWAVELENGTH LASER PROPAGATION
OBSCURANT OBSERVATION
EXTINCTION
BACKSCATTER
SMOKE WEEK

20. ABSTRACT (Continue on reverse side if necessary and identify by block number)

The SRI International four-wavelength (0.53, 1.06, 3.8, 10.6 μm) lidar system was used during the SNOW-ONE-B and Smoke Week XI/SNOW-TWO field experiments to validate its capabilities in assessing obscurant optical and physical properties. The lidar viewed along a horizontal path terminated by a passive reflector. Data examples were analyzed in terms of time-dependent transmission, wavelength dependence of optical depth, and range-resolved extinction coefficients. Three methods were used to derive extinction data

DD FORM 1 JAN 73 1473 EDITION OF 1 NOV 65 IS OBSOLETE

UNCLASSIFIED

SECURITY CLASSIFICATION OF THIS PAGE (When Data Entered)

from the lidar signatures. These were the target method, Klett method and experimental data method. The results of the field and analysis programs are reported in the journal and conference papers that are appended to this report, and include:

- "Comparison Study of Lidar Extinction Methods," submitted to Applied Optics
- "Error Analysis of Lidar Solution Techniques for Range-Resolved Extinction Coefficients Based on Observational Data," Smoke/Obscurants Symposium IX
- "Four-Wavelength Lidar Measurements from Smoke Week VI/SNOW-TWO," Smoke/Obscurants Symposium VIII
- "SNOW-ONE-B Multiple-Wavelength Lidar Measurements," Snow Symposium III
- "Lidar Applications for Obscurant Evaluations," Smoke/Obscurants Symposium VII.

The report also provides a summary of background work leading to this project, and of project results.

CONTENTS

ABSTRACT

The SRI International four-wavelength (0.53, 1.06, 3.8, 10.6 μm) lidar system was used during the SNOW-ONE-B and Smoke Week XI/SNOW-TWO field experiments to validate its capabilities in assessing obscurant optical and physical properties. The lidar viewed along a horizontal path terminated by a passive reflector. Data examples were analyzed in terms of time-dependent transmission, wavelength dependence of optical depth, and range-resolved extinction coefficients. Three methods were used to derive extinction data from the lidar signatures. These were the target method, Klett method and experimental data method. The results of the field and analysis programs are reported in the journal and conference papers that are appended to this report, and include:

- "Comparison Study of Lidar Extinction Methods," submitted to Applied Optics
- "Error Analysis of Lidar Solution Techniques for Range-Resolved Extinction Coefficients Based on Observational Data," Smoke/Obscurants Symposium IX
- "Four-Wavelength Lidar Measurements from Smoke Week VI/SNOW-TWO," Smoke/Obscurants Symposium VIII
- "SNOW-ONE-B Multiple-Wavelength Lidar Measurements," Snow Symposium III
- "Lidar Applications for Obscurant Evaluations," Smoke/Obscurants Symposium VII.

The report also provides a summary of background work leading to this project, and of project results.

I BACKGROUND

Earlier studies conducted for ARO used single (0.69 μm) and dual (0.69 and 10.6 μm) wavelength lidar systems to observe obscurant aerosols. Typically, the lidar viewed along a horizontal path terminated by a passive reflector with a uniform surface. The lidar target returns were interpreted in terms of transmission of laser energy as a function of event time. The transmission data was then correlated with the backscattered signal received from the obscurant aerosols. Experiments with the two-wavelength lidar during field tests DIRT-1 and Smoke Week II showed that the wavelength dependence of transmission (extinction) and backscatter could be used to identify the obscurant as smoke or dust, based on a strong wavelength dependence on particle size. However, relatively large data scatter occurred in plots of optical depth evaluated from the target returns plotted against path-integrated backscatter. Assuming the data scatter was a result of changing particle sizes, theoretical considerations indicated that a 3-to-4 μm wavelength lidar may provide higher correlation than a 0.69 or 10.6 μm wavelength system. In addition, a shorter wavelength would be useful to determine the mean particle size of smoke aerosols.

A four wavelength lidar system was constructed and initially tested at SRI under ARO Contract DAAG-20-80-C-0003. The lidar was designed to provide information on propagation at wavelengths commonly used by DoD laser systems, and to provide for multiple wavelength analysis in terms of particle characteristics and aerosol densities. Pulses at 0.53, 1.06, 3.8, and 10.6 μm can be transmitted along the same path within a 150 μs interval to overcome space and time separation problems associated with the earlier dual wavelength system. Initial tests at SRI indicated the lidar was ready for operation during scheduled Army Field tests which could provide the supplementary data needed to validate the lidar performance and data analysis procedures. This project provided that opportunity.

II SUMMARY OF PROJECT RESULTS

The results and findings obtained on this project are reported in the journal and conference papers reproduced as Appendixes to this report. A brief summary is presented below.

The four-wavelength lidar system was transported to Grayling, Michigan, to participate in the SNOW-ONE-B field test conducted during November and December 1983. Prior to this time, a new digital data acquisition system was installed within the lidar to improve digitization accuracy and reliability. The lidar operated on all SNOW-ONE-B tests without failure. Because of eye-safety considerations, only the 1.06, 3.8 and 10.6 μm wavelength energy were transmitted. The lidar van was positioned alongside transmissometer instrumentation vans operated by the U. S. Navy (NRL) and the U. S. Army Atmospheric Science Laboratory. The lidar and transmissiometers were aligned to observe parallel paths extending over a 600 m range. A passive reflector (target) was placed at the far end of the lidar path to provide for a constant reflectivity surface. The primary objective of the SNOW-ONE-B tests were to characterize electromagnetic propagation through dense snow. Only light snowfall occurred during the observational period.

Lidar target returns were interpreted in terms of transmission, and results were compared to data provided by the NRL transmissiometers. Excellent agreement was obtained as shown by the data example presented in Appendix D collected during an IR screener smoke test. The lidar results showed that the smoke attenuation (optical depth) was within 20% of being equal at the 1.06, 3.8 and 10.6 μm wavelengths. Data collected in snowfall showed that optical depth at 10.6 μm was 76% greater than at 1.06 μm, and 59% greater than at 3.8 μm. This enhanced attenuation at longer wavelengths is probably a result of multiple scattering effects from large scattering particles. Much of the large particle scattering is in the forward direction and, therefore, more scattered energy is directed back into the initial laser beam at longer wavelengths and results in less attenuation.

Plots of optical depth (target returns) against integrated back-

scatter (aerosol returns) show more data scatter than was anticipated--especially at 3.8 μm where theory had indicated that a better correlation might be obtained. However, further inspection of the lidar backscatter signatures indicated that the dynamic range of the log amplifiers used in the lidar receiver was not sufficiently large to accommodate the strong signals returned from dense aerosols, snow, and the target. Subsequently the four decade amplifiers were replaced with six-decade units. The SNOW-B-ONE data was also used to conduct a 'hole' and 'patch' analysis of smoke distributions. These results are further discussed in Appendices C and D.

As a second phase of the project, the improved four-wavelength lidar system participated in the Smoke Week XI/SNOW-TWO field tests conducted at Grayling, Michigan, during the 1983-84 winter. The lidar procedures were nearly identical to those used during the SNOW-ONE-B tests with the exception that permission was granted to transmit laser energy at all four wavelengths. The lidar operated without failure on 25 obscurant tests scheduled between 10 and 16 January. Unfortunately, a guy wire that intersected the lidar/target path was installed just prior to the test series, and reflections from the wire interfered with aerosol scattering on some tests. However, the lidar signatures showed more variability with smoke density and greater range response resulting from the enhanced dynamic range receivers. Plots of optical depth against path-integrated backscatter had substantially less data scatter, indicating that the lidar response to aerosol density had been improved.

The analysis program concentrated on methods to derive range-resolved extinction coefficients from the lidar signatures. Three methods were used. The target method uses the target-derived transmission and path-integrated backscatter to evaluate a single calibration constant for each lidar observation. The calibration constant can then be used with integrated backscatter to evaluate extinction along the lidar-to-target path. This method is based on the single-scatter lidar equation, and provides the best estimates of extinction along the path when multiple scattering is not important. The method does provide some correction for multiple scattering, as the constant is evaluated from the actual lidar signature. It was shown that the solution constant

varies from observation-to-observation so that a universal constant cannot be used to evaluate single-ended lidar observations.

The second method (Klett method) is a modification of a formal solution to the single-scattering lidar equation. The solution assumes a known relationship between backscatter and extinction coefficients and extinction near the far end of the lidar observation. Deviations (RMS differences) between the Klett and target method were computed for various solution parameters. The resulting extinction profile for solution parameters that yielded minimum RMS differences agreed well with the profile derived from the target method. This was expected, as both methods are derived from the single-scattering lidar equation. Contour plots of RMS values as a function of the two solution parameters were constructed, as were contour plots of transmission differences. These plots show that the Klett method is relatively sensitive to expected errors in assumed solution parameters.

The third method was the experimental data method which established an experimental relationship between the optical depth and the path-integrated backscatter evaluated from the lidar signature. Therefore, this method accounts for multiple scattering effects. Comparison of extinction profiles with those derived from the target method showed that the experimental data method provided for more attenuation in the near side of an obscurant cloud and for less attenuation in the far side, indicating the importance of multiple scattering. Before any one method is judged superior, an experiment should be conducted to validate the lidar methods for both low- and high-density obscurant events.

Finally, the range-resolved extinction coefficients evaluated as a function of obscurant event time were used to construct a contour plot of the time and range variability of smoke distribution along the propagation path. Such data are useful in evaluating obscurant effects on electrooptical systems operating within the obscurant cloud.

A more detailed accounting of project results and data examples is presented in the Appendices.

III RECOMMENDATIONS

The lidar technique is the best method available for evaluating spatial and temporal distributions of obscurant properties and obscurant effects on military laser-based weapon systems. However, uncertainties in relating backscatter data to extinction and density remain. Multiple-wavelength systems provide additional information to help analyze lidar signatures in terms of needed obscurant parameters. However, this approach is limited because of different lidar characteristics of multiple laser and detector systems, and because newer military obscurants do not follow available scattering theories. Nevertheless, the usefulness of lidar for obscurant evaluations has been demonstrated and further development is warranted.

The following recommendations are offered to further develop the lidar technique and enhance its value to military programs.

- Coordinated in situ sensing of aerosol densities along lidar propagation paths to provide data needed for validation and/or development of lidar signature analysis methods.
- Development of methods to deconvolute lidar performance factors from lidar signatures so that multiple wavelength data can be analyzed effectively in terms of atmospheric optical and physical properties.
- Addition of vertical scanning optics to the four-wavelength lidar system to investigate obscurant distributions in the vertical and their dependence on meteorological conditions and terrain properties.
- Investigation of airborne lidar systems for measurement of wide-area screening smoke distributions.
- Continued participation in the Smoke Week series and reporting of results at Smoke/Obscurants Symposia to promote interrelationships between lidar development, obscurant evaluations and electrooptical weapons testing programs.

IV LIST OF PUBLICATIONS

- "Comparison Study of Lidar Extinction Methods," submitted to Applied Optics
- "Error Analysis of Lidar Solution Techniques for Range-Resolved Extinction Coefficients Based on Observational Data," Smoke/Obscurants Symposium IX
- "Four-Wavelength Lidar Measurements from Smoke Week VI/SNOW-TWO," Smoke/Obscurants Symposium VIII
- "SNOW-ONE-B Multiple-Wavelength Lidar Measurements," Snow Symposium III
- "Lidar Applications for Obscurant Evaluations," Smoke/Obscurants Symposium VII.

V PARTICIPATING PERSONNEL

SRI staff members who participated in the research effort are listed below:

- Edward E. Uthe, Director, Remote Sensing Program
- Warren B. Johnson, Director, Atmospheric Science Center
- Norm B. Nielsen, Field Engineering Representative
- Jan van der Laan, Senior Research Engineer
- Stephen A. DeLateur, Research Engineer
- John M. Livingston, Research Meteorologist.

None of the project staff earned advanced degrees during the course of the project.

Appendix A

"COMPARISON STUDY OF LIDAR HORIZONTAL-PATH EXTINCTION METHODS"

Submitted to APPLIED OPTICS

COMPARISON STUDY OF LIDAR EXTINCTION METHODS

E. E. Uthe and J. M. Livingston
SRI International
Menlo Park, CA 94025, USA

ABSTRACT

The SRI four-wavelength (0.53, 1.06, 3.8 and 10.6 μm) lidar system was used during the Smoke Week XI/SNOW-TWO field experiments to observe range-resolved backscatter and target-reflected laser energy along a horizontal path intersected by test obscurant aerosols.

Target-reflected laser energy provided an excellent measure of time-dependent path-integrated extinction (e.g., transmission). These values allow the range-resolved backscatter to be analyzed in terms of range-resolved extinction when single-scattering is assumed. This two-ended (lidar and target) method provides extinction coefficients along the optical path that are consistent with independent transmissometer observations. The values are the most accurate that can be derived from the lidar technique when multiple scattering is limited.

Extinction profiles evaluated from the lidar/target method can be utilized to investigate the limitations and accuracies of algorithms which are used to derive extinction data from lidar backscatter signatures when no target return is available. Single-ended lidar methods are needed for vertical and slant-path measurements. Two single-ended techniques were investigated. The first is the well-known Klett modification of the analytic solution to the single-scattering lidar equation. The Klett technique can reproduce the extinction profile derived from the lidar/target method as expected since both are derived from the single-scattering lidar equation. However, this requires relatively accurate information on a boundary value of extinction and the backscatter-to-extinction relationship. Contour plots are presented which show deviation of the Klett extinction profile from the lidar/target extinction profile as a function of the solution parameters.

A second method of deriving extinction profiles from single-ended lidar measurements is based on an observed relationship of optical depth to path-integrated lidar signal. Such a relationship derived from lidar/target data includes multiple scattering effects on the extinction evaluation. The method does not reproduce the extinction profile derived from the single-scattering lidar/target and Klett methods -- indicating the importance of multiple scattering on the lidar backscatter signature.

I LIDAR DATA COLLECTION

The SRI four-wavelength (0.53, 1.06, 3.8 and 10.6 μm) lidar system was used during the Smoke Week XI/SNOW-TWO field experiments to collect data for analysis of obscurant extinction distributions. Basically, laser pulses at the four wavelengths were transmitted along a horizontal path terminated at a distance of 600 m from the lidar by a target of uniform reflective properties.

The laser pulses at each wavelength were emitted sequentially along the same path within a 60 μs interval to reduce effects of time- and space-varying aerosol concentrations on each four-wavelength pulse set. About 60 pulse sets were transmitted for each minute of operation. Both energy backscattered from atmospheric aerosols and energy reflected from the solid target was collected within a telescope and directed to appropriate detectors using dichroic filters. After logarithmic amplification, backscatter signatures were digitized by an 8-bit 100-MHz transient recorder, and the resulting digital records were stored on nine-track magnetic tape for subsequent analysis. Obscurant aerosols were generated upwind of the lidar/target path, and lidar observations were initiated just before the obscurants intersected the viewing path. Other details of the lidar system and its application to the Smoke Week VI/SNOW-TWO field test have been presented elsewhere (1).

II DATA ANALYSIS METHODS AND RESULTS

A. Target Method

Target returns observed by a lidar system can be interpreted in terms of transmission across the lidar-to-target path. Previous results have shown that lidar derived transmissions agree with independent data records collected with conventional two-ended transmissometers (2). Therefore, the four-wavelength lidar target returns collected during an obscurant event provide the time history of transmission at each

wavelength, and provide data to evaluate optical depth (u=-ln T) relationships between wavelengths, as shown by the example presented in Figure 1.

Fernald et al. (3), among others, have shown that if the ratio of the extinction coefficient to the backscatter coefficient, $k=\sigma(r)/\beta(r)$, remains constant over the range interval Δr being investigated, then the two-way transmittance, $T^2(r)$, follows directly from differentiation of the basic lidar equation, and is given by

$$T^2(R) = 1 - \frac{2k}{C}\int_0^R P(r)dr \qquad (1)$$

In this equation, P(r) is the signal whose amplitude is proportional to the power received from a scattering volume at range r, and is corrected for the geometric range-squared effect and transmitted energy variations. C is a lidar calibration constant.

The constant k/C can be determined by combining the known two-way transmittance between the laser and the target with the lidar return signature integrated over the same range. The value of the constant k/C may then be substituted back into (1), and combined with the integrals of the received backscatter signals to intermediate ranges to yield a horizontal transmission profile. Since transmission is directly related to optical depth through $T^2(R) = e^{-2u(R)}$, where optical depth $u(R) = \int_0^R \sigma(r)\,dr$, calculation of a transmission profile implies a corresponding extinction profile. We call this the "target" method of deriving an extinction profile because it requires the use of a target to derive the constant k/C value. Figure 2 presents an example of an extinction coefficient profile for a single lidar observation during an obscurant test for which the transmission history is presented in Figure 1. Figure 3 presents a contour plot of obscurant extinction (km^{-1}) distributions along the observed path as a function of event time.

If the value of k/C remains constant for a given type of obscurant, this value of k/C can be used to derive extinction and transmission values from single-ended lidar observations and, therefore, vertical and

slant-path measurements would be possible. Values of k/C have been calculated for each lidar shot for the test with data shown in Figure 1 by using the 1.06 μm wavelength target-derived transmissions. In addition, linear and best-fit Gaussian means and standard deviations of k/C have been calculated. These results are shown in Figures 4 and 5 where it can be seen that the two methods of computing a mean k/C yield similar results. Figure 4 shows that k/C can undergo both gradual and rapidly fluctuating variability that may be the result of pulse-to-pulse changes in lidar system performance (transmitted energy, pulse shape and detector response) as well as changes in the optical properties of the scattering obscurant. The mean value of k/C was used to recompute the transmission history shown in Figure 1. Many non-physical transmissions (17 percent of the data record) resulted because equation 1 can easily result in negative transmissions when improper k/C values are used. We conclude that the target method provides accurate lidar-to-target transmissions and consistent extinction coefficient profiles when multiple scattering is not important, but that k/C must be evaluated independently for each lidar observation. Therefore, the method does not appear suitable for single-ended vertical and slant path observations.

B. Klett Method

The extraction of extinction coefficients from lidar measurements taken in an inhomogeneous atmosphere, such as through a smoke or dust event, is a difficult task in the absence of a uniform reflective target. Early solutions to the single-scattering lidar equation assumed a backscatter-to-extinction relationship and a known value of extinction at a small distance from the lidar system (4, 5). However, as shown by Klett (6), these forward integration solutions typically yield numerically unstable results unless unrealistic solution parameters are assumed. This is related to the problem of evaluating equation 1 with small uncertainties in k/C.

Klett overcame the stability problem by assuming a power law relationship between backscatter and extinction and a known value of extinction near the end of the lidar signature, leading to a backward integration solution. In particular, the Klett solution for extinction is as follows:

$$\sigma(R) = \frac{\exp\left[(S(R) - S_m)/k'\right]}{\sigma_m^{-1} + \frac{2}{k}\int_R^{R_m} \exp\left\{[S(r) - S_m]/k'\right\} dr}, \qquad (2)$$

where $S(R) = \ln[P(R)]$, $S_m(R_m)$, $\sigma_m = \sigma(R_m)$, and $\beta = \text{const}\ \sigma^{k'}$. The Klett solution requires an assumed power law exponent k', and knowledge of the extinction coefficient σ_m at a reference range R_m near the end of the lidar backscatter signature. We have applied the Klett solution with several different values of k' and σ_m to derive extinction profiles for three different lidar shots made during the obscurant test for which transmission data are shown in Figure 1.

For each lidar signature, extinction profiles derived using the Klett method can be compared with the extinction profile calculated using the target method. Following the analysis of Sasano and Nakane (7), relative root mean square errors, defined as

$$\delta e = \frac{\left\{\frac{1}{n}\sum_{r=r_1}^{r_n} [\sigma_{\text{Klett}}(r) - \sigma_{\text{Target}}(r)]^2\right\}^{\frac{1}{2}}}{\frac{1}{n}\sum_{r=r_1}^{r_n} \sigma_{\text{Target}}(r)} \qquad (3)$$

where n is the number of range bins along the path, were computed for a range of k' and σ_m values. These errors are shown in Figure 6 as plots of δe percentage as a function of σ_m and k' for laser shot 546 of the test data shown in Figure 1. The Klett extinction profile yielding the smallest rms difference from the extinction profile derived from the

target method is shown in Figure 7. The σ_m and k' parameter used to derive this solution are indicated in Figure 6 by the central x. The near-equal extinction profiles of the Klett and target methods are expected, as both solutions are based on the single-scattering lidar equation. Figure 8 presents comparisons of the target method extinction profile with Klett method profiles for 10 percent changes in k' and factor of 3 changes in σ_m. The values of k' and σ_m for the four solutions shown in Figure 8 are marked on the contour plot of Figure 6 by x's surrounding the central x. The changes in k' lead to rms errors of about 30 percent, and the changes in σ_m lead to rms errors of nearly 60 percent. Figure 9 presents a contour analysis of transmission evaluated from the Klett extinction profile solutions as a function of the solution parameters. The transmission values for the 10% change in k' and factor of 3 change in σ_m also are listed in Figures 7 and 8. A 10 percent uncertainty in k' results in about 3 percent error in transmission. A factor of 3 uncertainty in σ_m results in about 10 percent error in transmission. The transmission evaluated from the target return was 19.9 percent, as indicated by the central x plotted in Figure 9.

Figure 10 presents a contour plot of rms differences between Klett and target solutions for lidar shot number 542. In this case, the transmission evaluated by using the target was 25.6 percent. Again, a 10 percent change in k' causes an rms error of about 60 percent. Resulting extinction profiles and transmission errors are shown in Figure 11, with differences from target-derived values about the same as for laser shot 546 presented above.

Figure 12 presents a contour plot of rms differences between Klett and target solutions for lidar shot number 550. In this case, the target derived transmission was 52.3 percent. The 10 percent change in k' and factor of 3 change in σ_m give higher rms errors (nearly 40 and 80 percent, respectively) than for the lower transmission laser firings presented above. Resulting extinction profiles and transmission errors are shown in Figure 13. Transmission errors are about 4 to 6 percent for 10 percent change in k' and are about 17 to 21 percent for a factor

of 3 change in σ_m. From this result, it appears that Klett solutions for conditions of higher transmissions are more sensitive to uncertainties in k' and σ_m.

C. Experimental Data Method

A number of researchers have found a linear correlation between backscatter and extinction coefficients for typical particle size distributions and visible or near-infrared radiation. This implies a linear relationship between optical depth and path-integrated range-corrected lidar signal for low density aerosols. Because of attenuation, the relationship becomes nonlinear for larger values of optical depth (e.g., higher density aerosols). Uthe (8) derived optical depth-to-integrated lidar signal relationships based on transmissions evaluated from target returns and corresponding lidar back-scatter signatures for smoke and dust events. Using the 1.06 μm wavelength transmissions shown in Figure 1 and corresponding lidar backscatter signatures, a plot of optical depth to path-integrated lidar signal is shown in Figure 14. Each data point is derived from a single lidar observation during the smoke event. A non-linear least-squares curve-fitting method (9) was used with the data presented in Figure 14 to evaluate the best fit a_1 and a_2 parameters of the following expression:

$$u(\Psi) = a_1 \Psi (1 + e^{-a_2 \Psi}) \qquad (4)$$

where Ψ is the path-integrated lidar signal and u is the optical depth evaluated from the target return method. The best-fit relationship (a_1, a_2) and the upper and lower uncertainty limits as defined by Bevington (9) ($a_1 + \delta a_1$, $a_2 - \delta a_2$) and ($a_1 - \delta a_1$, $a_2 + \delta a_2$) are shown in Figure 14.

For each lidar observation, an extinction profile can be evaluated by first integrating the lidar signature between the lidar location and range r_1 and then applying the resulting Ψ_1 values with the u(Ψ)

relationship (Equation 4) to determine an optical depth profile u_1. Differentiation yields the extinction profile $\sigma(r)$. An example of this technique applied to lidar shots 550, 542, and 546 (used for analysis of the Klett method in Section 2.2) is shown in Figure 15. Solutions of extinction profiles derived by the target method (Section 2.1) and by the experimental data method with optical depth-to-integrated lidar signal expressions defined by (a_1, a_2), $(a_1 + \delta a_1, a_2 - \delta a_2)$, and $(a_1 - \delta a_1, a_2 + \delta a_2)$ are shown in Figure 15. These results show the experimental data method provides extinction profiles in general agreement with the target method for high transmissions but with greater discrepancy for lower transmissions. This may be expected since the target method is based on the single-scattering lidar equation, while the experimental data method includes effects of multiple scattering. Because of multiple scattering, less attenuation correction is applied at greater depths within the smoke plume than with the single scattering solution. For this reason, the experimental data method may be more appropriate for evaluating extinction profiles through relatively dense smoke and dust events.

III CONCLUSIONS

In this paper, extinction profiles have been derived from lidar data using three different methods. The target method requires a lidar target return for each observation but provides extinction profiles that when range integrated give transmission data consistent with independent transmissometer observations. The Klett method, also based on the single scattering lidar equation, can reproduce the extinction profile derived from the target method when appropriate solution parameters are used. However, expected uncertainties in the solution parameters can result in unacceptable errors in the extinction profile. The experimental data method requires a known relationship between optical depth and path-integrated lidar signal. This relationship can be derived from lidar target and aerosol returns or can be estimated from

extinction-to-backscatter ratios. This method did not reproduce the extinction profiles of the target or Klett methods--probably because this method includes multiple scattering effects. Before any one method is judged superior, we believe an experiment is needed that is designed to validate lidar analysis methods. Such an experiment will require in situ measurement of aerosol optical and/or physical densities along the propagation path of lidar observations.

ACKNOWLEDGMENTS

This research was funded by the U.S. Army Research Office, Geosciences Division, under Contract DAAG29-82-K-0191. The authors thank Dr. Walter Flood of ARO for his suggestions on the conduct of this project.

Norman B. Nielsen and Steven A. DeLateur designed and constructed the four-wavelength lidar system, and operated the lidar during the SNOW-ONE-B and Smoke Week VI/SNOW TWO field programs.

REFERENCES

1. DeLateur, S.A., N.B. Nielsen, E.E. Uthe, and J.M. Livingston: "Four- wavelength Lidar Measurements from Smoke Week VI/SNOW-TWO," Smoke/
Obscurants Symposium VIII, Harry Diamond Laboratories, Adelphi, MD. Proceedings, Project Managers Office for Smoke and Obscurants, (1984).

2. Uthe, E.E., S.A. DeLateur, J.M. Livingston, and N.B. Nielsen: "SNOW-ONE-B Multiple-wavelength Lidar Measurements," Snow Symposium III, Hanover, NH, August 1983. Proceedings: U.S. Army Cold Regions Research and Engineering Laboratory, Hanover, NH.

3. Fernald, F.G., B.M. Herman, and J.A. Reagan: "Determination of Aerosol Height Distribution by Lidar. J. Appl. Meteorol., 11, 482-489, (1972).

4. Viezee, W., E.E. Uthe, and R.T.H. Collis: "Lidar Observations of Airfield Approach Conditions: An Exploratory Study." J. Appl. Meteorol., 8, 274-283, (1969).

5. Johnson, W.B. and E.E. Uthe: "Lidar Study of the Keystone Stack Plume," Atmos. Environ., 5, 703-724, (1971).

6. Klett, J.D.: "Stable Analytical Inversion Solution for Processing Lidar Returns." Appl. Opt., 20, 211-220, (1981).

7. Sasano, Y. and H. Nakane: "Significance of the Extinction/backscatter Ratio and the Boundary Value Term in the Solution for the Two-component Lidar Equation," Appl. Opt., 23, 11-13, (1984).

8. Uthe, E.E.: "Lidar Evaluation of Smoke and Dust Clouds," Appl. Opt., 20, 1503-1510, (1981).

9. Bevington, P.R.,: Data Reduction and Error Analysis for the Physical Sciences. McGraw-Hill, New York, New York, 188-189, 237-239, (1969).

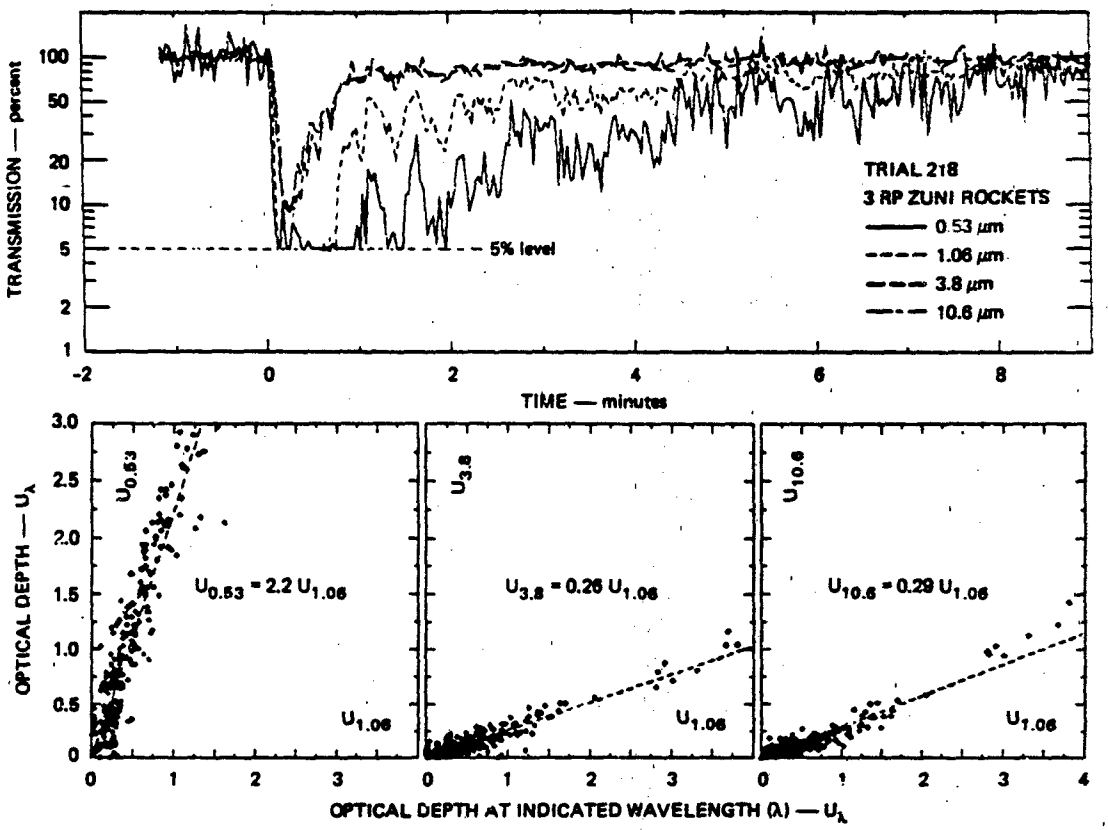

FIGURE 1 TRANSMISSION HISTORY AND OPTICAL DEPTH RELATIONSHIPS FOR SMOKE GENERATED DURING TRAIL 218 (3RP ZUNI ROCKETS)

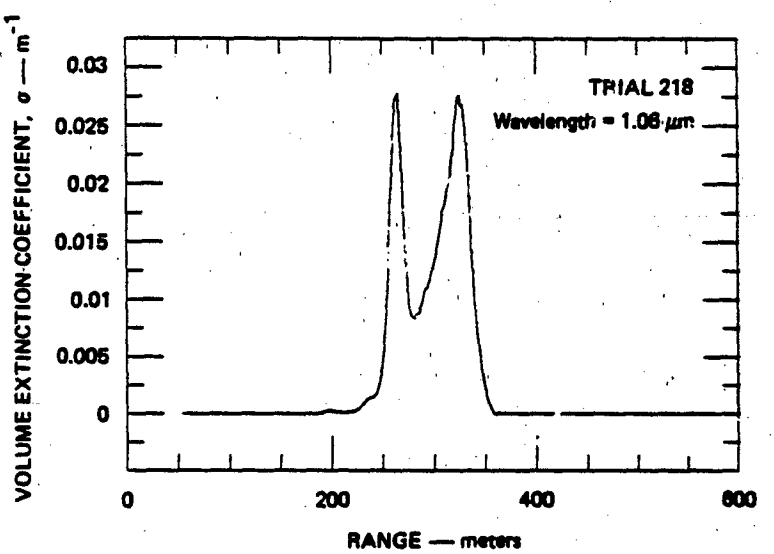

FIGURE 2. RANGE-RESOLVED VOLUME EXTINCTION COEFFICIENT (1.06 μm) ALONG THE OPTICAL PATH AT Z + 63 SECONDS OF TRIAL 218 (TARGET METHOD)

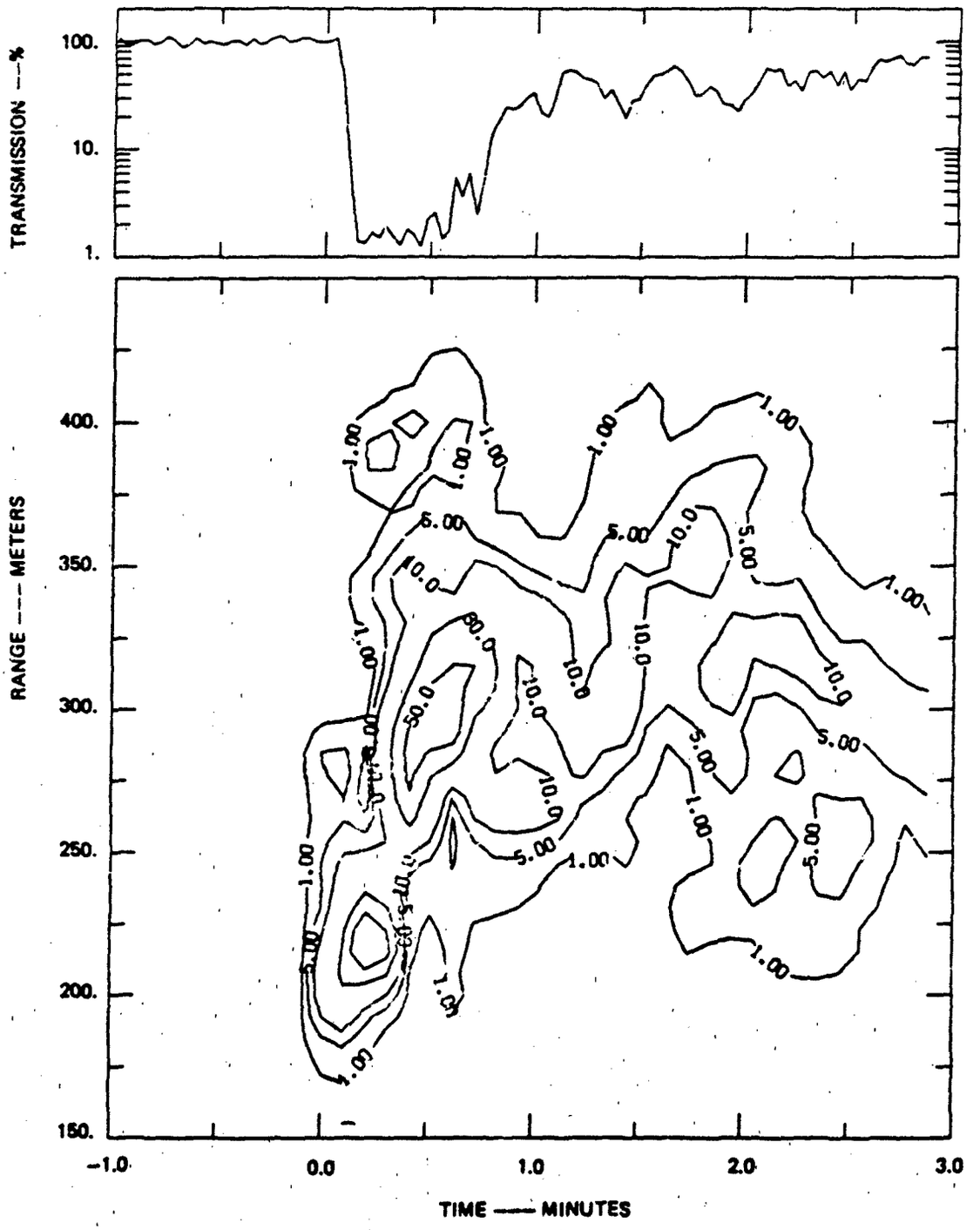

FIGURE 3 CONTOUR MAP OF 1.06 μm WAVELENGTH EXTINCTION COEFFICIENT (km^{-1}) DISTRIBUTION ALONG THE LIDAR OPTICAL PATH AS A FUNCTION OF SMOKE EVENT TIME. CORRESPONDING TRANSMISSION HISTORY IS PLOTTED ABOVE THE CONTOUR MAP.

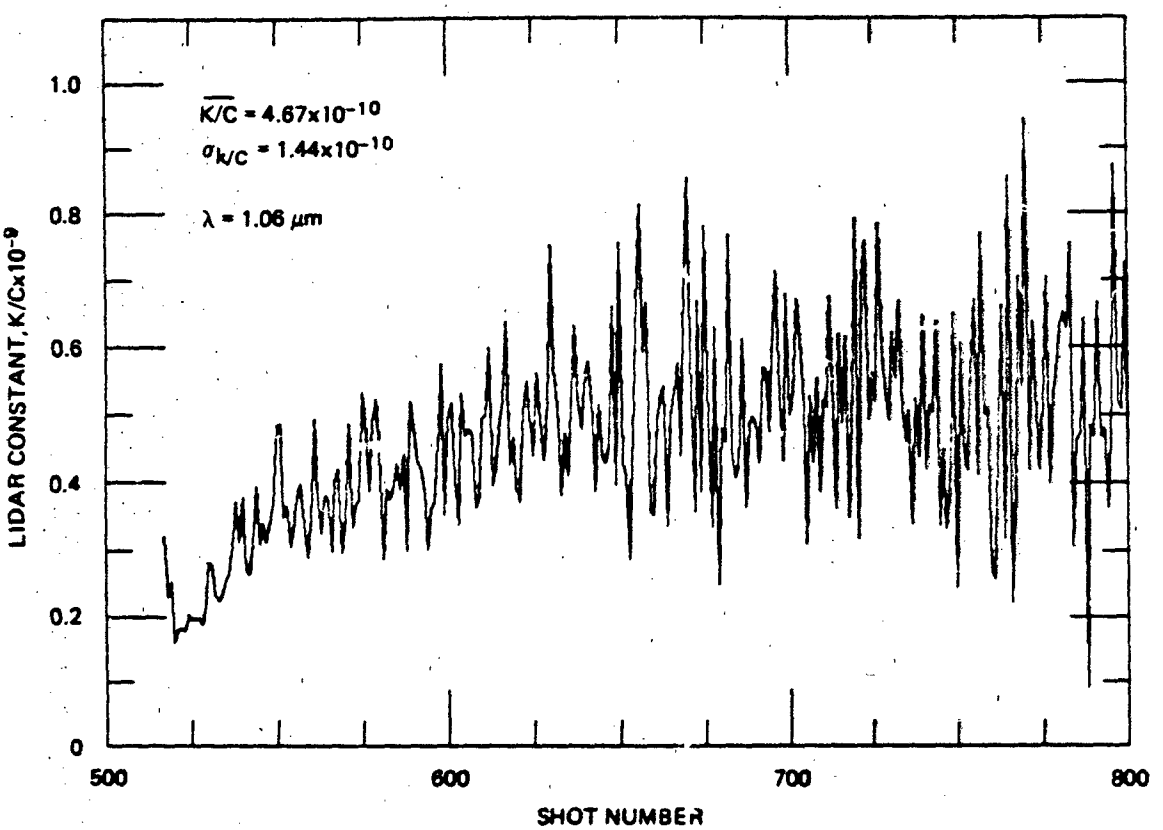

FIGURE 4 K/C HISTORY FOR SMOKE GENERATED DURING TRIAL 218

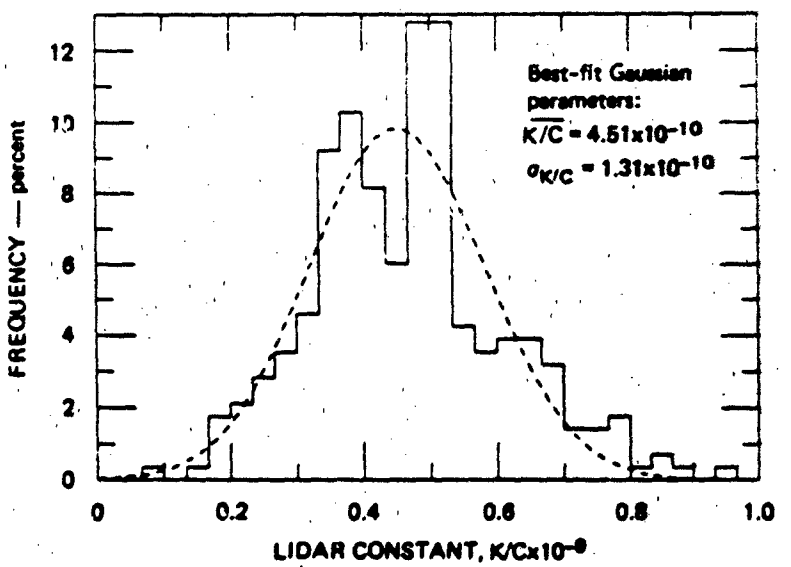

FIGURE 5 DISTRIBUTION OF K/C VALUES FOR SMOKE TRIAL 218.

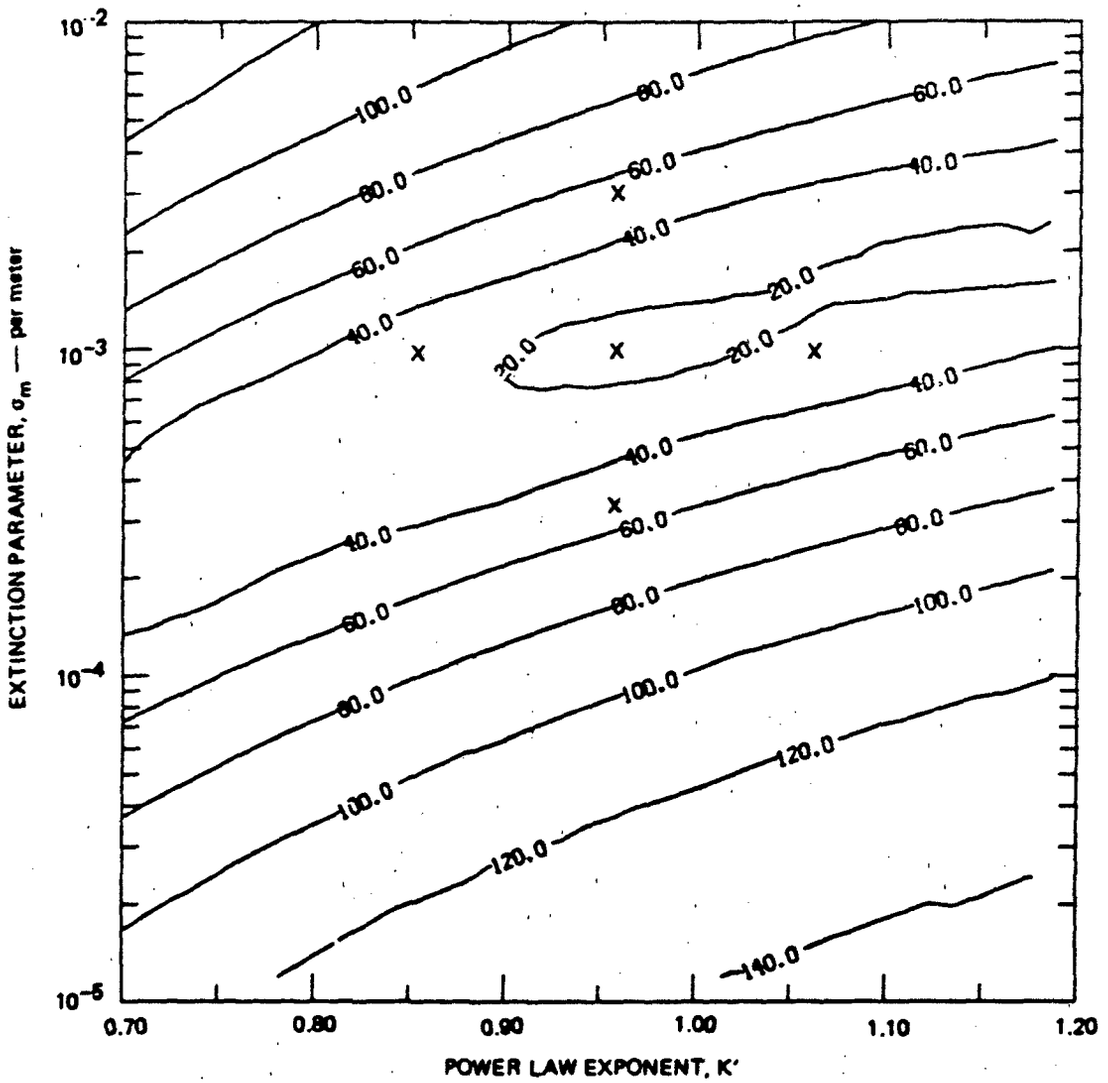

FIGURE 6 CONTOUR PLOT OF KLETT METHOD RMS ERRORS AS A FUNCTION OF THE SOLUTION PARAMETERS K' AND σ_{in} (LASER SHOT 546). THE X's INDICATE PARAMETER VALUES USED TO COMPUTE EXTINCTION PROFILES PRESENTED IN FIGURES 7 AND 8.

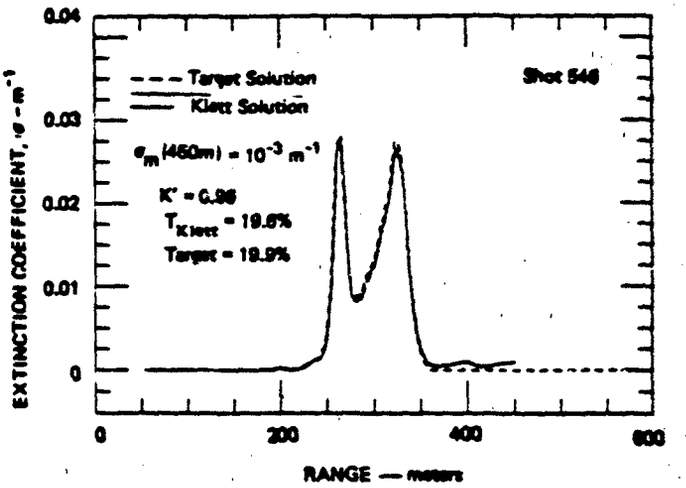

FIGURE 7 TARGET METHOD AND BEST-FIT KLETT METHOD EXTINCTION COEFFICIENT PROFILES (LASER SHOT 546)

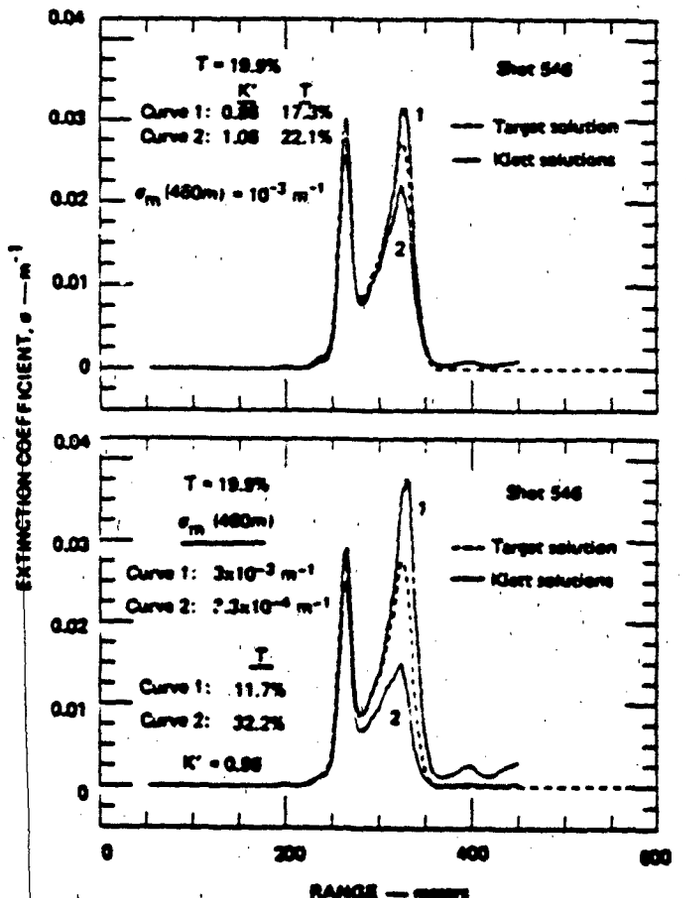

FIGURE 8 EXTINCTION COEFFICIENT PROFILES FOR INCREMENTED VALUES OF K' AND σ' (LASER SHOT 546).

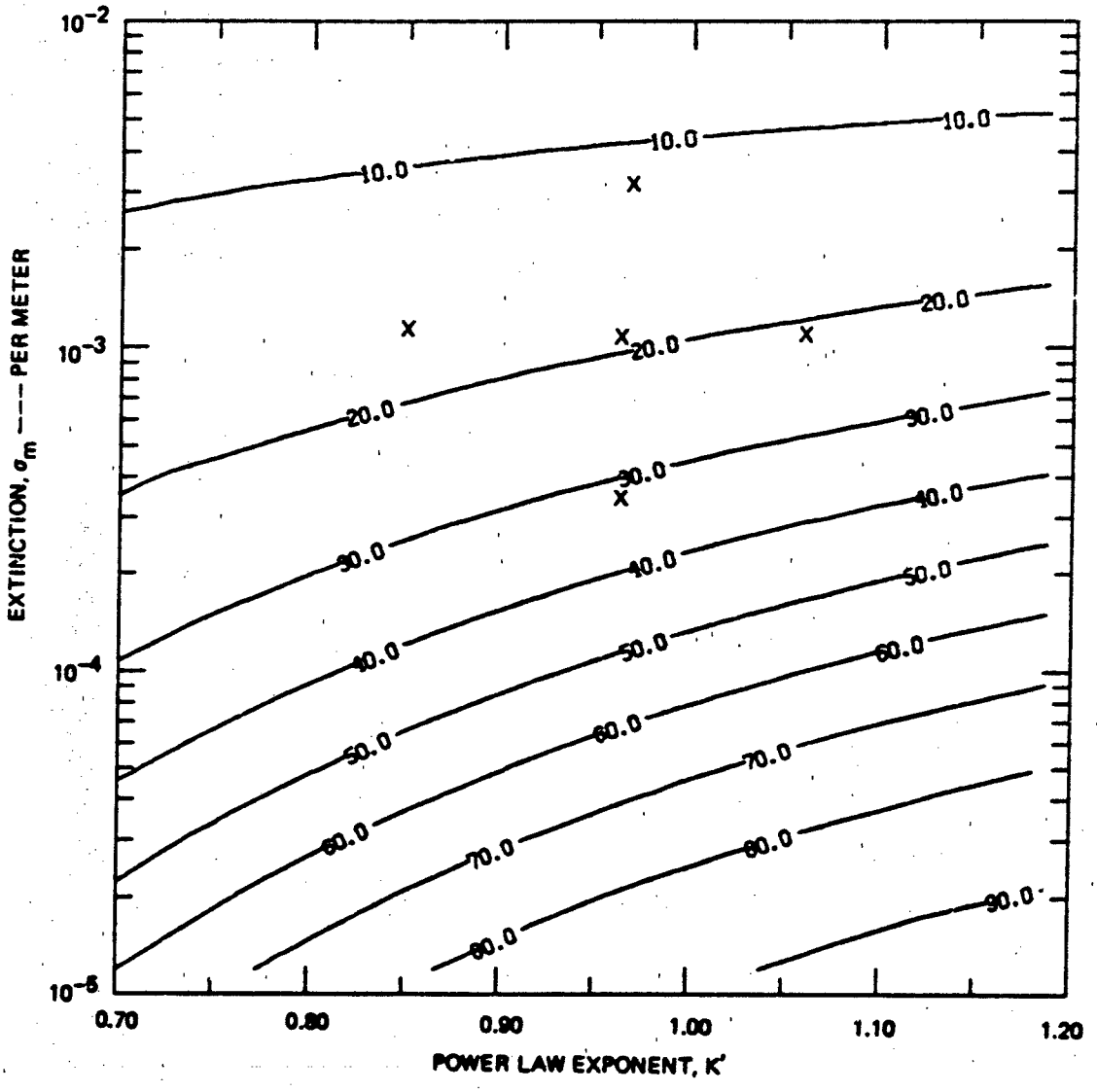

FIGURE 9 CONTOUR PLOT OF TRANSMISSIONS EVALUATED FROM THE KLETT METHOD AS A FUNCTION OF THE SOLUTION PARAMETERS σ_m, and K'. THE X's CORRESPOND TO THOSE OF FIGURE 8.

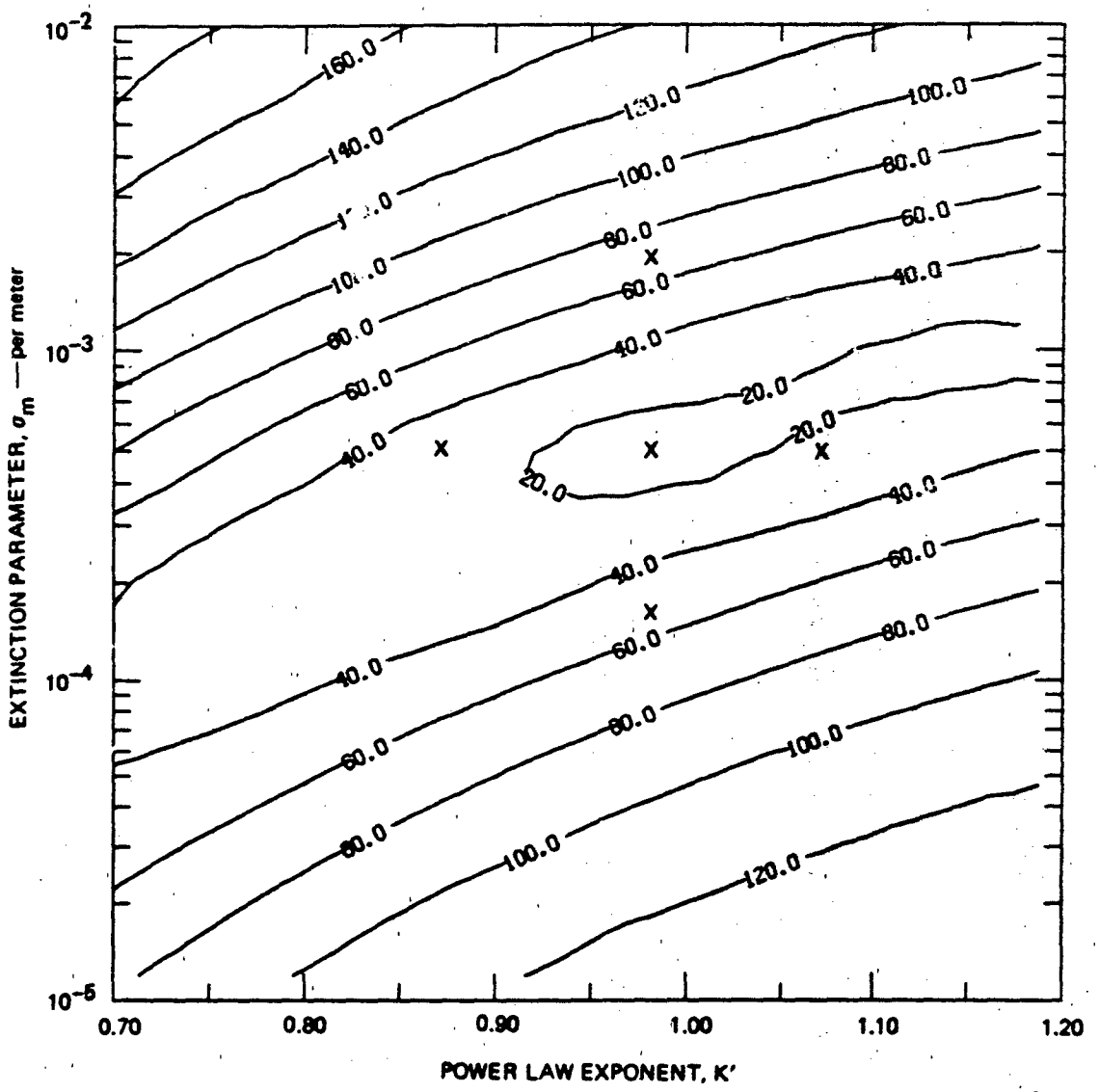

FIGURE 10 CONTOUR PLOT OF KLETT METHOD RMS ERRORS AS A FUNCTION OF THE SOLUTION PARAMETERS K' AND σ_m (LASER SHOT 542)

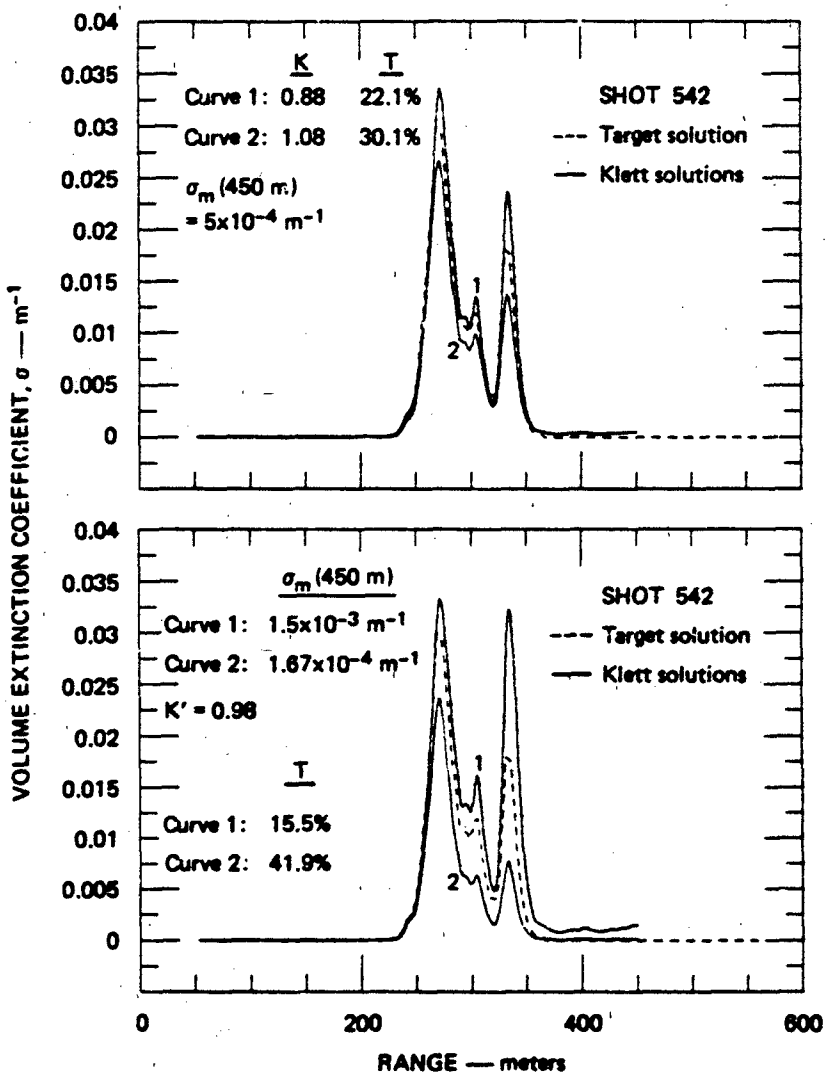

FIGURE 11 EXTINCTION COEFFICIENT PROFILES FOR INCREMENTED VALUES OF K' AND σ_m (LASER SHOT 542)

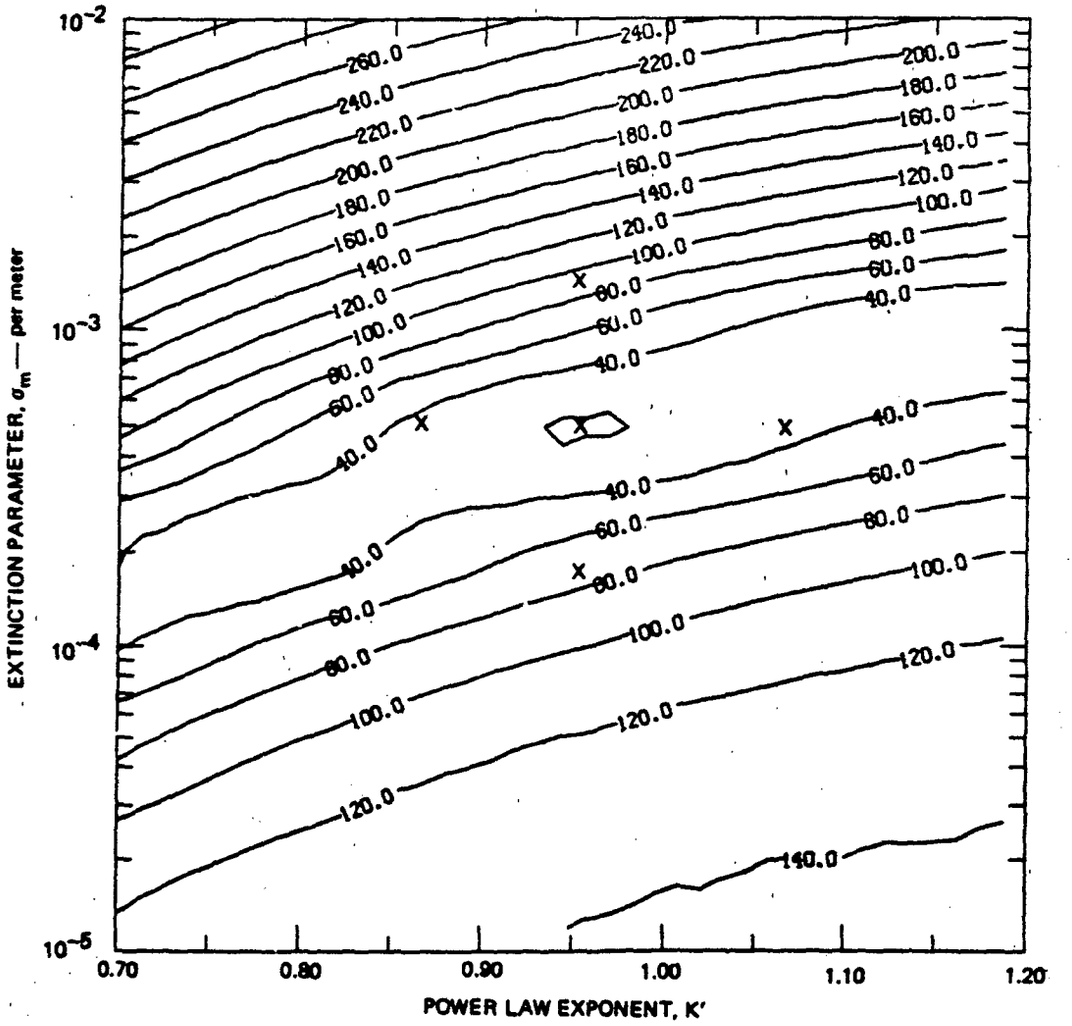

FIGURE 12 CONTOUR PLOT OF KLETT METHOD RMS ERRORS AS A FUNCTION OF THE SOLUTION PARAMETERS K' AND σ_m (LASER SHOT 548).

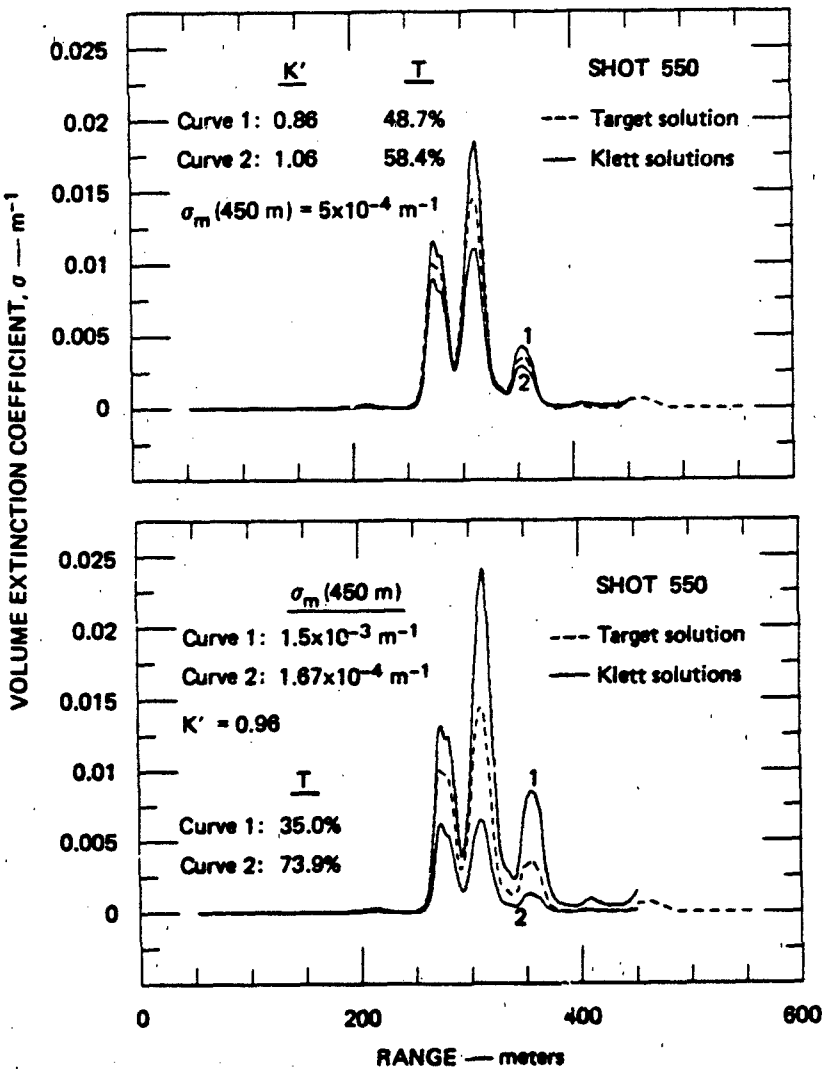

FIGURE 13 EXTINCTION COEFFICIENT PROFILES FOR INCREMENTED VALUES OF K′ AND σ_m (LASER SHOT 550)

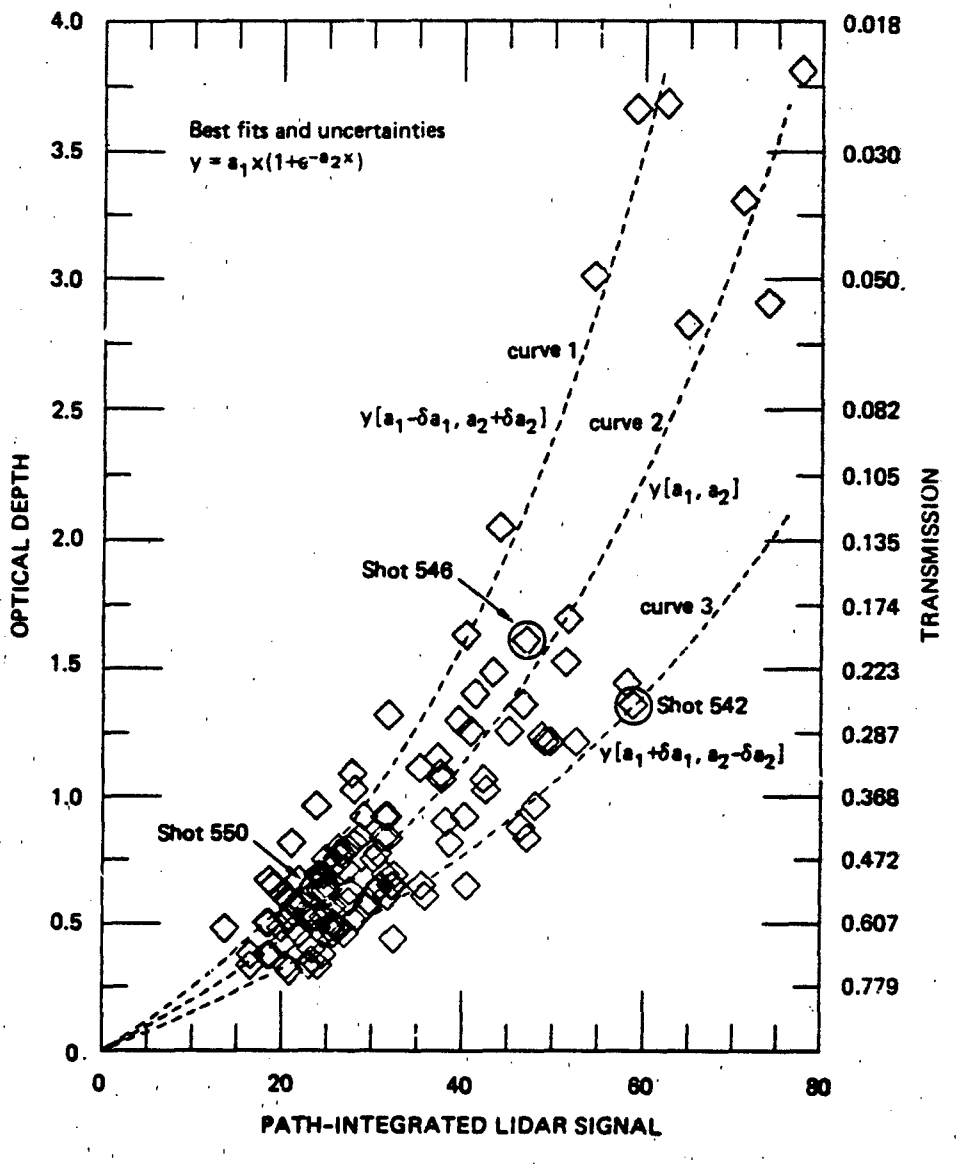

FIGURE 14 PLOT OF OPTICAL DEPTH AGAINST RANGE-INTEGRATED LIDAR SIGNAL FOR DATA COLLECTED DURING SMOKE TEST 218. BEST-FIT AND WORST-CASE MODEL FITS ARE INDICATED.

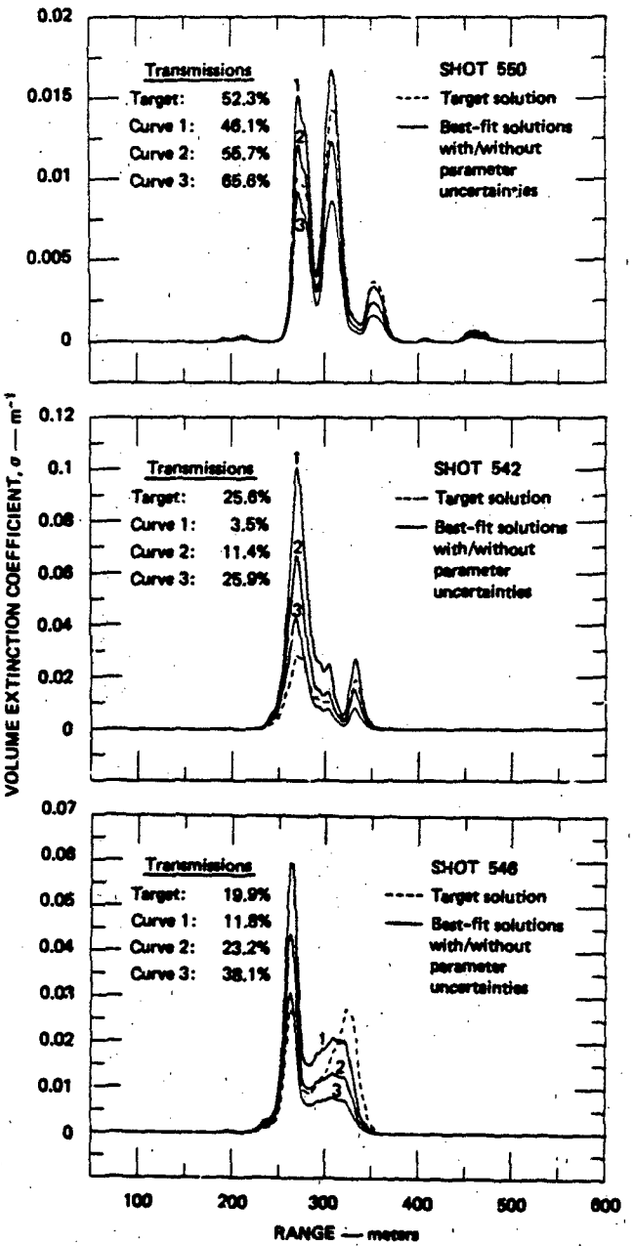

FIGURE 15. EXTINCTION COEFFICIENT PROFILES DERIVED USING EXPERIMENTAL DATA METHOD WITH OPTICAL DEPTH INTEGRATED LIDAR SIGNAL MODELS PRESENTED IN FIGURE 14

Appendix B

"ERROR ANALYSIS OF LIDAR SOLUTION TECHNIQUES FOR
RANGE-RESOLVED EXTINCTION COEFFICIENTS BASED ON OBSERVATIONAL DATA"

Presented at SMOKE/OBSCURANTS SYMPOSIUM IX.

ERROR ANALYSIS OF LIDAR SOLUTION TECHNIQUES FOR RANGE-RESOLVED EXTINCTION COEFFICIENTS BASED ON OBSERVATIONAL DATA*

E. E. Uthe and J. M. Livingston
SRI International
Menlo Park, CA 94025, USA

ABSTRACT

The SRI four-wavelength (0.53, 1.06, 3.8 and 10.6 μm) lidar system was used during the Smoke Week XI/SNOW-TWO field experiments to observe range-resolved backscatter and target-reflected laser energy along a horizontal path intersected by test obscurant aerosols.

Target reflected laser energy provided an excellent measure of time-dependent path-integrated extinction (e.g., transmission). These values allow the range-resolved backscatter to be analyzed in terms of range-resolved extinction when single-scattering is assumed. This two-ended (lidar and target) method provides extinction coefficients along the optical path that are consistent with independent transmissometer observations. The values are the most accurate that can be derived from the lidar technique when multiple scattering is limited.

Extinction profiles evaluated from the lidar/target method can be utilized to investigate the limitations and accuracies of algorithms which are used to derive extinction data from lidar backscatter signatures when no target return is available. Single-ended lidar methods are needed for vertical and slant-path measurements. Two single-ended techniques were investigated. The first is the well-known Klett modification of the analytic solution to the single-scattering lidar equation. The Klett technique can reproduce the extinction profile derived from the lidar/target method as expected since both are derived from the single-scattering lidar-equation. However, this requires relatively accurate information on a boundary value of extinction and the backscatter-to-extinction relationship. Contour plots showing deviation of the Klett extinction profile from the lidar/target extinction profile as a function of the solution parameters are presented.

A second method of deriving extinction profiles from single-ended lidar measurements is based on an observed relationship of optical depth to path-integrated lidar signal. Such a relationship derived from lidar/target data includes multiple scattering effects on the extinction evaluation. The method does not reproduce the extinction profile derived from the single-scattering lidar/target and Klett methods -- indicating the importance of multiple scattering on the lidar backscatter signature.

1. BACKGROUND

Description of the SRI van-mounted four-wavelength (0.53, 1.06, 3.8 and 10.6 μm) lidar system and its operation during the Smoke Week VI/SNOW-TWO field program was presented at the Smoke/Obscurants Symposium VIII (DeLateur et. al., 1984). Basically, laser pulses at the four wavelengths were transmitted along a horizontal path terminated at a distance of 600 m from the lidar by a target of uniform reflective properties over the illuminated area. The laser pulses at each wavelength were emitted sequentially within a 60 μs interval to reduce effects of time- and space-varying aerosol concentrations on each four-wavelength pulse set. About 60 pulse sets were transmitted for each minute of operation. Collected energy backscattered from atmospheric aerosols and energy reflected from the solid target was collected within a telescope and directed to appropriate detectors using dichroic filters. After logarithmic amplification, backscatter signatures were digitized by an 8-bit 100-MHz transient recorder and resulting digital records were stored on nine-track magnetic tape for subsequent analysis.

*This work was supported by the U.S. Army Research Office, Geosciences Division, under Contract DAAG29-82-K-0191.

2. DATA ANALYSIS METHODS AND RESULTS

2.1 Target Method

Target returns observed by a lidar system can be interpreted in terms of transmission across the lidar-to-target path. Previous results have shown that lidar derived transmissions agree with independent data records collected with conventional two-ended transmissometers (Uthe et al., 1983). Therefore, the four-wavelength lidar target returns collected during an obscurant event provide the time history of transmission at each wavelength and provide data to evaluate optical depth u=-ln T relationships between wavelengths, as shown by the example presented in Figure 1.

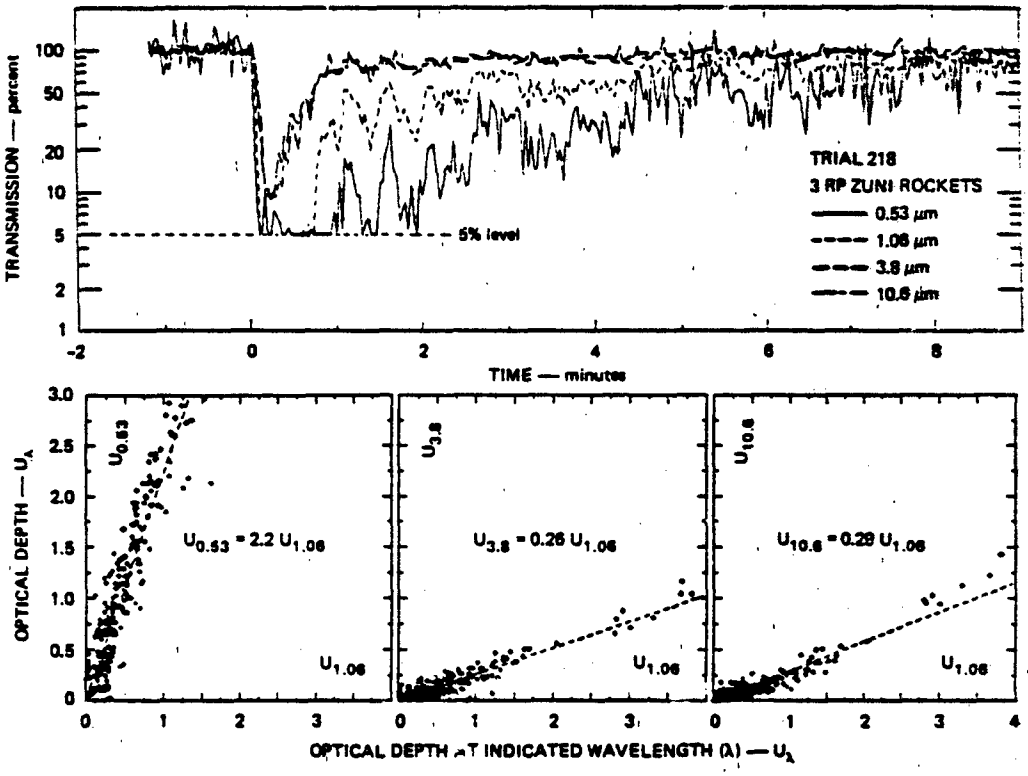

FIGURE 1 TRANSMISSION HISTORY AND OPTICAL DEPTH RELATIONSHIPS FOR SMOKE GENERATED DURING TRAIL 218 (3RP ZUNI ROCKETS)

Fernald et al. (1972), among others, have shown that if the ratio of the extinction coefficient to the backscatter coefficient, $k=\sigma(r)/\beta(r)$, remains constant over the range interval Δr being investigated, then the two-way transmittance, $T^2(r)$, follows directly from differentiation of the basic lidar equation and is given by

$$T^2(R) = 1 - \frac{2k}{C}\int_0^R P(r)dr \qquad (1)$$

In this equation, P(r) is the signal whose amplitude is proportional to the power received from a scattering volume at range r and is corrected for the geometric range-squared effect and transmitted energy variations. C is a lidar calibration constant.

The constant k/C can be determined by combining the known two-way transmittance between the laser and the target with the lidar return signature integrated over the same range. The value of this constant is then substituted back into (1) and combined with integrals of the received backscatter signals to intermediate ranges to yield a horizontal transmission profile. Since transmission is directly related to optical depth through $T^2(R) = e^{-2u(R)}$, where optical depth $u(R) = \int_0^R \sigma(r)\, dr$, calculation of a transmission profile implies a corresponding extinction profile. We call this the "target" method of deriving an extinction profile because it requires the use of a target to derive a constant k/C value. Figure 2 presents an example of an extinction coefficient profile for a single lidar observation during an obscurant test for which a transmission history is presented in Figure 1.

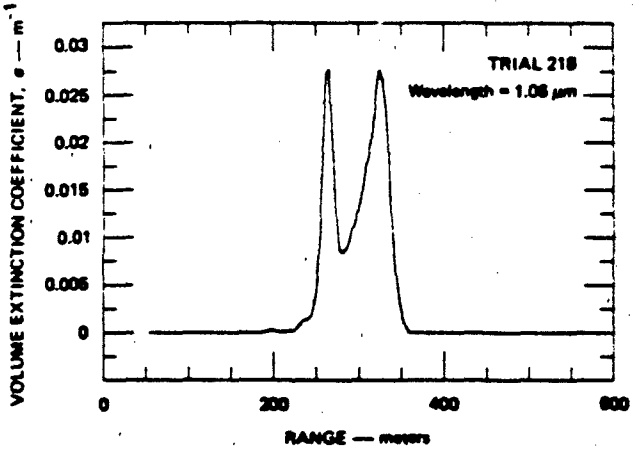

FIGURE 2. RANGE-RESOLVED VOLUME EXTINCTION COEFFICIENT (1.06 μm) ALONG THE OPTICAL PATH AT Z + 63 SECONDS OF TRIAL 218 (TARGET METHOD)

If the value of k/C remains constant for a given type of obscurant, this value of k/C can be used to derive extinction and transmission values from single-ended lidar observations and, therefore, vertical and slant-path measurements would be possible. Values of k/C have been calculated for each lidar shot for the test with data shown in Figure 1 by using the 1.06 μm wavelength target-derived transmissions. In addition, linear and best-fit Gaussian means and standard deviations of k/C have been calculated. These results are shown in Figures 3 and 4 where it can be seen that the two methods of computing a mean k/C yield similar results. Figure 3 shows that k/C can undergo both gradual and rapidly fluctuating variability that may be the result of pulse-to-pulse changes in lidar system performance (transmitted energy, pulse shape and detector response) as well as changes in the optical properties of the scattering obscurant. The mean value of k/C was used to recompute the transmission history shown in Figure 1. Many non-physical transmissions (17 percent of the data record) resulted because equation 1 can easily result in negative transmissions when improper k/C values are used. We conclude that the target method provides accurate lidar-to-target transmissions and consistent extinction coefficient profiles when multiple scattering is not important, but that k/C must be evaluated independently for each lidar observation. Therefore, the method does not appear suitable for single-ended vertical and slant path observations.

2.2 Klett Method

The extraction of extinction coefficients from lidar measurements taken in an inhomogeneous atmosphere, such as through a smoke or dust event, is a difficult task in the absence of a uniform reflective target. Early solutions to the single-scattering lidar equation assumed a backscatter-

to-extinction relationship and a known value of extinction at a small distance from the lidar system (Viezee et al., 1969; Johnson and Uthe, 1971). However, as shown by Klett (1981), these forward integration solutions typically yield numerically unstable results unless unrealistic solution parameters are assumed. This is similar to the problem of evaluating equation 1 with small uncertainties in k/C.

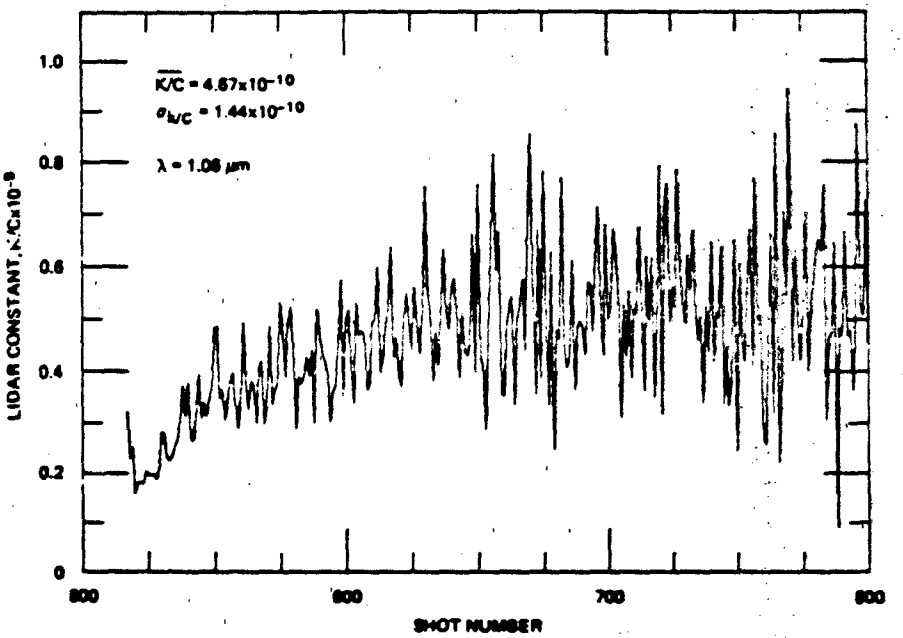

FIGURE 3. K/C HISTORY FOR SMOKE GENERATED DURING TRIAL 218

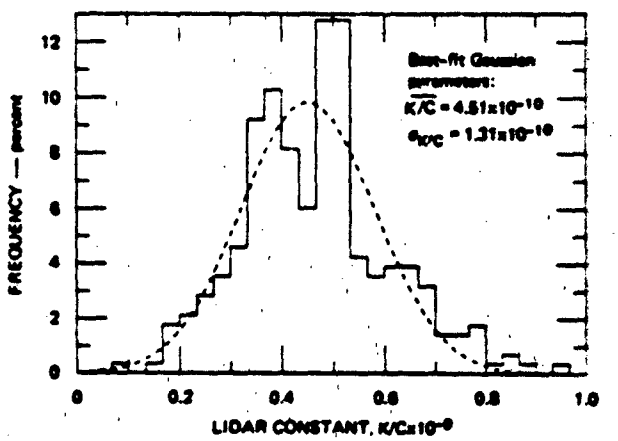

FIGURE 4. DISTRIBUTION OF K/C VALUES FOR SMOKE TRIAL 218.

Klett overcame the stability problem by assuming a power law relationship between backscatter and extinction and a known value of extinction near the end of the lidar signature, leading to a backward integration solution. In particular, the Klett solution for extinction is as follows:

$$\sigma(R) = \frac{\exp\left[(S(R) - S_m)/k'\right]}{\sigma_m^{-1} + \frac{2}{k'}\int_R^{R_m} \exp\left\{[S(r) - S_m]/k'\right\} dr}, \qquad (2)$$

where $S(R) = \ln[P(R)]$, $S_m = S(R_m)$, $\sigma_m = \sigma(R_m)$, and $\beta = \text{const}\ \sigma^{k'}$. The Klett solution requires an assumed power law exponent k', and knowledge of the extinction coefficient σ_m at the reference range R_m. We have applied the Klett solution with several different values of k' and σ_m to derive extinction profiles for three different lidar shots made during the obscurant test for which transmission data is shown in Figure 1.

For each lidar signature, extinction profiles derived using the Klett method can be compared with the extinction profile calculated using the target method. Following the analysis of Sasano and Nakane (1984), relative root mean square errors, defined as

$$\delta\sigma = \frac{\left\{\frac{1}{n}\sum_{r=r_1}^{r_n}\left[\sigma_{\text{Klett}}(r) - \sigma_{\text{Target}}(r)\right]^2\right\}^{\frac{1}{2}}}{\frac{1}{n}\sum_{r=r_1}^{r_n}\sigma_{\text{Target}}(r)} \qquad (3)$$

where n is the number of range bins along the path, were computed for a range of k' and σ_m values.

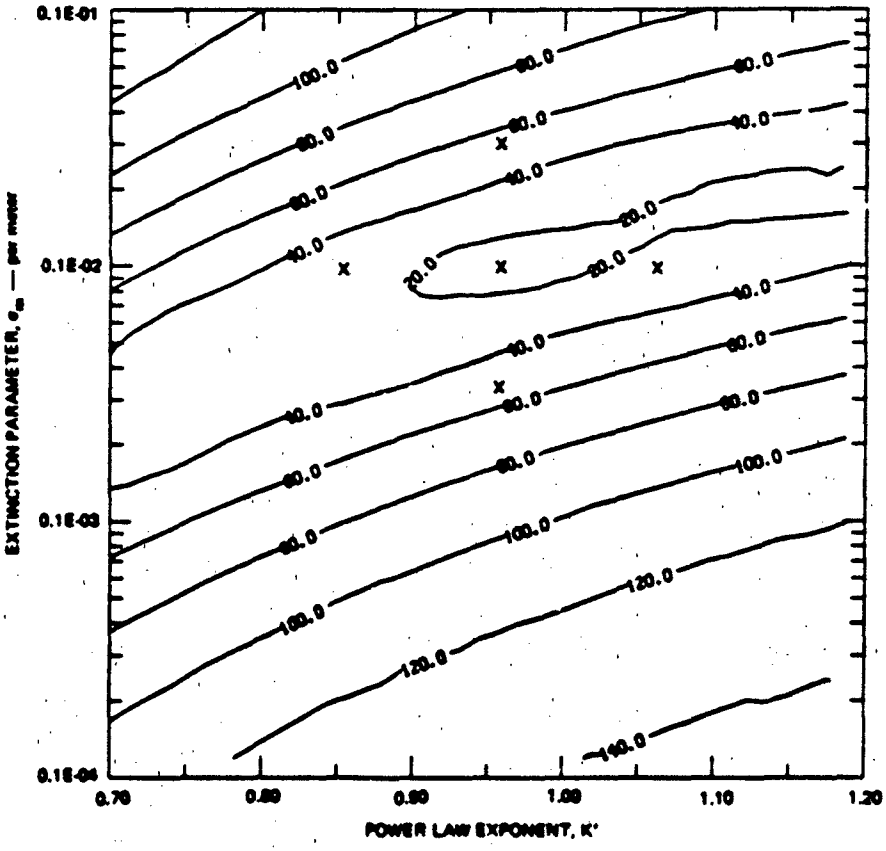

FIGURE 8 CONTOUR PLOT OF KLETT METHOD RMS ERRORS AS A FUNCTION OF THE SOLUTION PARAMETERS K' AND σ_m (LASER SHOT 846)

These errors are shown in Figure 5 as plots of δe percentage as a function of σ_m and k' for laser shot 546 of the test data shown in Figure 1. The Klett extinction profile yielding the smallest rms difference from the extinction profile derived from the target method is shown in Figure 6. The near-equal extinction profiles of the Klett and target methods are expected as both solutions are based on the single-scattering lidar equation. Figure 7 presents comparisons of the target method extinction profile with Klett method profiles for 10 percent changes in k' and factor of 3 changes in σ_m. The values of k' and σ_m for the four solutions shown in Figure 7 are marked on the contour plot of Figure 5 by x's. The changes in k' lead to rms errors of about 30 percent and the changes in σ_m lead to rms errors of nearly 60 percent. The resulting transmission errors are shown in Figure 7. A 10 percent uncertainty in k' results in about 3 percent

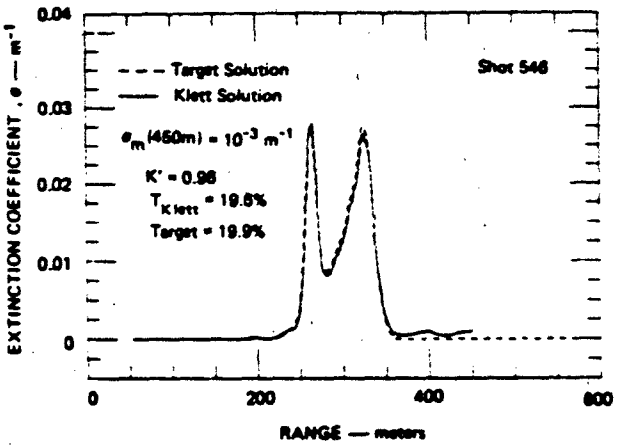

FIGURE 6 TARGET METHOD AND BEST-FIT KLETT METHOD EXTINCTION COEFFICIENT PROFILES (LASER SHOT 546)

uncertainty in transmission. A factor of 3 uncertainty in σ_m results in about 10 percent uncertainty of transmission. The transmission evaluated from the target return was 19.9 percent.

Figure 8 presents a contour plot of rms differences between Klett and target solutions for lidar shot number 542. In this case, the transmission evaluated by using the target was 25.6 percent. Again, a 10 percent change in k' causes an rms error of about 60 percent. Resulting extinction profiles and transmission uncertainties are shown in Figure 9 and differences from target-derived values are about the same as for laser shot 546 presented above.

Figure 10 presents a contour plot of rms differences between Klett and target solutions for lidar shot number 550. In this case, the target derived transmission was 52.3 percent. The 10 percent change in k' and factor of 3 change in σ_m give higher rms errors (nearly 40 and 80 percent respectively) than for the lower transmission

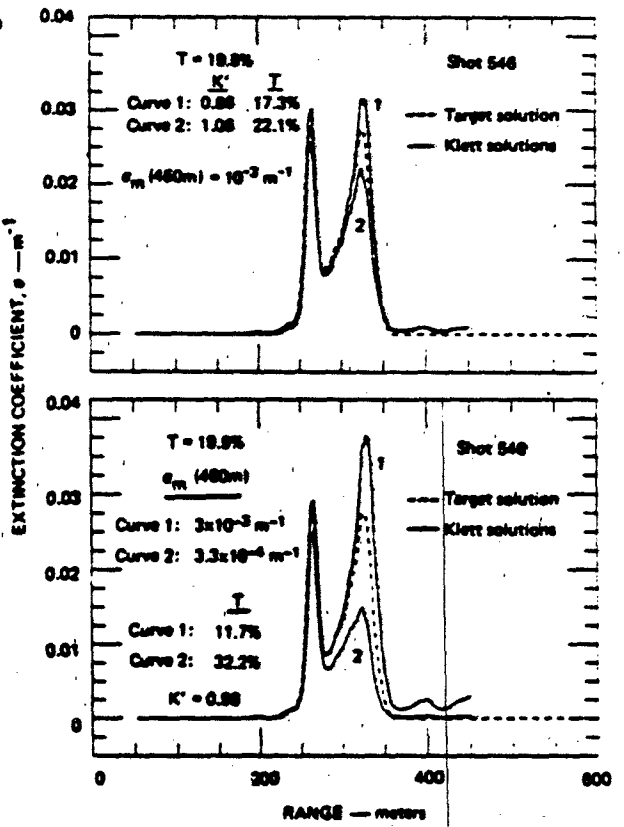

FIGURE 7. EXTINCTION COEFFICIENT PROFILES FOR INCREMENTED VALUES OF K' AND σ' (LASER SHOT 546).

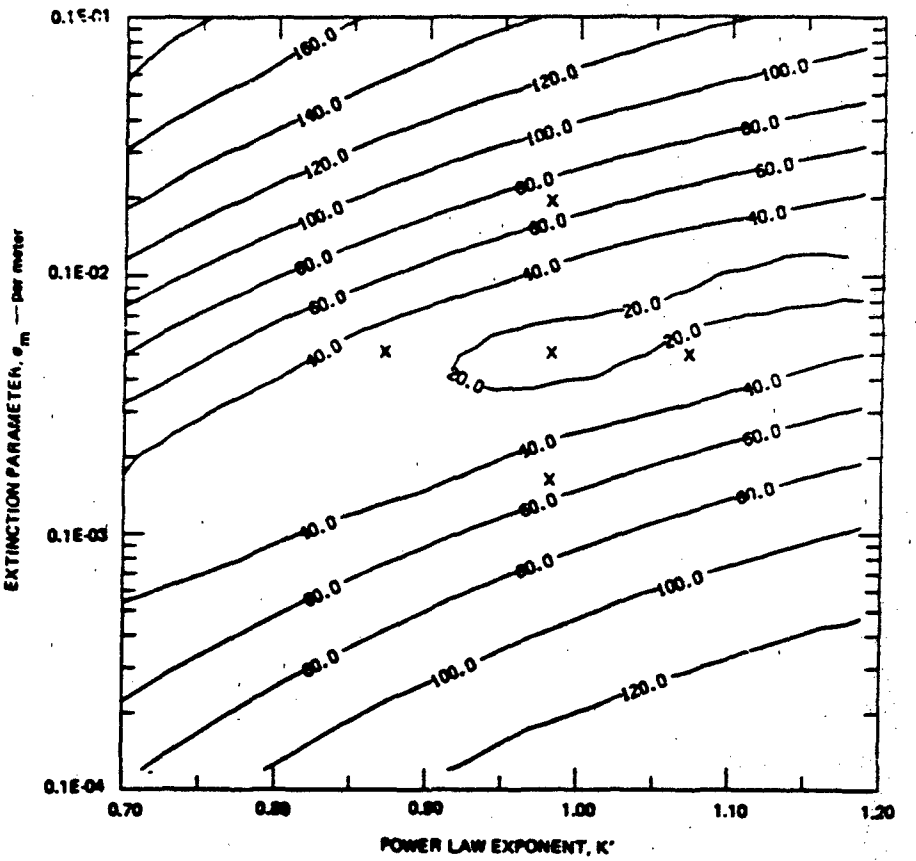

FIGURE 8 CONTOUR PLOT OF KLETT METHOD RMS ERRORS AS A FUNCTION OF THE SOLUTION PARAMETERS K' AND σ_m (LASER SHOT 542)

laser firings presented above. Resulting extinction profiles and transmission uncertainties are shown in Figure 11. Transmission differences are about 4 to 6 percent for 10 percent change in k' and are about 17 to 21 percent for a factor of 3 change in σ_m. From this result, it appears that Klett solutions for conditions of higher transmissions are more sensitive to uncertainties in k' and σ_m.

2.3 Experimental Data Method

A number of researchers have found a linear correlation between backscatter and extinction coefficients for typical particle size distributions and visible or near-infrared radiation. This implies a linear relationship between optical depth and path-integrated range-corrected lidar signal for low density aerosols. Uthe (1981) derived optical depth-to-integrated lidar signal relationships based on transmissions evaluated from target returns and corresponding lidar backscatter signatures for smoke and dust events. Using the 1.06 μm wavelength transmissions shown in Figure 1 and corresponding lidar backscatter signatures, a plot of optical depth to path integrated lidar signal is shown in Figure 12. Each data point is derived from a single lidar observation. A non-linear least-squares curve-fitting method (Bevington, 1969) was used with the

data presented in Figure 12 to evaluate the best fit a_1 and a_2 parameters of the following expression:

$$u(\mathcal{T}) = a_1 \mathcal{T} (1 + e^{-a_2 \mathcal{T}}) \qquad (4)$$

where $\mathcal{T}$ is the path-integrated lidar signal and u is the optical depth evaluated from the target return method. The best-fit relationship (a_1, a_2) and the upper and lower uncertainty limits as defined by Bevington ($a_1 + \delta a_1$, $a_2 - \delta a_2$) and ($a_1 - \delta a_1$, $a_2 + \delta a_2$) are shown in Figure 12.

For each lidar observation, an extinction profile can be evaluated by first integrating the lidar signature between the lidar location and range r_1 and then applying the resulting $\mathcal{T}_1$ values with the $u(\mathcal{T})$ relationship (Equation 4) to determine an optical depth profile u_1. Differentiation yields the extinction profile $\sigma(r)$. An example of this technique applied to lidar shots 550, 542, and 546 (used for analysis of the Klett method in Section 2.2) is shown in Figure 13. Solutions of extinction profiles derived by the target method (Section 2.1) and by the experimental data method with optical depth-to-integrated lidar signal expressions defined by (a_1, a_2), ($a_1 + \delta a_1$, $a_2 - \delta a_2$), and ($a_1 - \delta a_1$, $a_2 + \delta a_2$) are shown in Figure 13. These results show the experimental data method provides extinction profiles in general agreement with the target method for high transmissions but with greater discrepancy for lower transmissions. This may be expected since the target method is based on the single-scattering lidar equation while the experimental data method includes effects of multiple scattering. For this reason, the experimental data method may be more appropriate for evaluating extinction profiles through relatively dense smoke or dust events.

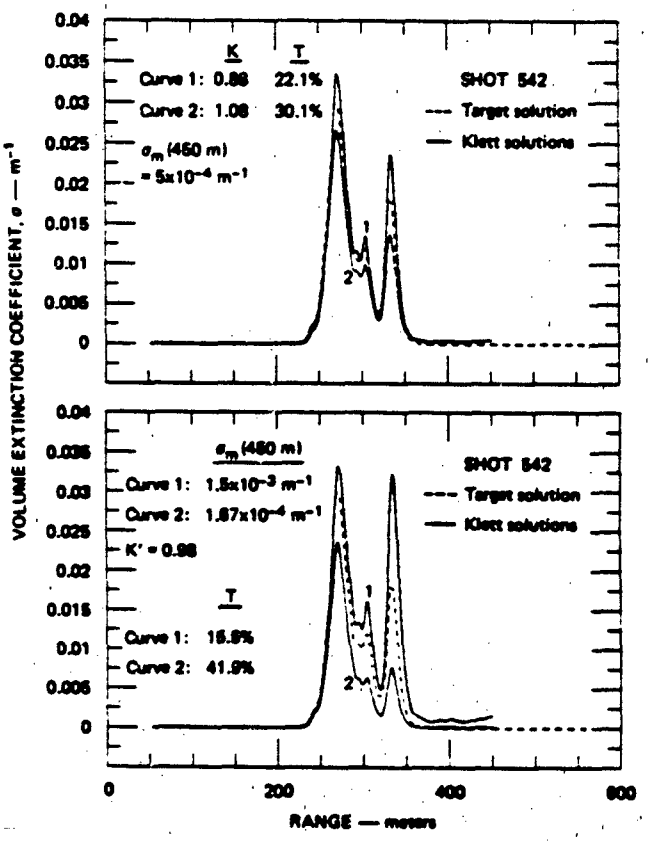

FIGURE 9 EXTINCTION COEFFICIENT PROFILES FOR INCREMENTED VALUES OF K' AND σ_m (LASER SHOT 542)

3. CONCLUSIONS

In this paper, extinction profiles have been derived from lidar data using three different methods. The target method requires a lidar target return for each observation but provides extinction profiles that when range integrated gives transmission data consistent with independent transmissometer observations. The Klett method, also based on the single scattering lidar equation,

can reproduce the extinction profile derived from the target method when appropriate solution parameters are used. However, expected uncertainties in the solution parameters can result in unacceptable errors in the extinction profile. The experimental data method requires a known relationship between optical depth derived from lidar target returns and path-integrated lidar signal derived from aerosol scattering. Extinction-to-backscatter ratios can provide estimates of the needed relationships. This method did not reproduce the extinction profiles of the target or Klett methods--probably because this method includes multiple scattering effects. Before any one method is judged superior, we believe an experiment is needed that is designed to validate lidar analysis methods. Such an experiment will require in situ measurement of aerosol optical and/or physical densities along the propagation path of lidar observations.

ACKNOWLEDGMENTS

This research was funded by the U.S. Army Research Office, Geosciences Division under Contract DAAG29-82-K-0191. The authors thank Dr. Walter Flood of ARO for his suggestions on the conduct of this project.

Norm Nielsen and Steve DeLateur designed and constructed the four-wavelength lidar system and operated the lidar during the SNOW-ONE-B and Smoke Week VI/SNOW TWO field programs.

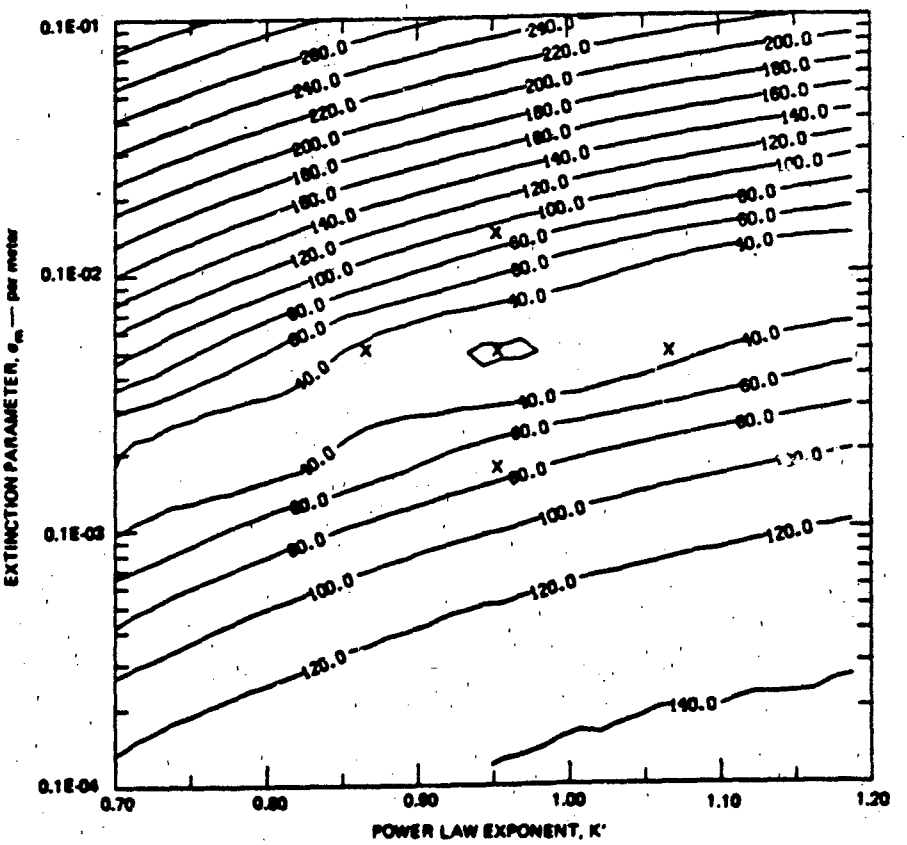

FIGURE 10. CONTOUR PLOT OF KLETT METHOD RMS ERRORS AS A FUNCTION OF THE SOLUTION PARAMETERS K' AND σ_m (LASER SHOT 648).

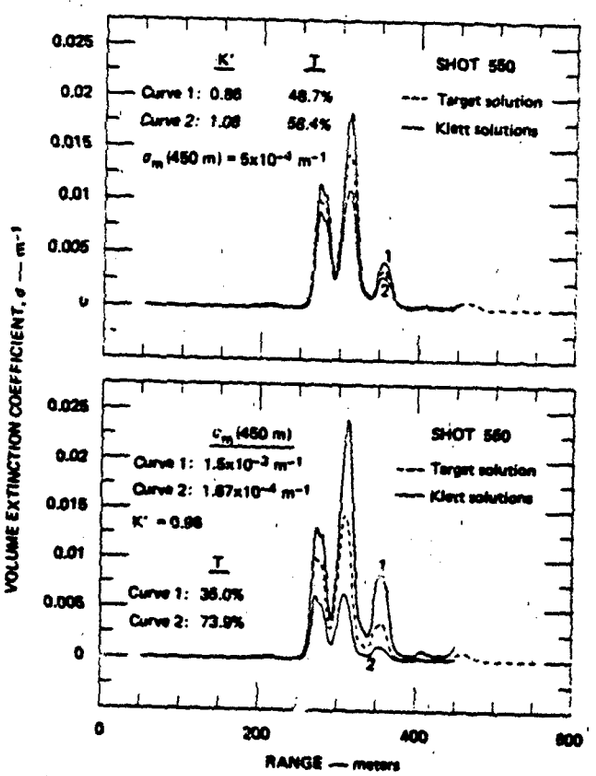

FIGURE 11 EXTINCTION COEFFICIENT PROFILES FOR INCREMENTED VALUES OF K' AND σ_m (LASER SHOT 550)

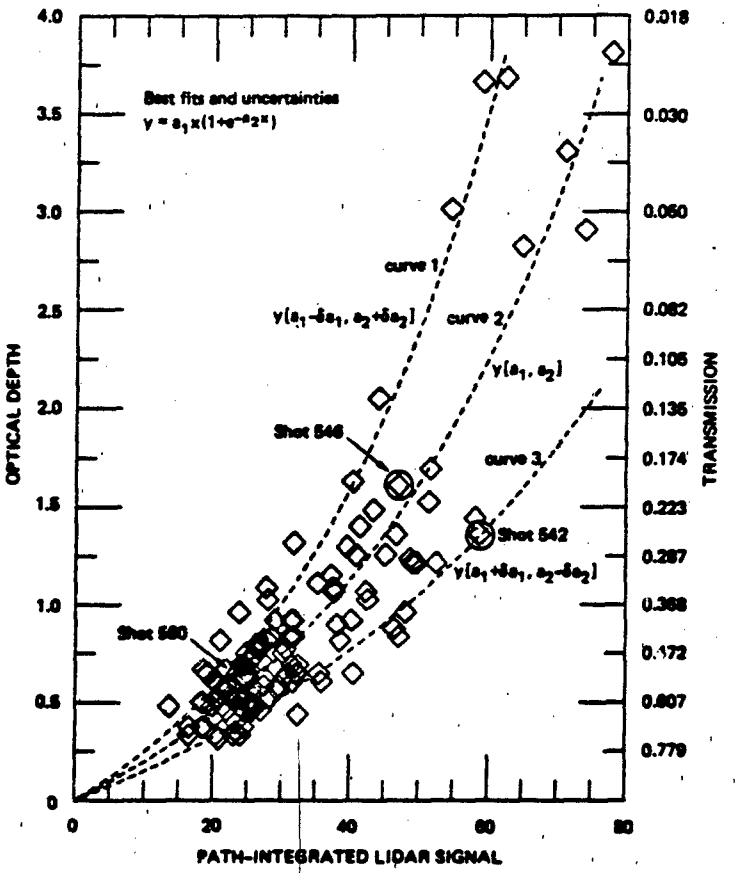

FIGURE 12. PLOT OF OPTICAL DEPTH AGAINST RANGE-INTEGRATED LIDAR SIGNAL FOR DATA COLLECTED DURING SMOKE TEST 218. BEST-FIT AND WORST-CASE MODEL FITS ARE INDICATED.

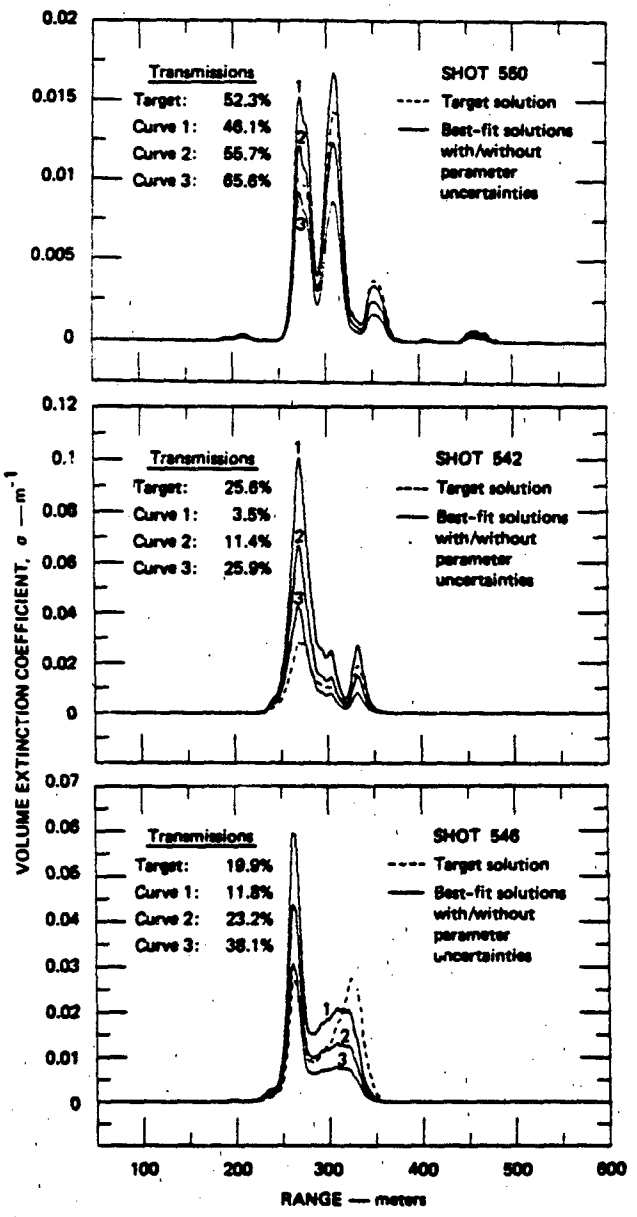

FIGURE 13 EXTINCTION COEFFICIENT PROFILES DERIVED USING EXPERIMENTAL DATA METHOD WITH OPTICAL DEPTH/INTEGRATED LIDAR SIGNAL MODELS PRESENTED IN FIGURE 12

REFERENCES

Bevington, P.R., 1969: Data reduction and error analysis for the Physical Sciences. McGraw-Hill, New York. New York, 188-189, 237-239.

DeLateur, S.A., N.B. Nielsen, E.E. Uthe, and J.M. Livingston, 1984: Four-wavelength lidar measurements from Smoke Week VI/SNOW-TWO. Smoke/Obscurants Symposium VIII, Harry Diamond Laboratories, Adelphi, MD. Proceedings, Project Managers Office for Smoke and Obscurants.

Fernald, F.G., B.M. Herman, and J.A. Reagan, 1972: Determination of aerosol height distribution by lidar. J. Appl. Meteorol., 11, 482-489.

Johnson, W.B. and E.E. Uthe, 1971: Lidar study of the keystone stack plume. Atmos. Environ., 5, 703-724.

Klett, J.D., 1981: Stable analytical inversion solution for processing lidar returns. Appl. Opt., 20, 211-220.

Sasano, Y. and H. Nakane, 1984: Significance of the extinction/backscatter ratio and the boundary value term in the solution for the two-component lidar equation. Appl. Opt., 23, 11-13.

Uthe, E.E., 1981: Lidar evaluation of smoke and dust clouds. Appl. Opt., 20, 1503-1510.

Uthe, E.E., S.A. DeLateur, J.M. Livingston, and N.B. Nielsen, 1983: SNOW-ONE-B multiple-wavelength lidar measurements. Snow Symposium III, Hanover, NH, August 1983. Proceedings, U.S. Army Cold Regions Research and Engineering Laboratory, Hanover, NH.

Viezee, W., E.E. Uthe, and R.T.H. Collis, 1969: Lidar observations of airfield approach conditions: An exploratory study. J. Appl. Meteorol., 8, 274-283.

Appendix C

"FOUR-WAVELENGTH LIDAR MEASUREMENTS FROM SMOKE WEEK VI/SNOW--TWO"

Presented at SMOKE/OBSCURANTS SYMPOSIUM VIII

Presented at
SMOKE/OBSCURANTS SYMPOSIUM V
Harry Diamond Laboratories
Adelphi, MD - 17-19 April 19

UNCLASSIFIED

FOUR-WAVELENGTH LIDAR MEASUREMENTS FROM SMOKE WEEK VI/SNOW-TWO

S.A. DeLateur, N.B. Nielsen,
E.E. Uthe and J.M. Livingston
SRI International
Menlo Park, CA 94025

ABSTRACT (U)

(U) SRI International's four-wavelength lidar system was used to make backscatter and transmission observations at laser wavelengths of 0.53, 1.06, 3.8, and 10.6 μm during the Smoke Week VI/SNOW-TWO field program. Laser pulses were transmitted along a horizontal path terminated at a distance of 600 m from the lidar by a target with uniform reflective properties over the illuminated area. Target returns are interpreted in terms of time-dependent laser energy transmission over the path, and provide the means to interpret lidar backscatter signatures in terms of range-dependent extinction coefficients. Although the data analysis program is in its early stage, an example of the technique is presented. Some results obtained from the SNOW-ONE-B tests are also included.

1. (U) INTRODUCTION

(U) The Smoke Week VI/SNOW-TWO program was conducted by the U.S. Army Smoke/Obscurants PM and CRREL during the 1983-84 winter at Grayling, Michigan. Various optical sensors were used to make propagation measurements through both natural and man-made obscurants. With funding from the U.S. Army Research Office, SRI International participated by making lidar measurements simultaneously at wavelengths of 0.53, 1.06, 3.8, and 10.6 μm.

(U) The objectives of this program were to

- Evaluate transmissions for natural and generated obscurants at DoD laser wavelengths
- Evaluate multiple-scattering effects with multi-wavelength lidar observations
- Interpret multi-wavelength backscatter signatures in terms of aerosol optical and physical densities, and particle characteristics, along the propagation paths
- Derive statistical models describing the spatial and temporal variability of obscurants along propagation paths.

2. (U) MULTIWAVELENGTH LIDAR SYSTEM

(U) The multiwavelength lidar system is installed within a 6-meter long van to facilitate operations at remote sites (Figure 1). Laser pulses are transmitted either vertically or horizontally at

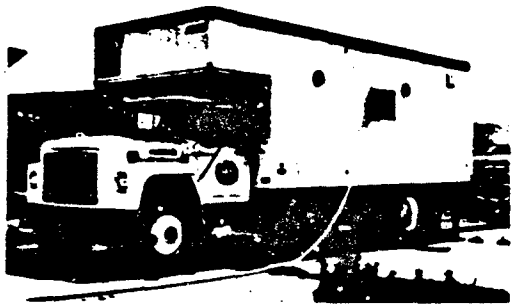

(a) EXTERNAL VIEW SHOWING LASER PORT FOR HORIZONTAL MEASUREMENTS

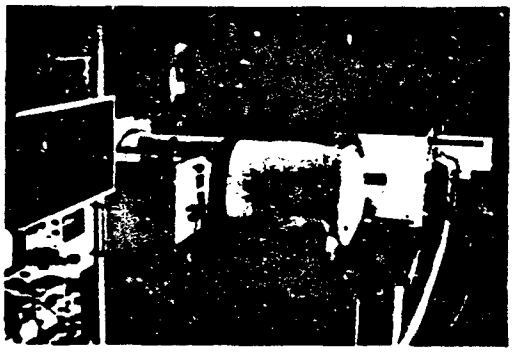

(b) INTERNAL VIEW SHOWING LASER/OPTICS TABLE AND DATA RECORDING SYSTEM

FIGURE 1 FOUR-WAVELENGTH LIDAR SYSTEM IN 6-METER-LONG VAN

wavelengths of 0.53, 1.06, 3.8 and 10.6 μm by using Nd:YAG, DF, and CO_2 lasers. The transmitter optics direct the laser pulses to a common path coaxial with a 12-in Newtonian telescope, as shown in Figure 2. A series of laser pulses at each of the four wavelengths are transmitted sequentially within a 60 μs interval. Therefore, effects of time- and space-varying aerosol distributions on the multi-wavelength lidar measurements are minimized.

(U) Collected energy backscattered from atmospheric targets, and energy reflected from solid targets, is collected within the telescope and directed to appropriate detectors using dichroic filters. Detector outputs are logarithmically amplified and digitized by 8-bit 100-MHz and 12-bit 10-MHz transient recorders. Transient recorder outputs are displayed on an oscilloscope, and are written on magnetic tape under control of an LSI-11 microcomputer system.

(U) The four-wavelength system was first used during the SNOW-ONE-B tests conducted at Grayling, Michigan, during November and December 1983. Data collected showed that greater receiver dynamic range and shorter recovery time from large amplitude

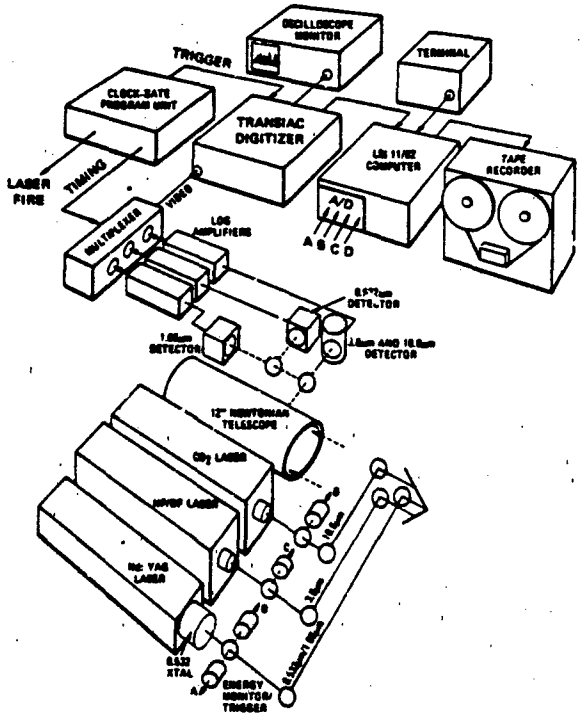

FIGURE 2 BLOCK DIAGRAM OF THE SRI FOUR-WAVELENGTH LIDAR

signals were needed to evaluate dense obscurant distributions along the propagation path. A significant part of our program was directed to improvement of the lidar receivers for application to the Smoke Week VI/SNOW-TWO experiments. New extended-range logarithmic amplifiers were installed on the 0.53 μm and 1.06 μm wavelength channels. The new amplifiers extended the dynamic range from four to six orders of magnitude (i.e., from 40 to 60 dB). Because the detector for the 3.8 and 10.6 μm wavelength channels was the limiting component, a time-gate circuit was added to the detector pre-amplifier so that dense aerosol returns near the lidar could be electrically attenuated, while returns at greater distances could be fully amplified.

(U) In addition to the receiver modifications, the computer-controlled data digitization and components in the computer system were updated. New 8-bit 100-MHz and 12-bit 10-MHz transient recorders were installed within a CAMAC chassis along with the LSI-11 computer. Software was stored on 5-1/4 inch floppy disk units which were also installed within the CAMAC chassis. Therefore, the system was substantially reduced in size while increasing capabilities and improving rejection of RFI noise from laser firings. The Smoke Week VI/SNOW-TWO program was the first test of these new lidar modifications.

3. (U) DATA COLLECTION PROGRAM

(U) The four-wavelength lidar van was transported to Grayling, Michigan, and positioned alongside transmissometer systems operated by the U.S. Army Atmospheric Science Laboratory (ASL) and the U.S. Navy (NRL). A solid lidar target was installed about 600 m distant from the lidar, and near the path-termination hardware for the transmissometer sensors. Therefore, the lidar-target path was nearly parallel and separated by only a few meters from the transmissometer paths.

(U) Lidar observational periods were restricted in duration because of laser eye-safety considerations. Operations were conducted only at times when approval was granted by the field coordinator. Because of these restrictions, only limited lidar calibration data were obtained. The lidar normally operated about five minutes before the start of each obscurant test until five-to-ten minutes after the test start. Unlike lidar operations on the SNOW-ONE tests, laser transmissions at all four wavelengths were allowed. The lidar operational times and obscurants observed are given in Table I.

TABLE I. (U) LIDAR OPERATIONS
Smoke Week VI/SNOW-TWO

TRIAL	DATE	TIME	TAPE	MATERIAL TYPE
101	1/10/84	10:42-10:50	6	Diesel Fuel Generator
102	1/11/84	11:07-11:16	10	Fog Oil Generator
202	1/11/84	11:42-11:55	10	Fog Oil Generator
114	1/11/84	13:58-14:06	11	RP from L8A3
214	1/11/84	14:38-14:46	11	RP from L8A3
203	1/12/84	8:58-9:12	12	IR2 Generator
118	1/12/84	11:35-11:45	12	RP Zuni Rocket
210	1/12/84	12:00-12:24	13	FWP Zuni Rocket
218	1/12/84	14:58-15:11	13	(3) RP Zuni Rockets
107	1/12/84	15:43-15:56	14	Foreign HC Pots
105	1/12/84	16:56-17:02	15	Experimental "C" Generator
122	1/13/84	8:58-19:16	16	Fog Oil Generator in Snow
222	1/13/84	9:28-9:36	16	Fog Oil Generator in Snow
104	1/13/84	13:03-13:11	17	IR2 + Fog Oil Generator
204	1/13/84	13:21-13:30	17	IR2 + Fog Oil Generator
116	1/13/84	14:24-14:31	18	Simulated 155mm HE
310	1/13/84	15:03-15:22	18	(3) FWP Zuni Rockets
418	1/13/84	15:53-16:06	19	(3) RP Zuni Rockets
111	1/13/84	16:49-17:02	19	WP LUST
216	1/14/84	9:04-9:10	20	Simulated 155mm HE
213	1/14/84	9:52-10:01	20	IR2 XM76
125	1/16/84	8:39-9:14	21	Experimental "C" Generator
128	1/16/84	12:30-12:47	22	Foreign Pots
302	1/16/84	13:45-13:55	23	Fog Oil Generator
316	1/16/84	16:30-16:42	23	Simulated 155mm HE

4. (U) DATA RECORDS

(U) A four-wavelength backscatter digital record is shown in Figure 3. The transient recorder is initiated just prior to the first laser firing, and digitizes continuously at 10 ns (1.5m) intervals for about 60 μs. The time period between the 0.53 μm / 1.06 μm wavelength data is determined by the separation time between two laser pulses derived from the same flash lamp excitation of the Nd:YAG laser. A relatively long period was used between the 3.8 μm and 10.6 μm laser firings as the same detector is used, and ample time is needed for detector stabilization after observing the large amplitude 3.8 μm target return. Figure 3 shows that the 1.5 m (100-MHz) resolution of the 8-bit digitizer provides valid target amplitude signals at all wavelengths. The 15-m resolution (10-MHz) of the 12-bit digitizer did

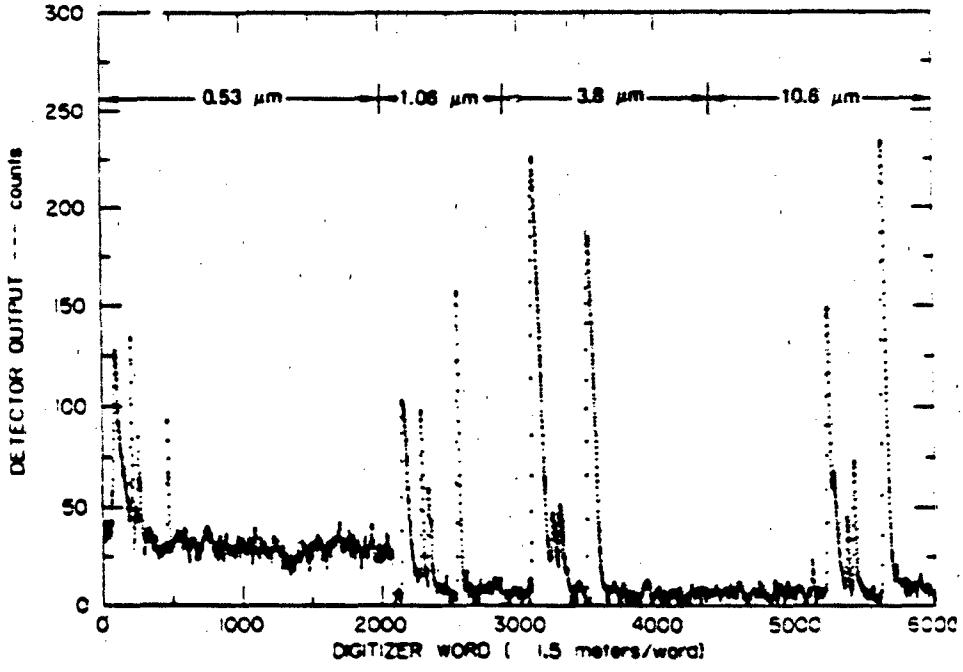

FIGURE 3 DIGITAL BACKSCATTER SIGNATURE RECORDED USING THE FOUR-WAVELENGTH LIDAR

not provide suitable target amplitude data at 0.53 μm and 1.06 μm. Accordingly, the 8-bit 100-MHz data recordings are being used on the data analysis program.

(U) The four-wavelength backscatter signature stored within the transient recorder memory (Figure 3) can be used to generate individual wavelength backscatter signatures on the display oscilloscope (see Figure 2). Figure 4 presents oscilloscope displays for clear air conditions on 13 January. The initial signal rise is a result of the convergence of the transmitted pulse with the receiver field of view. The clear-air range-resolved signal falls off as inverse range-squared. The target return is 600 m from the lidar position. The return at about 300 m results from a guy wire used to support the meteorological tower. The guy wire was installed after lidar-target positioning and just before the Smoke Week VI series of tests. Wire and target returns provide information on pulse shape at each laser wavelength. The shortest laser pulse duration is at 0.53 μm followed by the 1.06, 10.6 and 3.8 μm wavelength pulses.

(U) Because the clear-air scattering decreases with increasing wavelength while the target returns remain relatively constant with wavelength, the target-to-clear air ratio increases with wavelength as shown on the 0.53 and 1.06 μm wavelength signatures. Clear air scattering at 3.8 and 10.6 μm is observed only at short ranges. Therefore, observation of clear air scattering and target returns requires a

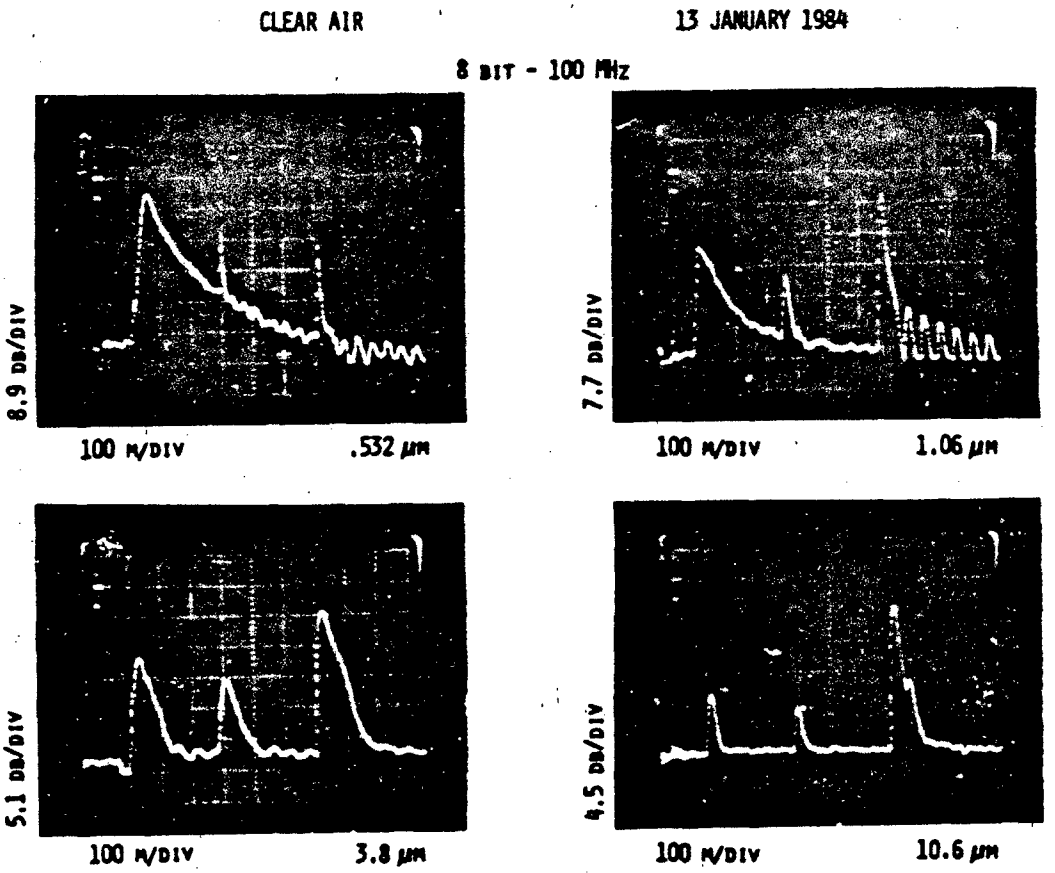

FIGURE 4 LIDAR BACKSCATTER SIGNATURES AT 0.53, 3.8 and 10.6 μm FOR CLEAR AIR CONDITIONS

greater receiver dynamic range at longer wavelengths. As discussed in Section 2, the dynamic range of the 0.53 and 1.06 μm wavelength receivers was increased by adding extended dynamic range (60dB) logarithmic amplifiers. A preamplifier gating circuit was installed to improve the dynamic range of the 3.8 and 10.6 μm wavelength receivers. The extended dynamic range amplifiers at 0.53 and 1.06 μm performed as expected. However, the gating circuit for 3.8 and 10.6 μm was designed for use with a specific detector. This detector failed during the field program, and was replaced. When used with the replaced detector, the gating introduced a transient noise that interfered with the target return. Therefore, the gating was not used on the Smoke Week VI/SNOW-TWO tests. Rather, optical filters were used on the 3.8 and 10.6 μm wavelength systems to prevent target and dense aerosol saturation of receiver electronics. As a consequence, low-level clear-air scattering normally was not observed.

(U) Figure 5 presents individual wavelength backscatter signatures recorded during a light snowfall. A 3dB optical filter was added to the 0.53 μm and 1.06 μm wavelength receivers to prevent receiver saturation by the large amplitude returns from the snow near the lidar van. Range-resolved snow returns are observed almost to the target with the 3.8 μm and 10.6 μm lidar wavelengths.

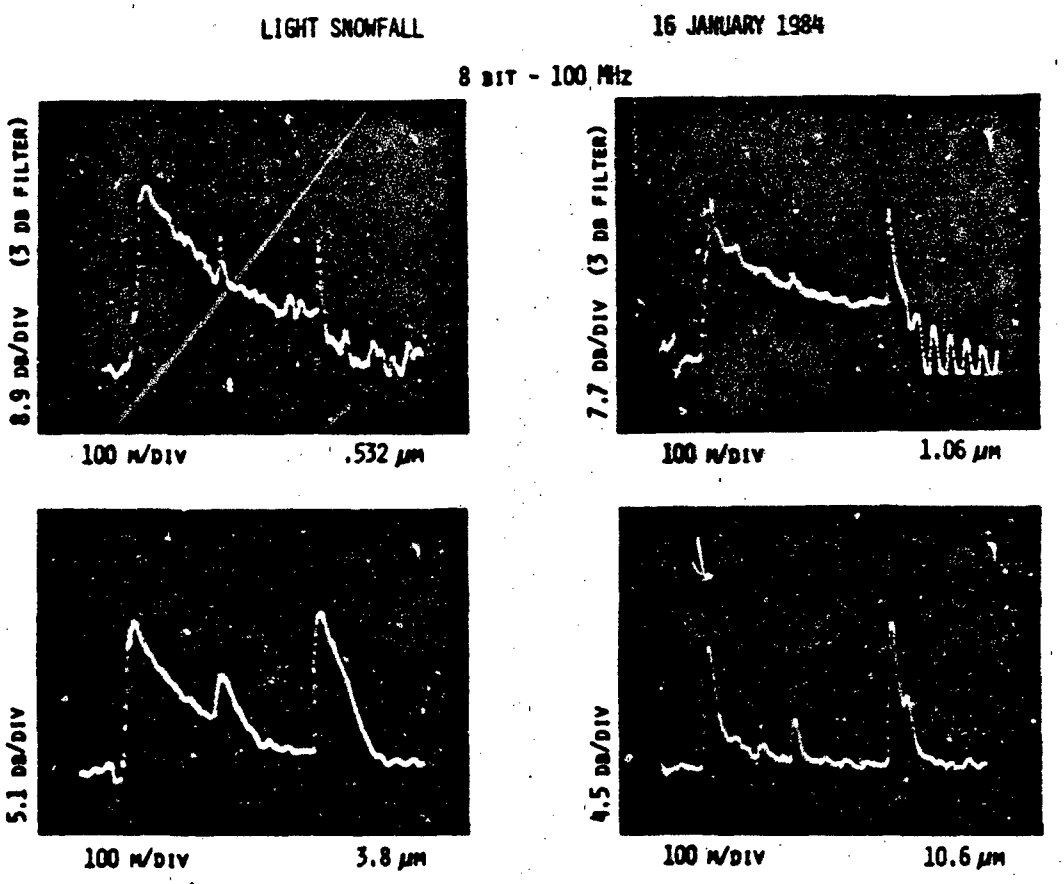

FIGURE 5 LIDAR BACKSCATTER SIGNATURES AT 0.53, 1.06, 3.8, and 10.6 μm FOR LIGHT SNOWFALL CONDITIONS

(U) Figure 6 presents oscilloscope-photographed lidar backscatter signatures that were recorded near the end of Trial 310 (2+9 min). The smoke event was generated by three white phosphorous rockets. The lidar returns from the relatively tenuous smoke are of greater amplitude than the target return. Also, the patchy smoke structure results in 0.53 μm wavelength smoke returns that are nearly identical in shape to the target returns. As the laser pulse duration increases (as for the longer wavelengths), the smoke patches are spatially averaged, and the resulting smoke returns are easily identifiable from target returns. (In addition, it can be noted that the guy wire returns in Figure 6 are more difficult to separate from the smoke returns for the longer pulse systems.)

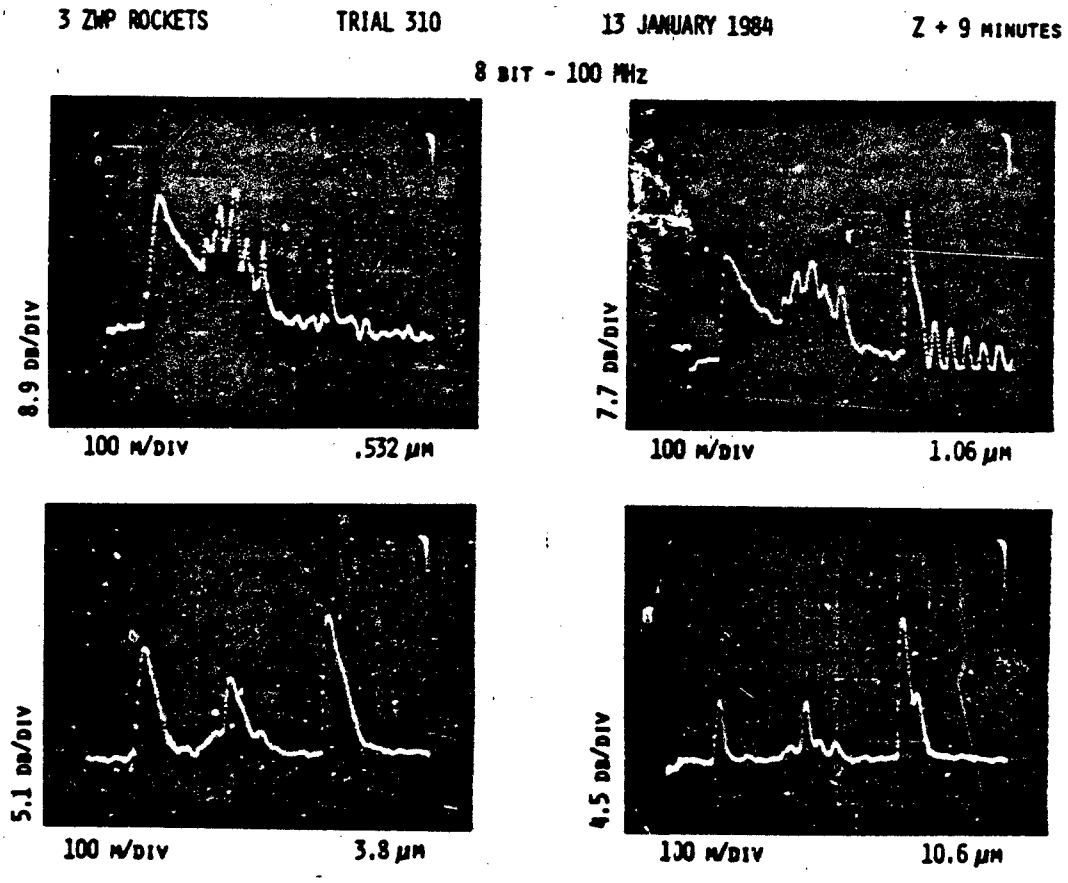

FIGURE 8 LIDAR BACKSCATTER SIGNATURES AT 0.53, 1.06, 3.8 and 10.6 μm FOR WHITE PHOSPHOROUS SMOKE AT Z + 9 MINUTES OF TRIAL 310

(U) The four-wavelength backscatter signatures stored on magnetic tape can be processed as intensity modulated displays which illustrate the time and space variability of smoke and target lidar returns occurring during a smoke trial. Figure 7 presents such a display for data collected during Trial 218 on 12 January 1984. The smoke event was generated by three red phosphorous Zuni rockets. Figure 7 indicates that the smoke completely obscured the target at all four lidar-wavelengths. However, the target was again observed within a half-minute at the 1.06 μm, 3.8 μm, and 10.6 μm wavelengths. The target was obscured for about 2 minutes at 0.53 μm. Detailed structure of the smoke dispersion is observed at 0.53 and 1.06 μm but not at 3.8 and 10.6 μm because of longer pulse lengths and lower detector bandwidths of the far infrared systems.

(U) Figure 8 presents an intensity modulated display for Trial 128 conducted on 16 January 1984. Smoke from foreign pots was very effective in obscuring the target at 0.53 and 1.06 μm, but not at

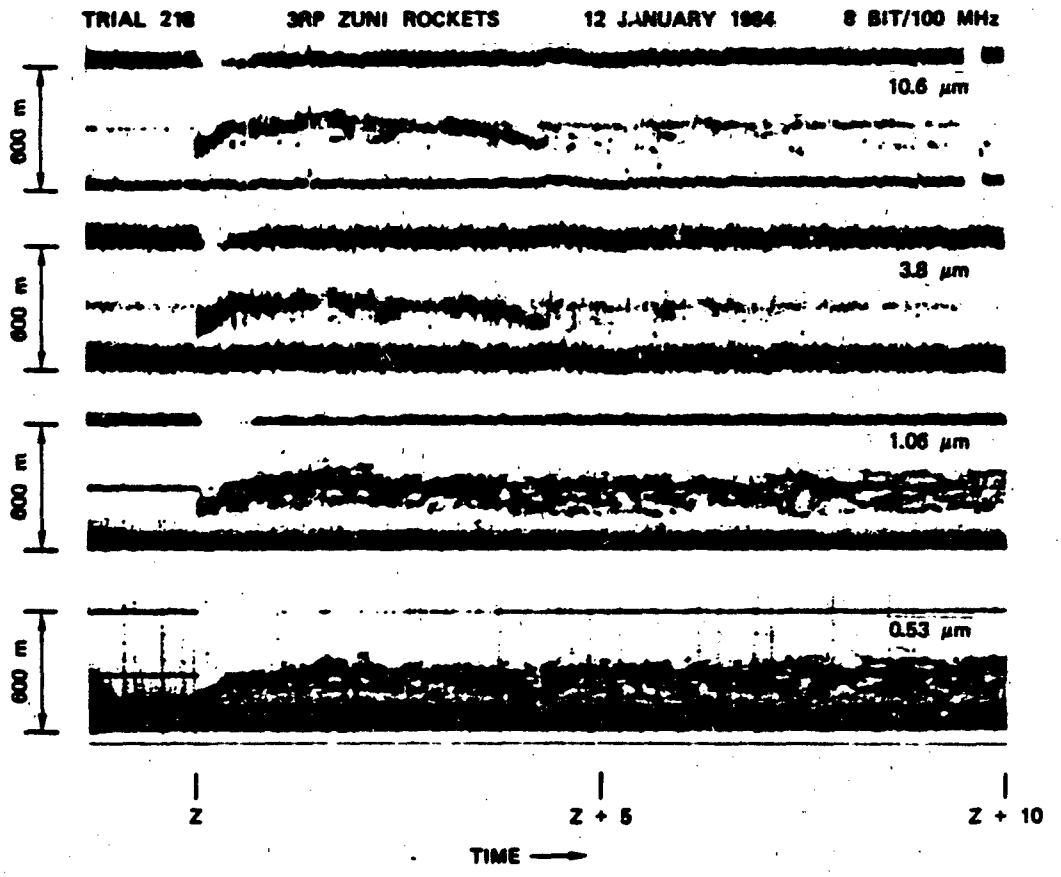

FIGURE 7 RANGE/TIME INTENSITY MODULATED DISPLAY GENERATED FROM FOUR-WAVELENGTH LIDAR BACKSCATTER SIGNATURES COLLECTED DURING TRIAL 218

3.8 μm and 10.6 μm. Because of the large attenuation at 0.53 μm and 1.06 μm, structure of the internal plume is not observed. For this case, plume structure is best determined from the longer wavelength systems even though they are limited in spatial resolution.

4. (U) EXPERIMENTAL RESULTS

(U) The analysis program was in its early stages at the time this paper was written. Therefore, only preliminary data will be presented here, and final results will be published elsewhere. Also some results obtained from the SNOW-ONE-B program are used to illustrate analysis methods not yet applied to the Smoke Week VI/SNOW-TWO data base.

(U) The first task of the analysis program was to evaluate the response of the lidar receiver from calibration data collected during the Smoke Week VI/SNOW-TWO period. Receiver calibration consisted of inserting optical filters of known attenuation in front of the detector, and of making lidar observations. The decrease in target returns introduced by the optical filter provides a measurement of the response of the lidar receiver in terms of the number of digitizer counts per dB of attenuation. In practice, three filters of different attenuation were used to evaluate linearity and response over the dynamic range of the receiver. The response factors then are used to correct backscatter signatures in terms of relative light input into the lidar receiver. Pulse-to-pulse transmit energy variations were recorded and these data were used to normalize the backscatter signatures to a constant transmit level.

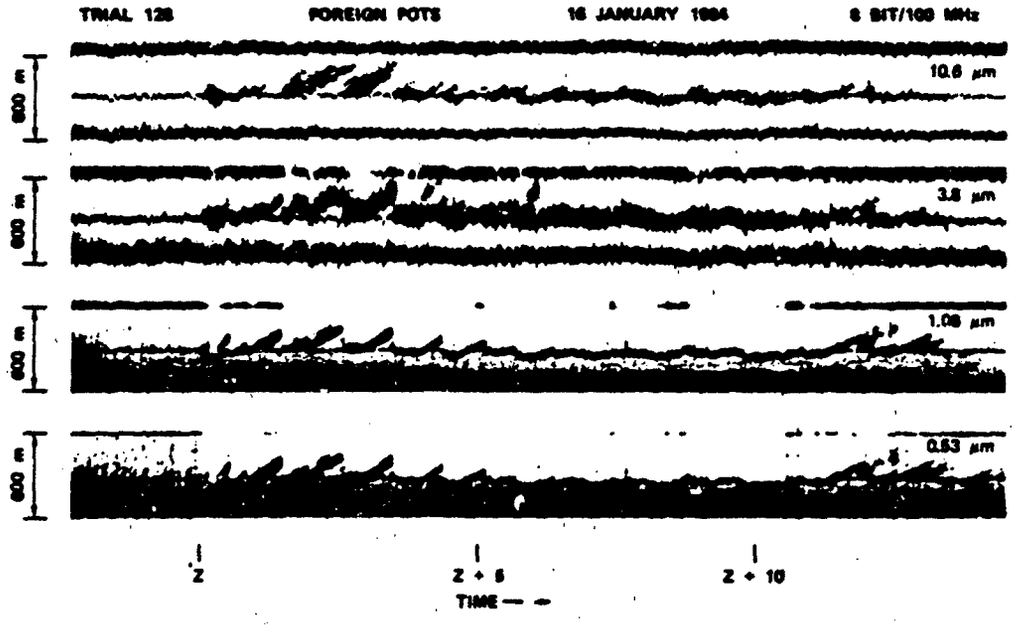

FIGURE 8 RANGE/TIME INTENSITY MODULATED DISPLAY GENERATED FROM FOUR-WAVELENGTH LIDAR BACKSCATTER SIGNATURES COLLECTED DURING TRIAL 128

(U) Lidar data collected during the SNOW-ONE-8 tests showed that the target returns could be interpreted in terms of transmission that agreed well with transmissions measured by two-ended transmissometer systems (Uthe et al., 1983). For example, Figure 9 presents lidar and NRL transmissometer records obtained at a wavelength of 1.06 μm during an IR screener smoke event conducted on 8 December

1982. Excellent agreement is obtained, although the two observational paths were separated by about 3m in the horizontal. Therefore, the lidar/target transmission values are considered valid, and can be used to validate various methods for interpreting aerosol backscatter signatures in terms of optical density.

(U) Figure 10 presents an example of four-wavelength lidar-evaluated transmissions for the Smoke Week VI Trial 218 (see Figure 7). The smoke event was generated by three red-phosphorous rockets. The pre-event target returns are used to normalize the transmission evaluations to 100%. Fluctuations in the 0.53 μm wavelength may be the result of digitizer errors for large amplitude (target) signals. However, the fluctuations are not a problem at lower transmission values (e.g., small target returns). Figure 10 shows that the attenuation at 0.53 μm is over two times greater than at 1.06 μm. Attenuation at 3.8 μm and 10.6 μm is only about one-four of that at 1.06 μm. The relatively little data-point scatter in the optical depth plots indicates that space and time variations of the obscurant cloud did not effect the sequential multiple-wavelength laser transmissions. Also, the wavelength dependence remained relatively constant during the test, indicating that particle sizes, shapes, and compositions also remain relatively constant. Lower attenuation than expected at 1.06 μm for large optical depths can be explained by multiple-scattering, as discussed later in this paper.

(U) Analysis of lidar backscatter signatures in terms of aerosol optical density along the propagation path normally begins by assuming the volume extinction coefficient σ is related to the volume backscatter coefficient β by the expression $\sigma = k\beta$. Then, the range-corrected single-scattering lidar equation $P(R) = C\beta(R) \exp\left[-2\int\sigma(R)dR\right]$ can be analytically solved for $\sigma(R)$ when k and a boundary value of σ at range R_0 are known (Klett, 1981; Viezee et al., 1969). However, the single scattering assumption is not valid for large optical depths; and, therefore, this technique may be of little use for evaluating dense

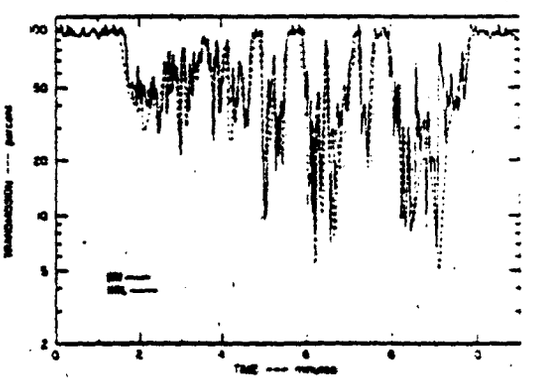

FIGURE 9 COMPARISON OF TRANSMISSION HISTORIES MEASURED BY THE 1.06 μm SRI LIDAR AND THE NRL TRANSMISSOMETER FOR IR SCREENER SMOKE EVENT ON 8 DECEMBER 1982

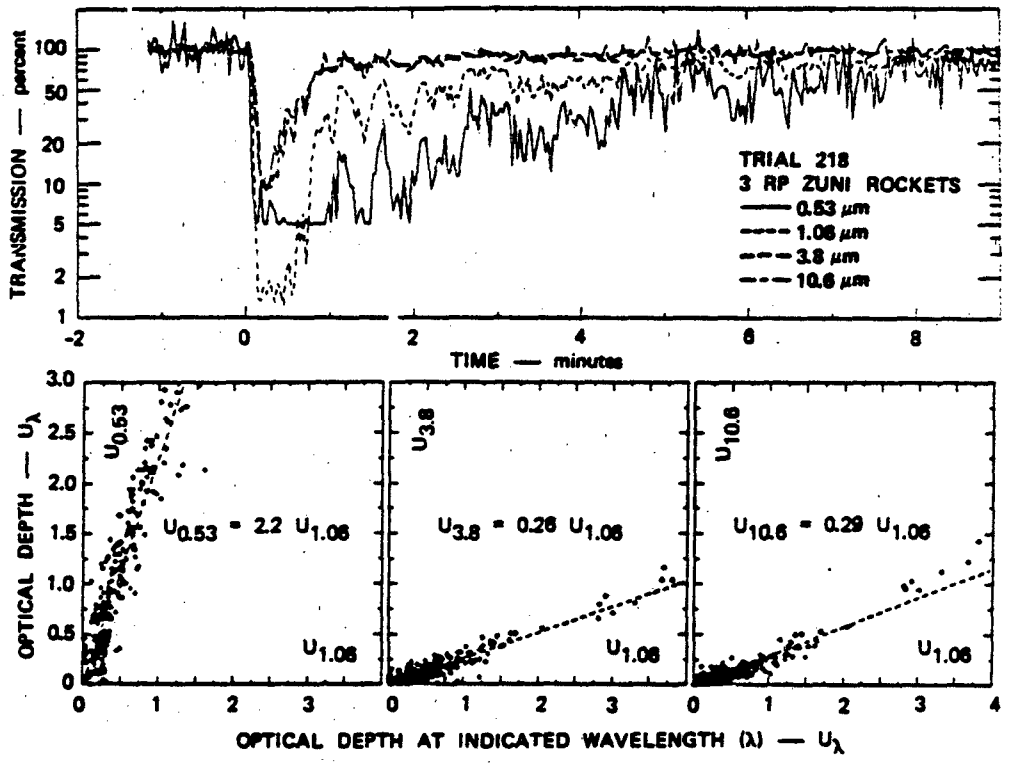

FIGURE 10 TRANSMISSION HISTORY AND OPTICAL DEPTH RELATIONSHIPS FOR SMOKE GENERATED DURING TRIAL 218 (3 RP ZUNI ROCKETS)

obscurants. The $\sigma = k\beta$ relationship can be investigated by relating target-evaluated optical depth $U = -\ln T = \int \sigma dR$ to path-integrated lidar signal $\int P dR$. For small U, $k = \sigma/\beta$ can be evaluated from a calibrated lidar. The relationship of optical depth-to-integrated lidar return includes effects of attenuation and multiple scattering, and therefore, may be useful for interpreting single-ended lidar observations in terms of transmission of laser energy through dense obscurant events. However, previous results (Uthe, 1981) have shown relatively large data point scatter between U and $\int P dR$. This may be a result of experimental errors associated with lidar receivers of limited dynamic range and bandwidth, and was a major reason for extending the dynamic range and response of the four-wavelength lidar receivers (see Section 2).

(U) Figure 11 presents 1.06 μm wavelength optical depths plotted against 1.06 μm path-integrated lidar signals for data collected during Trial 218. Although the guy wire introduces additional uncertainty in the integrated backscatter values, the data point scatter is less than that observed in previous studies. This indicates that improving the dynamic range and response of the lidar receiver

has improved the relationship of the lidar signal to optical density terms. At low optical depth values, a near linear relationship is obtained, indicating that the $\sigma = k\beta$ relationship is valid. At large optical depths, less lidar signal is observed because of the attenuation.

(U) Another method is being investigated for providing profiles of extinction coefficients. We assume that the maximum target return results from non-scattered and near-forward scattered light. Other multiply-scattered light incident on the target arrives later than the non-scattered and forward-scattered light. Therefore, the lidar target-derived extinction coefficient (e.g., transmission) is representative of small-angle multiple-scattering (i.e., the single-scattering coefficient σ_s is reduced by the forward-scattering):

$$\sigma_m = \sigma_s - \int_{\text{forward direction}} \beta(\theta)\, d\omega$$

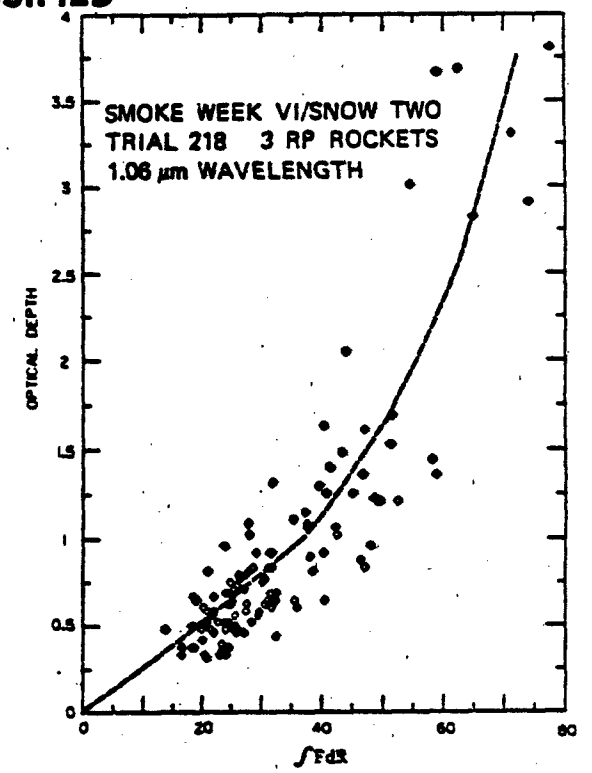

FIGURE 11 OPTICAL DEPTH-TO-PATH-INTEGRATED LIDAR SIGNAL RELATIONSHIP DERIVED FROM 1.06 μm WAVELENGTH LIDAR SIGNATURES RECORDED DURING TRIAL 218

If the scattering particles are of small size, the forward-scattering term is small and $\sigma_m \approx \sigma_s$ for target evaluated transmission, even for dense obscurants. When the scattering particles are large (>10 μm), the forward-scattering term at shorter wavelengths is large and effectively increases lidar-derived transmissions. Transmissometer values may be increased even more if receiver aperture sizes are larger than those used for the lidar. Therefore, larger lidar-observed transmissions are expected at shorter wavelengths for obscurants with large particle sizes. This is illustrated in Figure 12 for data collected during a snowfall at the SNOW-ONE-B program. Attenuation at 10.6 μm is about 80% greater (e.g., smaller transmissions) than attenuation at 1.06 μm. Longer wavelength systems designed to better penetrate smoke obscurants may be less effective in penetrating snowfall.

(U) The single-scattering lidar equation can be solved in terms of the single constant $\frac{k}{C}$ (after Fernald et al., 1972):

$$\frac{k}{C} = \left[1 - T^2\right]\left[2\int_0^{R_t} P(R)dR\right]^{-1}$$

where T is the target-evaluated transmission, and R_t is the range to the target. Then $\frac{k}{C}$ can be used with the path-integrated range-corrected lidar signal $\int_0^R P(R)dR$, and the solution equation, to evaluate

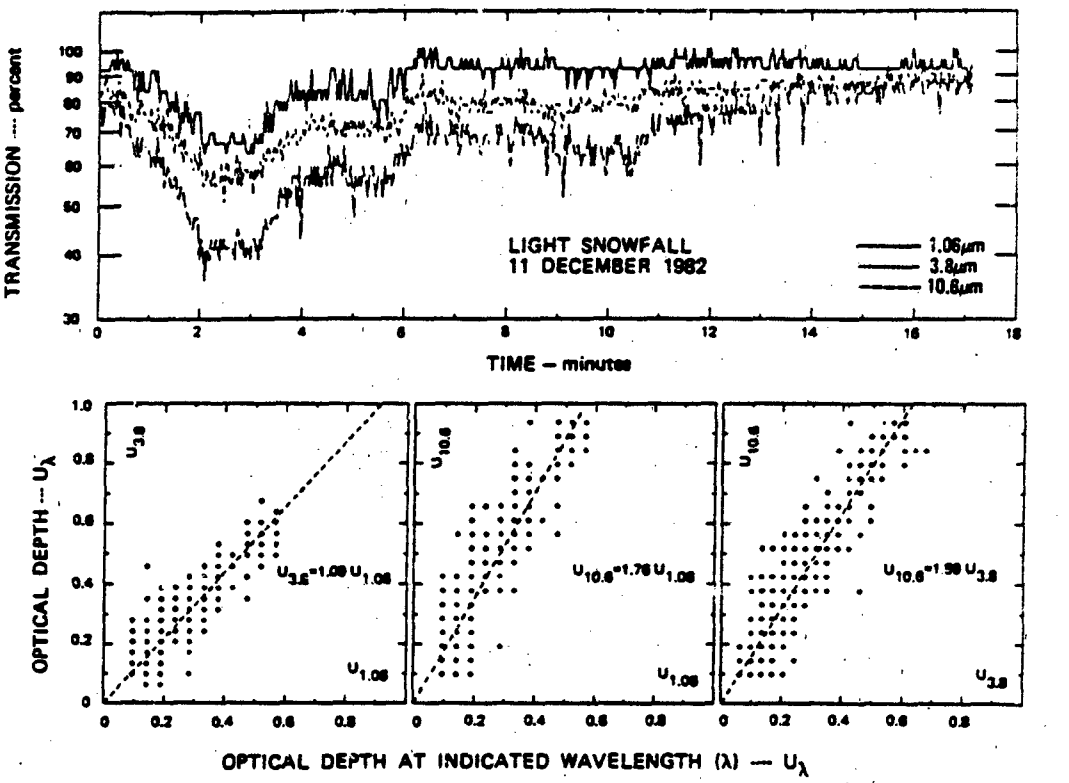

FIGURE 12 TRANSMISSION HISTORY AND OPTICAL DEPTH RELATIONSHIPS FOR LIGHT SNOWFALL AT 0100 ON 11 DECEMBER 1982

optical depth (or extinction) to range R. Because the lidar target evaluated transmissions are used to determine $\frac{k}{c}$, the solution provides range-resolved optical parameters that include approximate multiple-scattering effects. An example of range-resolved optical depth and transmission at 1.06 μm is presented in Figure 13 for Z+63 seconds of Trial 218. The resulting extinction coefficient profile is presented in Figure 14. The lidar solution greatly amplified the optical density of the far side of the obscurant cloud, as viewed from the lidar.

(U) Another objective of this study was to investigate methods of describing spatial and temporal variability of obscurant densities along propagation paths. One method is illustrated in Figure 15. The lidar transmission record presented in Figure 9 (IR Screener Smoke — 1.06 μm wavelength) was used to compute the number and duration of smoke 'holes.' A hole occurs when the transmission becomes greater than a specified (threshold) transmission value, and then later becomes less than the specified value. Figure 15 shows that the number of holes is greatest at 50% transmission. However, duration of the holes is greatest for lower transmission values. Similar analysis has been conducted for transmission 'patches.' These results provide a measure of obscurant effectiveness at DoD laser wavelengths. Ludwig

et al. (1984 — in this proceedings) are examining lidar two-dimensional cross sections of smoke events to describe the spatial distribution of smoke and clear air parcels.

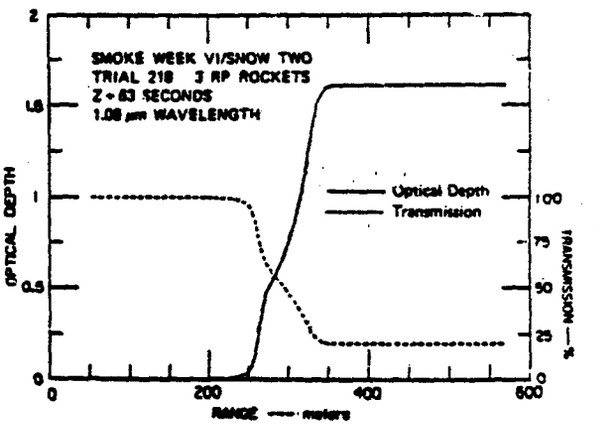

FIGURE 13 RANGE-RESOLVED OPTICAL DEPTH AND TRANSMISSION (1.06 μm) ALONG THE OPTICAL PATH AT Z + 63 SECONDS OF TRIAL 218

5. (U) CONCLUSIONS

(U) Lidar is the best method to remotely observe the spatial and temporal distribution of obscurant clouds. Although lidar also provides a method to remotely evaluate aerosol densities and particle characteristics, the technique is limited by receiver dynamic range and bandwidth, and by uncertainties in various analysis techniques. For dense obscurants, multiple-scattering affects are important, and analytical solutions to the single scattering lidar equation normally are not appropriate and other methods must be used.

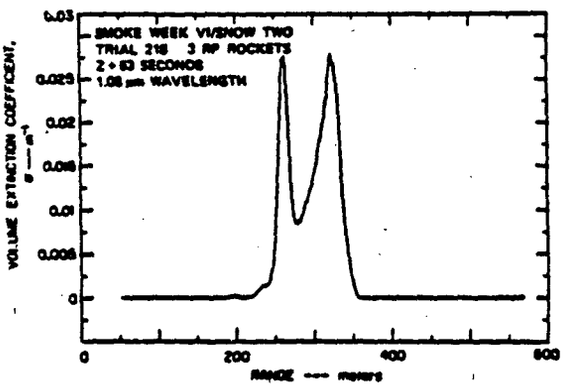

FIGURE 14 RANGE-RESOLVED VOLUME EXTINCTION COEFFICIENT (1.06 μm) ALONG THE OPTICAL PATH AT Z + 63 SECONDS OF TRIAL 218

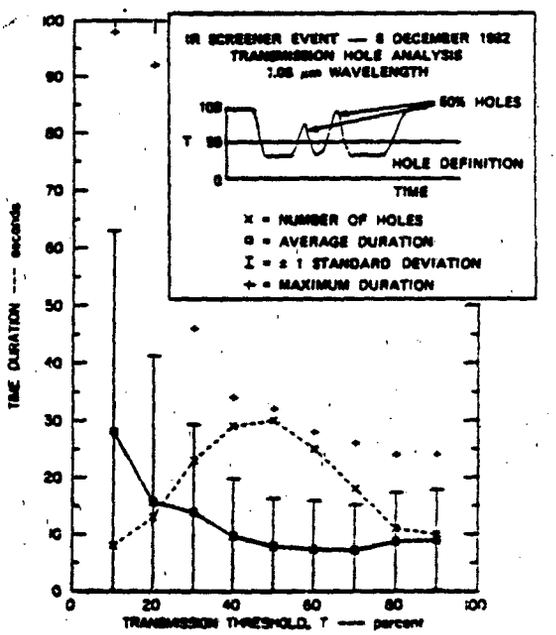

FIGURE 15 NUMBER AND DURATION OF HOLES AT A WAVELENGTH OF 1.0 μm FOR AN IR SCREENER SMOKE EVENT OF SNOW-ONE-8

(U) This paper presents two methods to provide useful information on the density of obscurant clouds. However, one of the methods relies on the use of a target to evaluate the extinction-to-backscatter ratio and lidar-calibration constant. The other method requires a target to derive an integrated lidar signal-to-optical depth relationship, and assumes this relationship is characteristic of the same smoke type so that it can be applied to similar smoke events. Both methods can be used to evaluate optical density along the propagation path. The target methods would be particularly useful in the case of a downward-viewing airborne lidar where the ground surface provides a target return, and the system can make observations over large regional areas, or track smoke clouds to greater downwind distances. This technique already has been used to make vertical transmission measurements of forest fire smoke at 0.53 μm and 1.06 μm (Uthe et al., 1982). Of course, if $\frac{k}{C}$ is determined to be a constant, single-ended measurements of optical density are feasible.

(U) The data analysis program is continuing with support from the Army Research Office, Geosciences Division, and final results will be presented in the near future. Results already obtained have shown the importance of lidar receiver dynamic range and response for making quantitative density measurements along propagation paths.

6. (U) REFERENCES

Fernald, F.G., B.M. Herman, and J.A. Reagan, 1972: Determination of Aerosol Height Distributions by Lidar. J. Applied Meteorology, 11, 482-489.

Ludwig, F.L., K.C. Nitz and A. Valdes, 1984: Techniques for Studying the Spatial Distribution of Clear Patches in Smoke Plumes (U). Smoke/Obscurants Symposium VIII, Harry Diamond Laboratories, Adelphi, MD, 17-19 April 1984.

Uthe, E.E., S.A. DeLateur, J. Livingston and N.B. Nielsen, 1983: SNOW-ONE-B Multiple-Wavelength Lidar Measurements. Snow Symposium III, Hanover, New Hampshire, August 1983. U.S. Army Cold Regions Research and Engineering Laboratory, Hanover, New Hampshire.

Uthe, E.E., B.M. Morley, and N.B. Nielsen, 1982: Airborne Lidar Measurements of Smoke Plume Distribution, Vertical Transmission, and Particle Size. Applied Optics, 21, 460-463.

Uthe, E.E., 1981: Lidar Evaluation of Smoke and Dust Clouds. Applied Optics, 20, 1503-1510.

Appendix D

"SNOW-ONE-B MULTIPLE-WAVELENGTH LIDAR MEASUREMENTS"

Presented at SNOW SYMPOSIUM III

(U) SNOW-ONE-B MULTIPLE-WAVELENGTH LIDAR MEASUREMENTS

Edward E. Uthe, SRI International
Stephen A. DeLateur, SRI International
John Livingston, SRI International
Norman B. Nielsen, SRI International

(U) ABSTRACT

(U) Lidar observations of natural and generated obscurants were made during the SNOW-ONE-B field program. Laser pulses at infrared wavelengths of 1.06 μm, 3.8 μm, and 10.6 μm were transmitted along a common path terminated by a passive reflector located about 600 m from the lidar. Each pulse set (30 sets/minute) was transmitted within a 150-μs time interval. Laser energy backscattered by aerosols and reflected by the target was collected within a 12-inch telescope and optically directed to appropriate detectors. Resulting range-dependent lidar signals were logarithmically amplified, digitized at a 3-m resolution, and stored on magnetic tape for subsequent analysis.

(U) Analysis examples are presented illustrating the evaluation of the time history of transmission based on observed target returns. High correlations between optical depths at different wavelengths indicate that time and space variation of aerosol concentrations have little effect on a pulse set. Linear relationships between the optical depths indicate that multiple scattering effects are minimal. Slopes of the linear relationships provide estimates of the relative effectiveness of the obscurant at each wavelength.

(U) Lidar transmission histories are compared to transmissometer values, and are analyzed in terms of the total time for which transmission was less than any specified value. The data is described in terms of transmission holes and patches. In addition, preliminary backscatter analyses are presented.

(U) INTRODUCTION

(U) SNOW-ONE-B was part of a field test series conducted by the U.S. Army Cold Regions Research and Engineering Laboratory (CRREL) to determine the effects of natural and man-made obscurants on ultraviolet through millimeter-wave propagation in winter environments. The SNOW-ONE-B tests were conducted at Grayling, Michigan, during November and December 1983. The tests included electromagnetic propagation, aerosol characterization, and meteorological data collection.

(U) Under sponsorship of the U.S. Army Research Office (ARO), SRI International participated in the SNOW-ONE-B field program by making multiple-wavelength lidar measurements of backscatter and attenuation of aerosol clouds at laser wavelengths of 1.06 μm, 3.8 μm, and 10.6 μm. This paper presents first results from analysis of the SNOW-ONE-B lidar records. The analysis program is continuing.

(U) MULTIWAVELENGTH LIDAR SYSTEM

(U) The SNOW-ONE-B experiment was the first application of a new multiple-wavelength van-mounted lidar system especially designed for remote characterization of aerosol densities and particle

characteristics. As shown in Figure 1, the lidar can transmit laser pulses at four wavelengths: 0.53 μm and 1.06 μm using a Nd:YAG laser that includes a doubling crystal, 3.8 μm using a DF laser, and 10.6 μm using a CO_2 laser. The lasers pulse at each wavelength sequentially and transmit into the atmosphere within a 150-μs interval. This is achieved by double pulsing the Nd:YAG laser during a single flash-lamp excitation. The laser pulses are directed along a path coaxial with a 12-in Newtonian telescope. Collected backscattered energy is directed to an appropriate detector, and the detector outputs are logarithmically amplified. A multiplexer circuit provides a single-channel

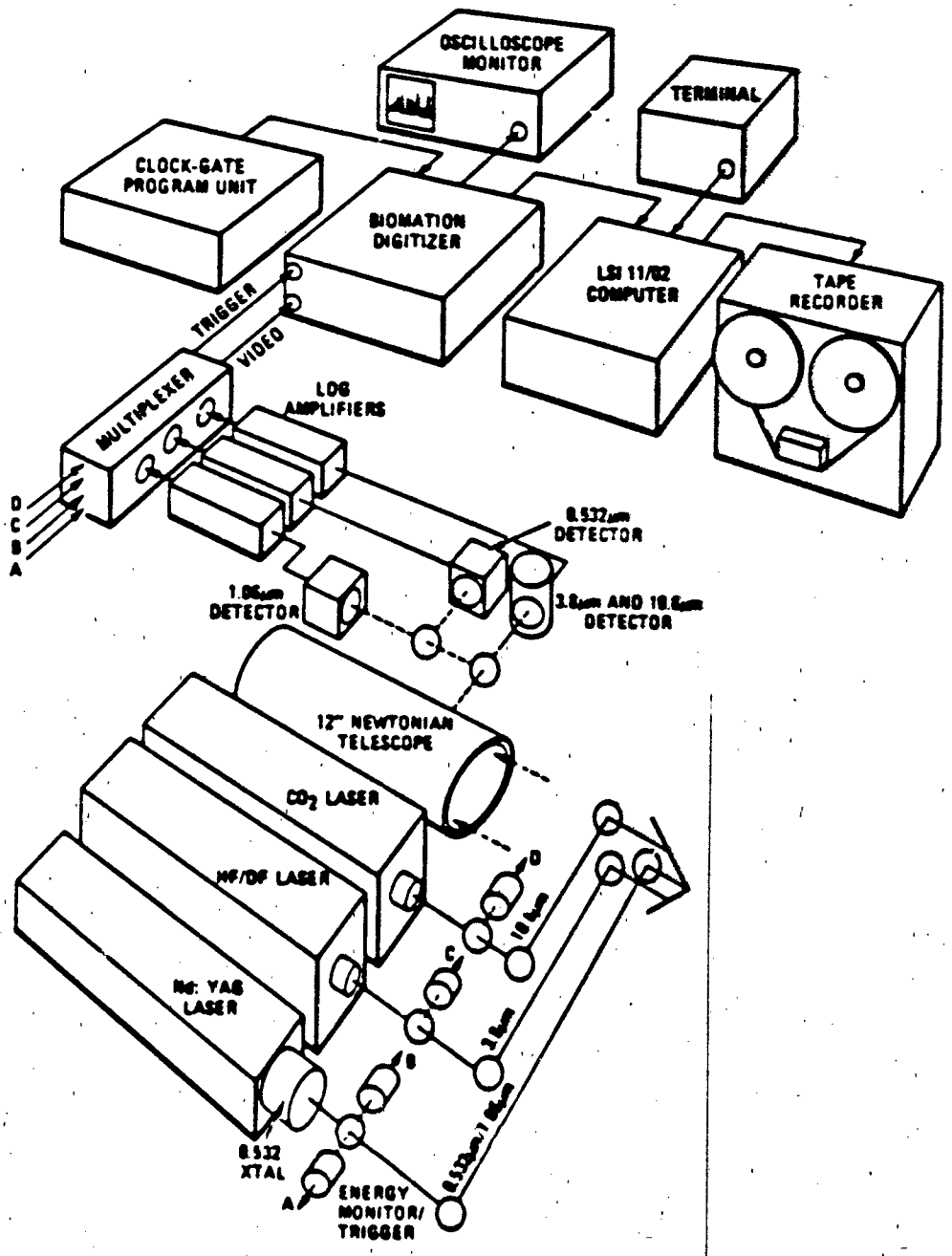

Figure 1 Block Diagram of the Four-Wavelength Lidar System for Remote Aerosol Measurement

waveform consisting of the output of four energy monitors (pyroelectric detectors) in addition to the four backscatter signatures. Therefore, a single transient recorder (Biomation 8100) can be used to digitize the lidar records. A clock-gate program unit provides for transient recorder interrupts. Data for each pulse set is contained in the 2048 8-bit Biomation memory. A sample rate of 20 ns (3-m resolution) is typically used, and 30 pulse sets can be transmitted each minute of operation. The digital record for each pulse set is transferred to a Digital Equipment Corp. LSI-11 microcomputer, and written onto magnetic tape (nine-track, 1600 BPI) along with date and time information. The lidar system is installed in a 7-m van (Figure 2) to facilitate the experimental setup at remote field sites.

(U) EXPERIMENTAL PROGRAM

(U) The SNOW-ONE-B field program was conducted over flat terrain near Grayling,

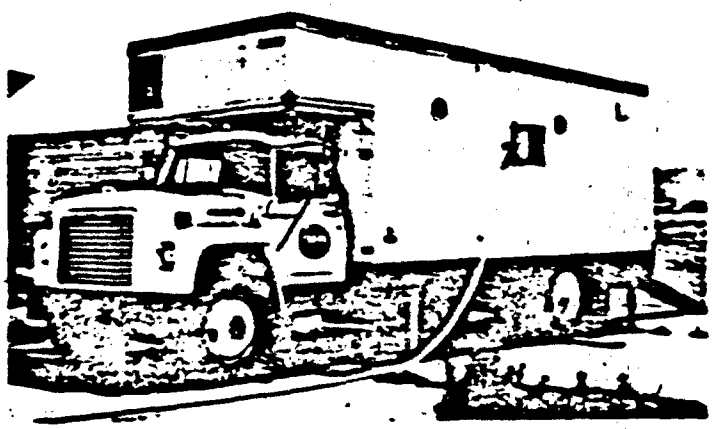

(a) EXTERNAL VIEW SHOWING LASER PORT FOR HORIZONTAL MEASUREMENTS

(b) INTERNAL VIEW SHOWING LASER/OPTICS TABLE AND DATA RECORDING SYSTEM

Figure 2 Four-Wavelength Lidar System in 6-Meter-Long Van

Michigan, during November and December 1982. The lidar van was positioned alongside transmissometer instrumentation vans operated by the U.S. Navy and the U.S. Army Atmospheric Science Laboratory. The lidar and transmissometers were aligned to observe parallel paths extending over a 600-m range. A passive (plywood) target of 64 square feet was erected at the far end of the lidar path, and transmissometer energy sources were located near the lidar target. The target provided a constant reflectivity surface such that variation in lidar-observed target returns can be interpreted in terms of atmospheric attenuation over the lidar-to-target path.

(U) Because of eye-safety requirements, the 0.53 μm laser wavelength was not transmitted during the experiment. Therefore, lidar observations were made only at the infrared wavelengths of 1.06 μm, 3.8 μm, and 10.6 μm. The lidar was allowed to operate the first 20 minutes of each hour during measurement periods. Occasionally, vertical lidar measurements were made by placing a 45° mirror outside the laser van.

(U) The primary objective of the field program was to characterize electromagnetic propagation through dense snowfall. Unfortunately, only light snowfall occurred during the experimental period. However, on several days a relatively dense fog occurred, and measurements were made. (Observations also were conducted for several generated-smoke events.) Table 1 presents a summary of the lidar operations.

(U) EXPERIMENTAL RESULTS (Preliminary)

(U) In this section, we present some of the results obtained thus far by a

Table 1. Lidar Measurements taken During SNOW-ONE-B Experiment

SNOW-ONE-B
Data Collection Runs
Grayling, Michigan

Date	Begin (EST)	End (EST)	Weather Conditions	Data Type	Tape No.
11/18/82	17:23	17:39	clear air	calib	A
11/19/82	16:37	17:02	high humidity	calib	B
11/29/82	16:40	17:02	high humidity	calib	1
11/30/82	7:29	7:53	clear air	calib	2
12/1/82	7:22	7:53	fog	horiz	3
12/1/82	7:55	8:01	fog	vert	3
12/2/82	7:14	7:37	light rain	calib	4
12/2/82	7:41	8:02	light rain	horiz	5
12/4/82	16:17	16:37	clear air	calib	6
12/4/82	16:38	16:43	clear air	calib	6
12/6/82	9:00	9:19	clear air	calib	7
12/8/82	10:00	10:30	light snowfall	calib	8
12/8/82	11:00	11:10	clear air	horiz	9
12/8/82	12:05	12:19	oil fog smoke	horiz	9
12/8/82	13:05	13:20	IR screener smoke	horiz	10
12/8/82	14:05	14:20	fly ash smoke	horiz	11
12/8/82	15:06	15:20	diesel smoke	horiz	11
12/10/82	22:05	22:20	light snowfall	horiz	12
12/10/82	23:04	23:20	snowfall	horiz	13
12/10/82	24:00	00:20	light snowfall	horiz	13
12/11/82	1:00	1:20	light snowfall	horiz	13
12/11/82	2:01	2:20	light snowfall	horiz	14
12/11/82	3:00	3:10	light snowfall	horiz	14
12/11/82	3:11	3:20	light snowfall	vert	14
12/12/82	9:00	9:20	light snowfall	horiz	15
12/12/82	10:06	10:20	light snowfall	horiz	15
12/12/82	11:00	11:20	light snowfall	horiz	15
12/12/82	12:00	12:20	clear air	calib	15

data analysis program. The analysis program is being directed to the following objectives:

- Evaluation of 1.06 μm, 3.8 μm, and 10.6 μm transmission histories over the lidar-to-target path for each obscuration event
- Evaluation of the accuracy of the lidar transmissions by estimating their correlation to other transmission measurements
- Derivation of transmission distribution models that may be more useful to weapons analysts than transmission histories
- Evaluation of the relationship of lidar backscatter along the observed path to transmission measurements
- Evaluation of the information content on particle characteristics and multiple-scattering effects, in order to form better estimates of absolute aerosol concentrations from single-ended lidar measurements.

(U) Figure 3 presents a single multi-wavelength lidar backscatter waveform for an oil fog aerosol cloud. Returns from clear air, the aerosol cloud, and the solid target can be identified for each infrared wavelength. The solid target returns were analyzed for time histories of transmission by assuming the target is of constant reflectivity during each experiment. Target returns during clear-air conditions were used to establish the 100 percent transmission value, and optical filters with known attenuation at each lidar wavelength were used to calibrate the lidar receiver response to target returns in terms of atmospheric transmission.

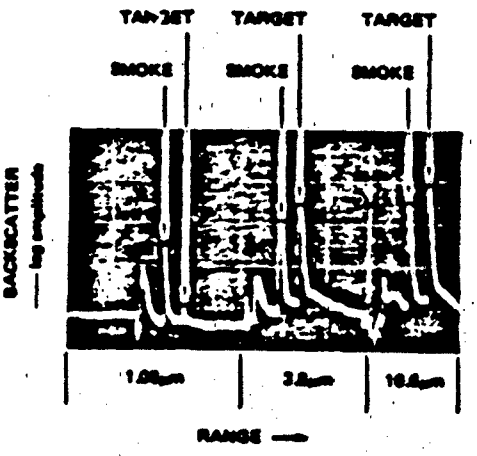

Figure 3 Three-Wavelength Lidar Backscatter Signature for Oil Fog Release Along 600m Path Between Lidar Van and Target

Greyling, Michigan, 8 December 1982

(U) Figure 4 presents an example of a transmission history result obtained from lidar target returns recorded during the IR screener event on 8 December 1982. The event observed by the lidar extended over an 8-minute interval, with rapid changes in transmission occurring at all three infrared wavelengths. The high correlation of transmission with time between wavelengths results because nearly equal paths are viewed at nearly equal times. Previous multiple-wavelength lidar measurements indicated that path separations—especially in the vertical—resulted in uncorrelated transmission histories so that multiple-wavelength analysis could not be applied.

(U) Also presented in Figure 4 are plots of the optical depth ($U = -\ln T$) between wavelengths. Again, the relatively good correlation indicates minimal time and space variability of transmission between the multiple wavelength observations. Moreover, the linear relationships between the optical depths indicate that multiple-scattering may not be an important factor for the lidar transmission analysis. The plots indicate that the IR screener is 17 percent more effective at 10.6 μm wavelength than at 1.06 μm, and 20 percent more effective at 3.8 μm than at 1.06 μm.

(U) Figure 5 presents a comparison of lidar transmission history at 1.06 μm and the equivalent history recorded by the Navy transmissometer system. Excellent agreement is obtained, although the two observational paths were separated by about 3 to 4 m in the horizontal.

(U) Transmission histories such as those presented in Figure 4 are useful for evaluating the effectiveness of an aerosol event against various electro-optical systems. However, models presenting transmission values as frequency distributions may be more readily useful to weapon system designers and evaluators. Several examples are presented below to illustrate the type of transmission models that can be derived from transmission histories. Figure 6 presents histograms of the total time

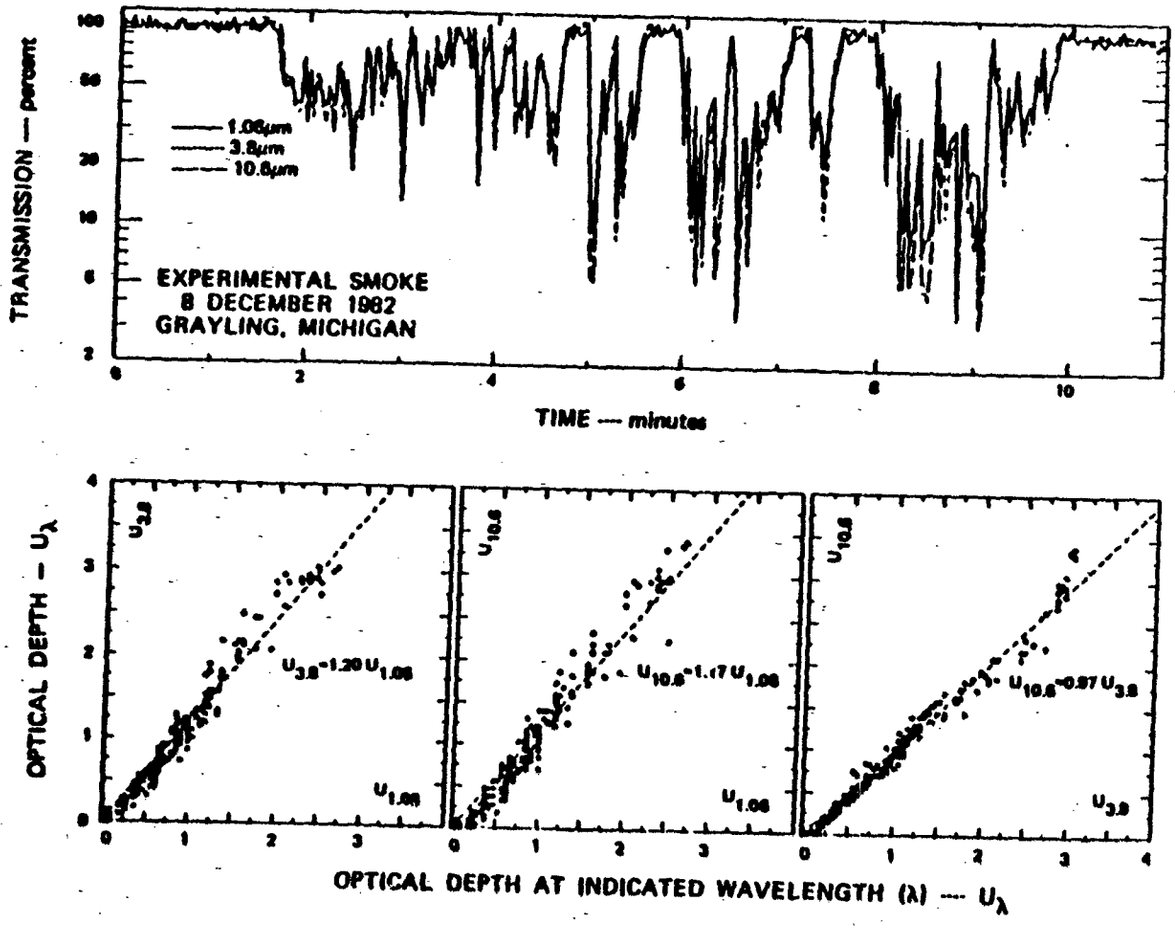

Figure 4 Transmission History and Optical Depth Relationships for IR Screener Smoke Event on 8 December 1982

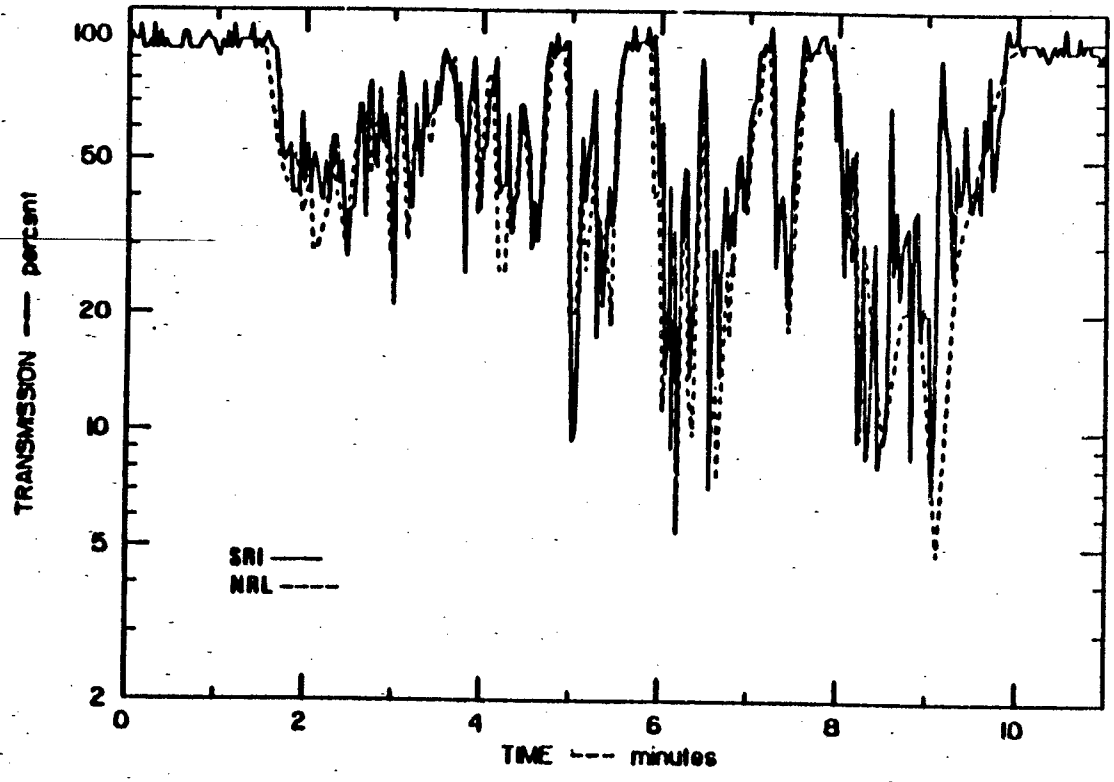

Figure 5 Comparison of Transmission Histories Measured by the 1.06 μm SRI Lidar and the NRL Transmissometer for IR Screener Smoke Event on 8 December 1982

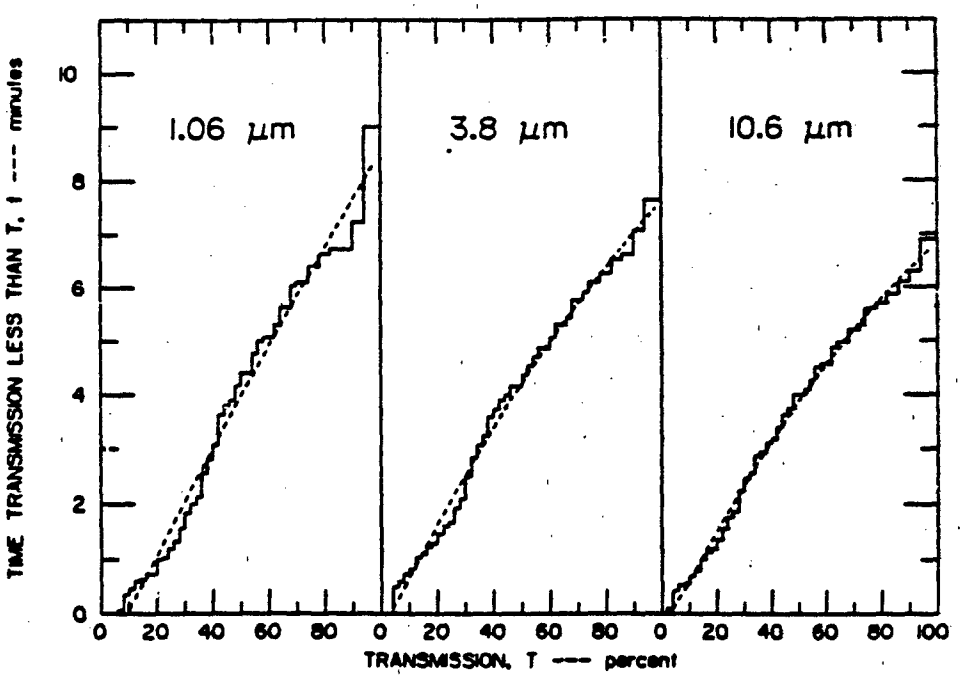

Figure 6 Histograms of the Time That Transmission Was Less Than a Specified Value, T, for the IR Screener Smoke Event on 8 December 1982

increment that transmission was below any specified value for the IR screener smoke test. For example, at a wavelength of 10.6 μm, the transmission was less than 50 percent for about 4 minutes during the smoke event. The transmission was less than 20 percent for only about 1 minute during the smoke event. Therefore, if a weapon system is rendered inoperative only if transmission is less than 20 percent at the 10.6 μm wavelength, the IR screener smoke event will be effective for about 1 minute of total time. However, the effective time may be extended because of variable transmissions extending over longer time periods. Figure 7 presents an analysis of the time duration of transmission "holes" (i.e., time duration when transmission is greater than or equal to a specified value). For example, only 10 holes occurred for transmission of 10 percent, but these can be of relatively long duration. At 50 percent, more holes can occur (28 in this example), but with shorter time durations.

(U) A similar analysis can be performed for transmission "patches" (i.e., time durations when transmission is less than a specified value). Figure 8 presents a transmission "patch" analysis for the 10.6 μm wavelength transmission

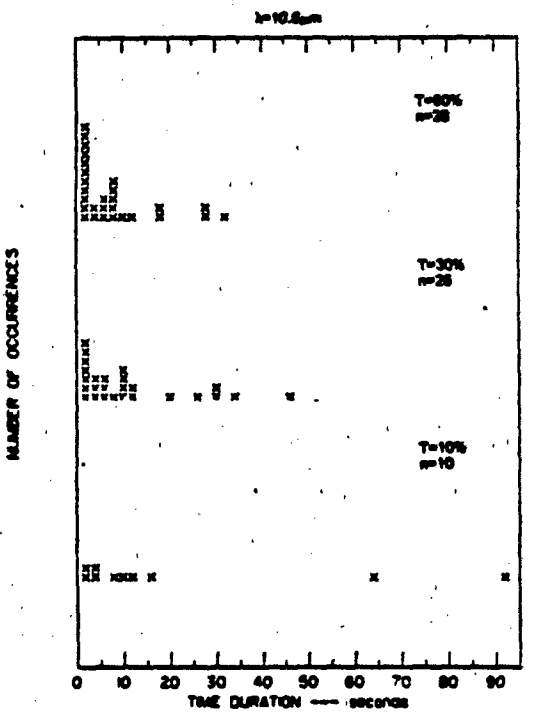

Figure 7 Number and Time Distribution of "Holes" (When Transmission is Greater Than or Equal to a Specified Value, T) for the IR Screener Smoke Event on 8 December 1982

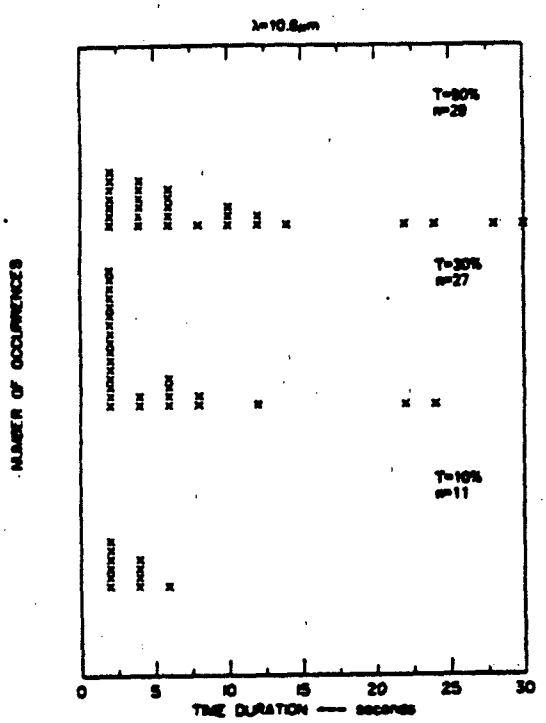

Figure 8 Number and Time Duration of "Patches" (When Transmission is Less Than a Specified Value, T) for the IR Screener Smoke Event on 8 December 1982

history data presented in Figure 4. For patches with less than 50 percent transmission, 50 events occurred with a maximum duration of 30 sec. Only 11 patches with transmission less than 10 percent occurred with a maximum duration of only 6 sec.

(U) The examples presented above were derived from target returns. However, the primary objective of the lidar program is to derive quantitative information using single-ended backscatter data. Several methods have been used to relate lidar atmospheric backscatter observations to extinction or concentration. For relatively dense aerosols, single-scattering formulations may not be valid and, therefore, the typically-used lidar equation and its various solution forms may not be appropriate.

(U) One method for evaluating attenuation from backscatter data is to relate the path-integrated backscatter to the optical depth evaluated from target returns. For example, Figure 9 presents a plot of these two quantities for lidar data collected at a wavelength of 3.8 μm during the IR screener test (c.f. Figure 4). The integrated backscatter ratio was calculated using a clear air return obtained before the smoke release.

(U) Although a relatively large scatter of data points occur, a near-linear relationship can be evaluated for optical depths less than 1.5 (i.e., transmissions from 100 to 22 percent). This linear relation can be used to infer transmission from single-ended backscatter measurements. The near constant path-integrated backscatter and the relatively large scatter of data points above optical depths of 1.5 have been associated with dynamic range limitations of the lidar receiver, and possibly with a wide secondary pulse superimposed on the primary narrow pulse of the gas lasers (this introduces false scattering at ranges greater than the aerosol target).

(U) Figure 10 shows the transmission of three laser wavelengths during light snowfall (approximately .03 grams/m^3) starting at 0100 on 11 December. During this snowstorm, transmission is generally decreased with increasing wavelength. Figure 10 also contains the relationships of the optical depths for this period. In summary, $U_{10.6} > U_{3.8} > U_{1.06}$.

(U) Figure 11 presents the relationship between optical depth and integrated backscatter ratio for the 3.8 μm data of Figure 10. Because a clear air profile was not available during this period, the backscatter ratio is normalized to the minimum profile obtained for the data set. As with the smoke data presented in Figure 9, there is large scatter in the data points. Because of equipment limitations, identified by the smoke and snow data at SNOW-ONE-B, backscatter analysis of relatively dense aerosol events (e.g., smoke tests) are not being pursued. Rather, extended-range log amplifiers and time-gated detectors are being incorporated to expand the system dynamic range for use on future tests.

(U) This research was sponsored by the Geosciences Division of the U.S. Army Research Office.

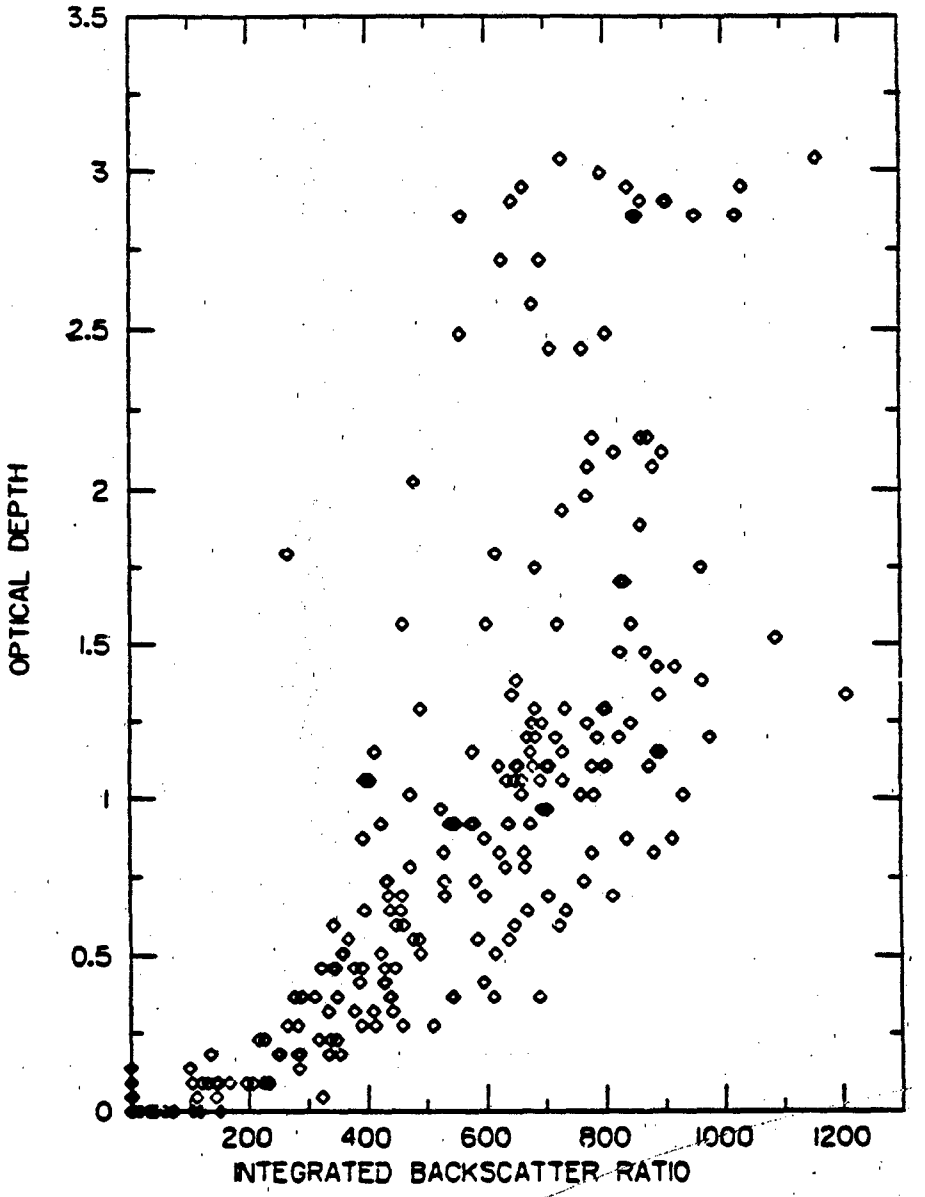

Figure 9 Relationship of Optical Depth and Integrated Backscatter Ratio for 3.8 μm During the IR Screener Smoke Event on 8 December 1982

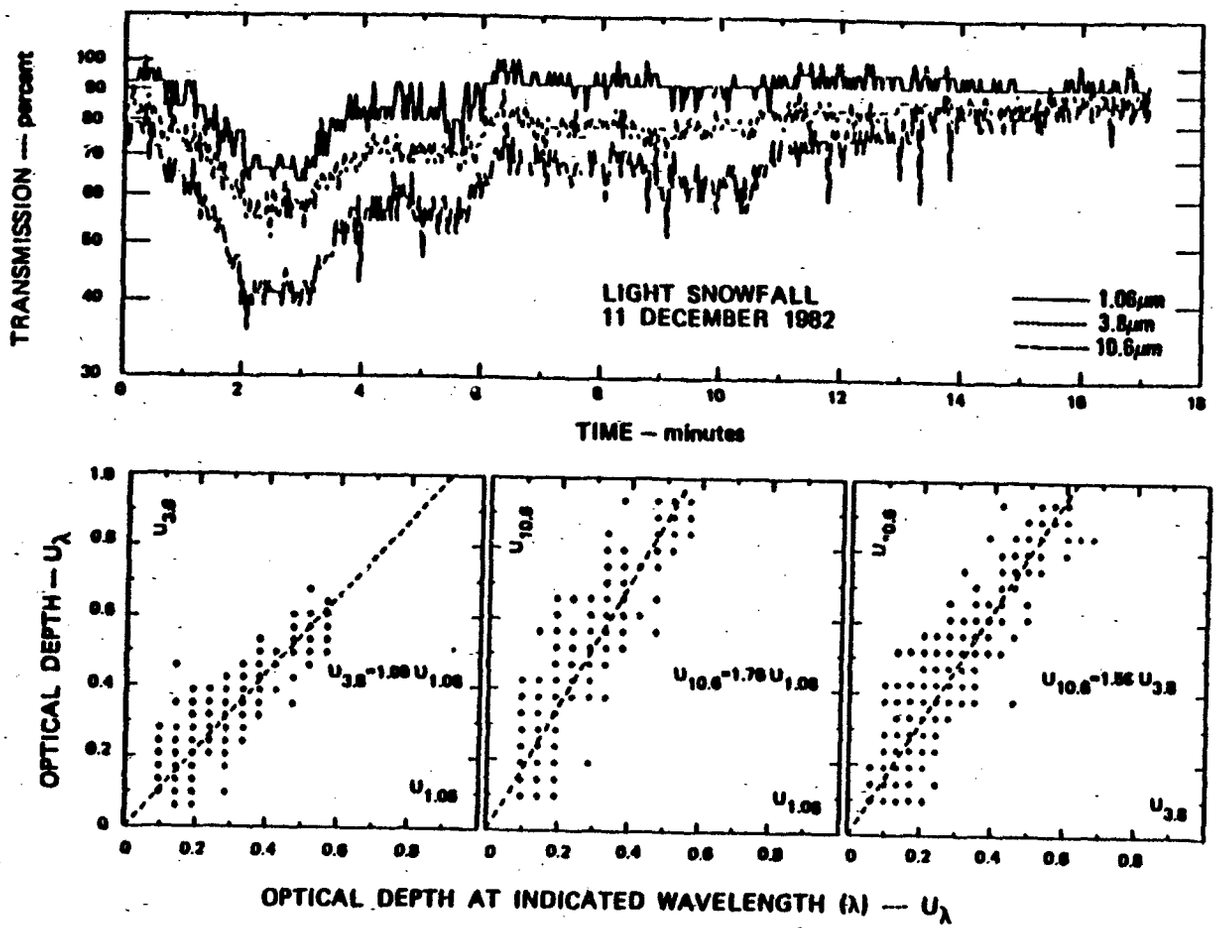

Figure 10 Transmission History and Optical Depth Relationships for Light Snowfall at 0100 on 11 December 1982

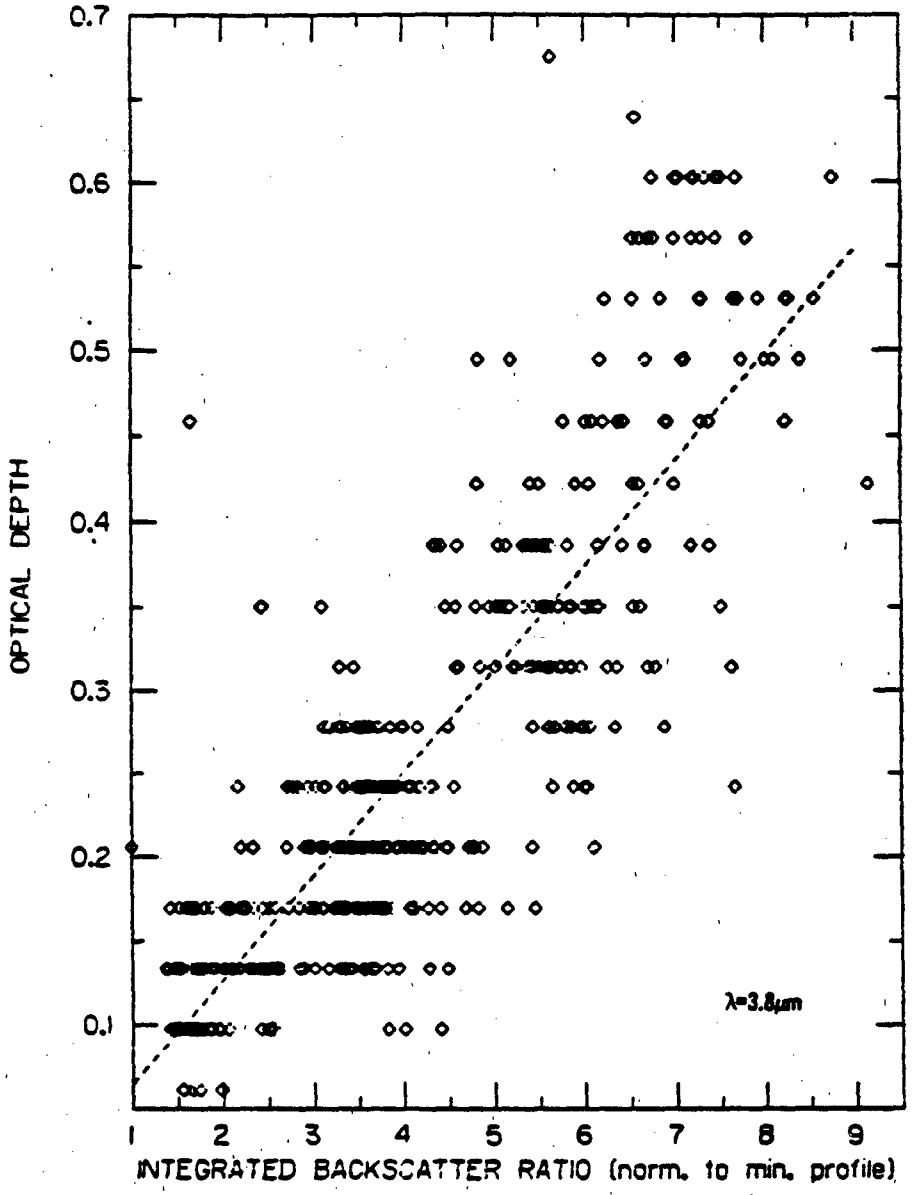

Figure 11 Relationship of Optical Depth and Integrated Backscatter Ratio for 3.8 μm During Light Snowfall on 11 December 1962

Appendix E

"LIDAR APPLICATIONS FOR OBSCURANT EVALUATIONS"

Presented at SMOKE/OBSCURANTS SYMPOSIUM VII

LIDAR APPLICATIONS FOR OBSCURANT EVALUATIONS (U)

Edward E. Uthe
SRI International
Menlo Park, California 94025 U.S.A.

ABSTRACT (U)

(U) Lidar provides a unique method for observing temporal and spatial distributions of obscurants along optical paths. However, attenuation and multiple scattering effects introduced by very dense obscurant clouds can (1) severely limit observational ranges, and (2) complicate interpretation of backscatter signatures in terms of absolute density and other properties. Nevertheless, lidar properly used can provide needed information that is nearly impossible to obtain by other means. This paper reviews applications for obscurant evaluations of several existing lidars, including a four-wavelength van-mounted and a two-wavelength airborne system. Examples are presented that illustrate the evaluation of:

- Aerosol plume transport over complex terrain and water surfaces
- Cross-plume diffusion during active convection
- Multiwavelength transmissions over lidar-to-target horizontal paths
- Vertical-path transmissions using the earth's surface as a passive reflector
- Particle-size distribution parameters derived from multiwavelength data
- Backscatter properties of natural and generated obscurants
- Optical and physical density inferences from single-ended observations.

1. (U) LIDAR SYSTEMS

(U) Lidar applies short-wavelength laser sources in radar fashion for remote observation of scattering aerosols and reflective surfaces. High-speed digitization and logarithmic processing, coupled with computer-based video displays, provide for real-time generation of pictorial views of atmospheric structure. This is derived from range-dependent backscatter signatures collected with high-pulse rate lasers. Van-mounted and airborne lidar systems have been developed for observing atmospheric aerosols over large volumes with high spatial and temporal resolutions. This paper presents examples derived from several lidar systems operated by SRI. Although these examples mostly have been derived on environmental studies, they clearly relate to applications for obscurant evaluations. System details have been presented elsewhere.

2. (U) AEROSOL PLUME TRANSPORT OVER COMPLEX TERRAIN AND WATER SURFACES

(U) Downward-viewing airborne lidar systems are particularly well suited for evaluating terrain effects on the transport and diffusion of aerosol plumes. For example, Figure 1 presents plume cross sections collected with the ALPHA-1 (Airborne Lidar Plume and Haze Analyzer) at different downwind distances from a coal-burning power plant. The plume was being channeled by complex terrain to the west of the plant. Other data collected show mountain restrictions and barriers to plume transport (Uthe, et al., 1980).

Paper to be included in the Proceedings of Smoke/Obscurant Symposium VII, Harry Diamond Laboratories Adelphi, Maryland, 26-28 April 1983

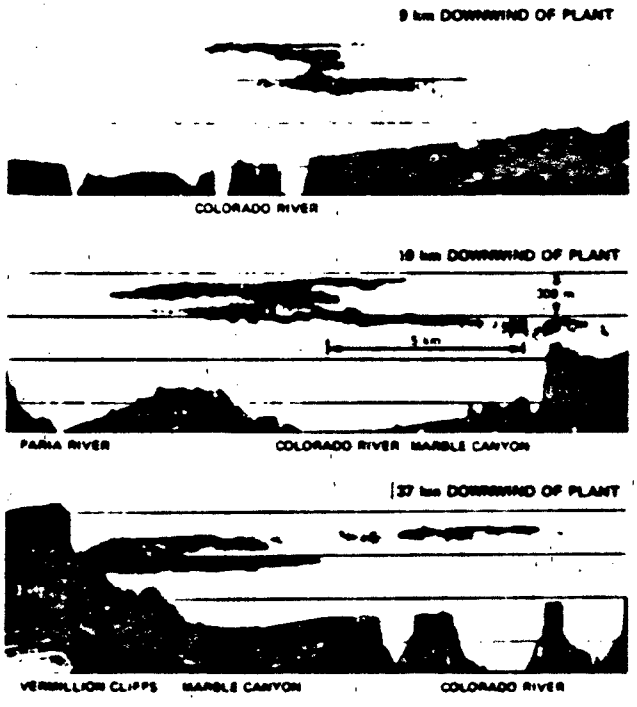

FIGURE 1. (U) AIRBORNE LIDAR OBSERVATIONS OF THE CROSS-PLUME STRUCTURE OF A SUBVISIBLE POWER PLANT PLUME AT DIFFERENT DOWNWIND DISTANCES FROM THE PLANT.

(U) Airborne systems are also well suited for making observations over water surfaces. For example, Figure 2 presents an example of air pollution layers over Los Angeles, and extending over the ocean area. The data show increasing density and depth of the pollution layer during the day, and indications of elevated wind flow reversal near the San Gabriel Mountains. The ALPHA-1 transmits energy simultaneously at 0.53 and 1.06 μm. The ratio of surface returns at these wavelengths provides a good indication of land or water surface, as shown by Figure 3. Therefore, the ALPHA-1 can be used to map terrain elevation and surface type, to correlate with observed atmospheric transport and diffusion characteristics.

3. (U) CROSS-PLUME DIFFUSION DURING ACTIVE CONVECTION

(U) Figure 4 shows examples of ALPHA-1 flights across a power plume at 10 km downwind from a source located in flat terrain. Early morning observations show a well-defined plume above the developing mixing layer while subsequent passes across the plume show structure of clear-air convective cells and entrainment of the plume particulates. These data show that highest plume concentrations during active convection are associated with compensating downdraft motions. Darker areas at the top of convective cells probably result by hygroscopic particle growth as the relatively warm and humid air is lifted into cooler surroundings. These data illustrate the dramatic effect of daytime convection on aerosol concentration distributions.

4. (U) MULTIWAVELENGTH TRANSMISSIONS OVER LIDAR-TO-TARGET PATHS

(U) A four-wavelength van-mounted lidar system recently has been developed to investigate techniques for remote measurement of aerosol optical and physical densities and of particle characteristics.

LOS ANGELES, CALIFORNIA – 16 DECEMBER 1979

(a) 1120 – 1150 PST, 1.06 μm, 190° TRUE COURSE

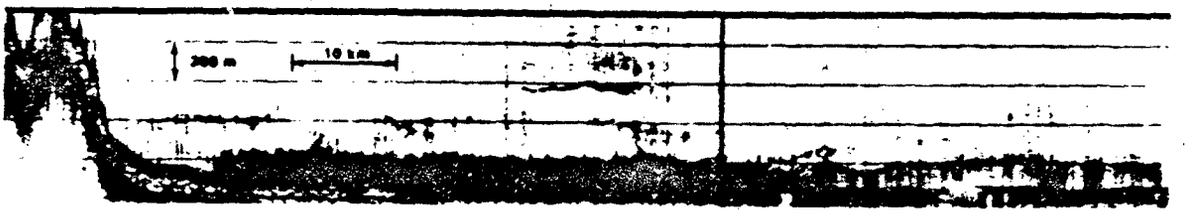

(b) 1602 – 1634 PST, 1.06 μm, 190° TRUE COURSE

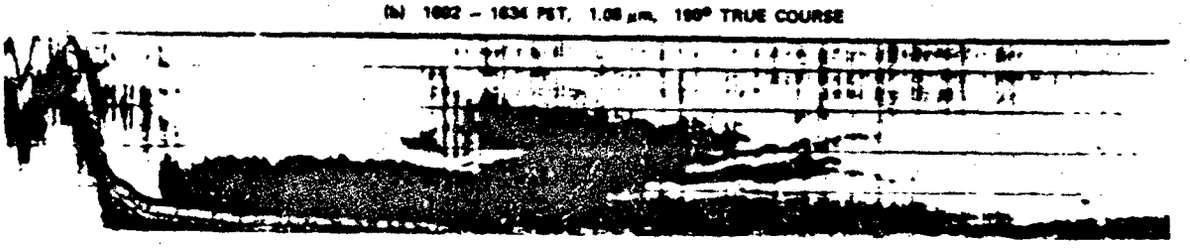

FIGURE 2. (U) LOS ANGELES BOUNDARY LAYER STRUCTURE DERIVED FROM ALPHA-1 MAGNETIC TAPE RECORDS, 16 December 1979 (300 m/div altitude).

The system transmits energy at 0.53 μm and 1.06 μm wavelengths using a neodymium-Yag laser, 3.8 μm using a DF laser and 10.6 μm using a CO_2 laser. Pulses from the three lasers are transmitted coaxially with a 12-inch Newtonian telescope. Four-wavelength backscatter and transmission measurements are made along the same viewing path within 150 μs to reduce effects of time-varying aerosol distributions.

(U) A local test of the four-wavelength lidar was conducted to evaluate system performance in environments similar to those experienced during previous lidar operations at Army range facilities (Uthe, 1981). The lidar van was located about 600 m from an 8-ft square passive reflector constructed on the Stanford University field site. Both dust and smoke aerosols were generated near the midpoint of the lidar-to-target path. Figure 5 shows an oscilloscope presentation of a single lidar signature showing atmospheric backscatter and target returns at each of the four wavelengths. The larger ratio of dust-to-clear-air backscatter for longer

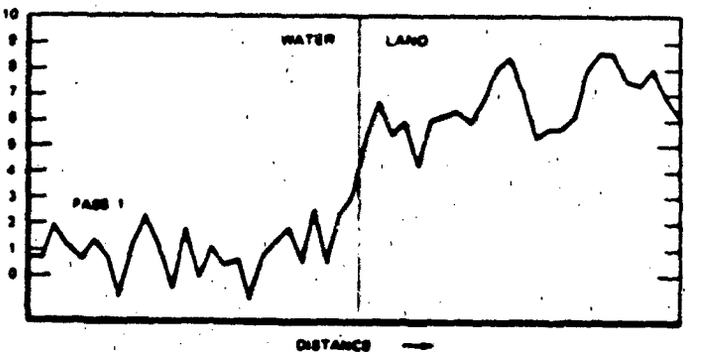

FIGURE 3. (U) RATIO OF SURFACE RETURNS AT 1.06-μm AND 0.53-μm WAVELENGTHS OBSERVED BY ALPHA-1 DURING A FLIGHT OVER WATER-TO-LAND

wavelengths is expected, as the large-particle dust scattering is nearly wavelength independant. However the clear-air scattering is proportional to the inverse fourth power of wavelength (assuming Rayleigh scattering).

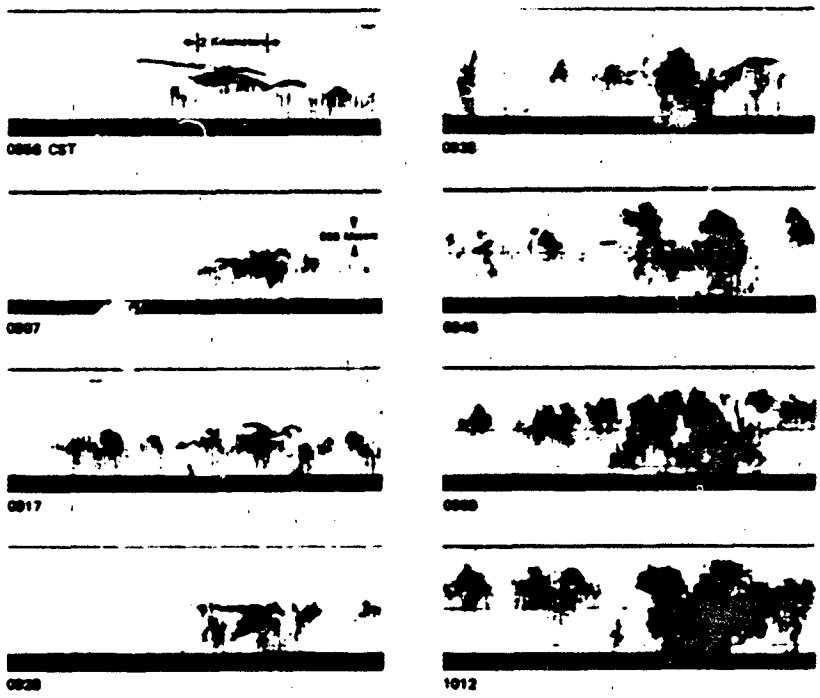

FIGURE 4. (U) PLUME CROSS SECTIONS DURING CONVECTION, 10-km DOWNWIND OF KINCAID POWER PLANT, 4 May 1980.

(U) The target returns provide a means to evaluate obscurant transmission along the lidar-to-target path, quantitatively. Figure 6 presents a time history of transmission derived from data collected during a red-smoke test. These data indicate that the optical properties of smoke are nearly equal at 0.53 and 1.06 μm, with substantially less attenuation at 3.8 μm and almost no attenuation at 10.6 μm. Transmission values evaluated from target returns can be used to develop and validate transmission values derived from the range-resolved backscatter data, so that measurements can be made along vertical and slant paths.

(U) The four-wavelength lidar was recently used to collect backscatter and transmission data during the SNOW-ONE-8 Tests conducted at Grayling, Michigan; the data are now being analyzed.

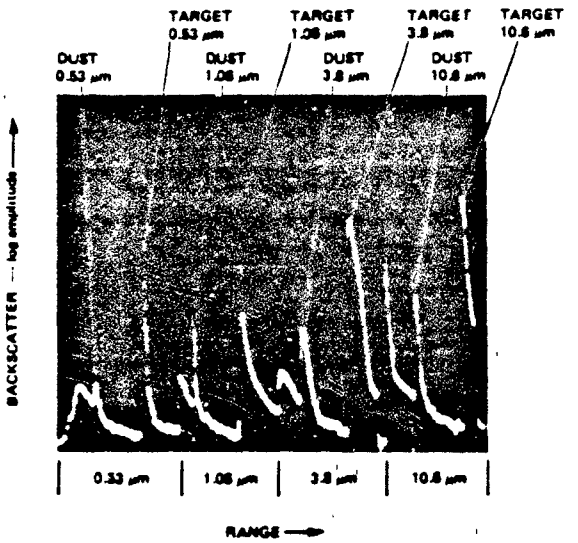

FIGURE 5 FOUR-WAVELENGTH LIDAR BACKSCATTER SIGNATURE FOR DUST GENERATED ALONG 600m PATH BETWEEN LIDAR AND TARGET Stanford Field Site, 7 July 1982.

5. (U) VERTICAL-PATH TRANSMISSIONS USING THE EARTH'S SURFACE AS A PASSIVE REFLECTOR

(U) During a flight test of the ALPHA-1, observations were made downwind of a forest fire located near the California coast (Uthe et al., 1982). Visually, the fire appeared to be contained within a small area; the resulting smoke plume towered over the source, but was transported downwind at lower altitudes.

(U) Figure 7 shows plume cross-sections derived from infrared and visible backscatter signatures recorded during the second pass of ALPHA-1 across the plume. For these data, receiver gain was reduced so that surface returns did not saturate receiver electronics; as a result, clear air haze layers were not as well observed on this data. Greater plume attenuation of the visible energy than of the infrared energy is evident by the absence of plume visible backscatter following penetration by the laser pulse of the denser plume elements. Plume

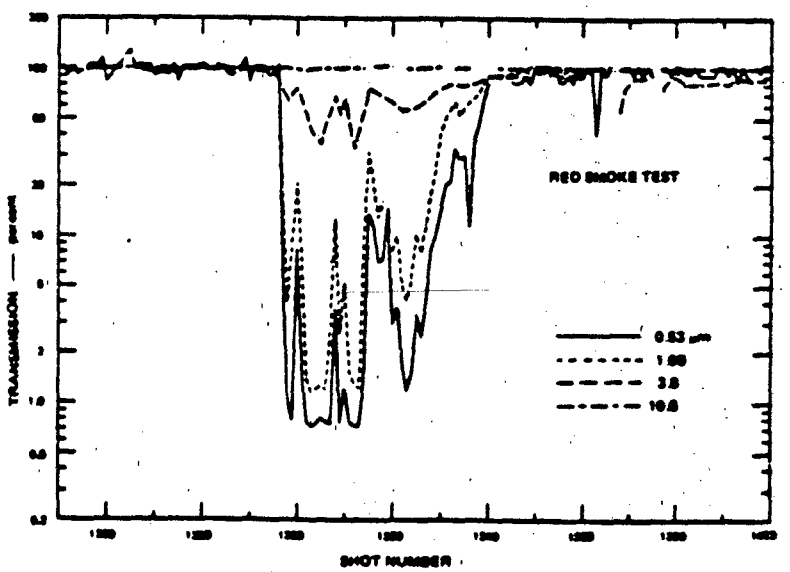

FIGURE 6. IUB LIDAR TEST TRANSMISSION HISTORY. Stanford Field Site, 7 July 1982

transmissions in the vertical were evaluated by normalizing to 100 percent-observed surface returns in the absence of plume backscatter, and by assuming constant surface reflectivity and laser-transmitted peak power for each laser firing made along the cross-plume path. Lidar response information required for quantitative analysis of backscatter signatures was derived using standard calibration techniques with neutral density filters of known attenuation. Vertical transmissions for one-way passage of the laser energy through the smoke plume are plotted in Figure 7. The results show minimum plume transmissions of about 50 percent at 1.06 μm and about 6 percent at 0.53 μm. The strong wavelength dependence of attenuation suggests submicron particle sizes, although strong absorption in the visible, and weak absorption in the infrared, by plume constituents could also explain the observations. A mean particle size is derived from the observations in the following section of this paper.

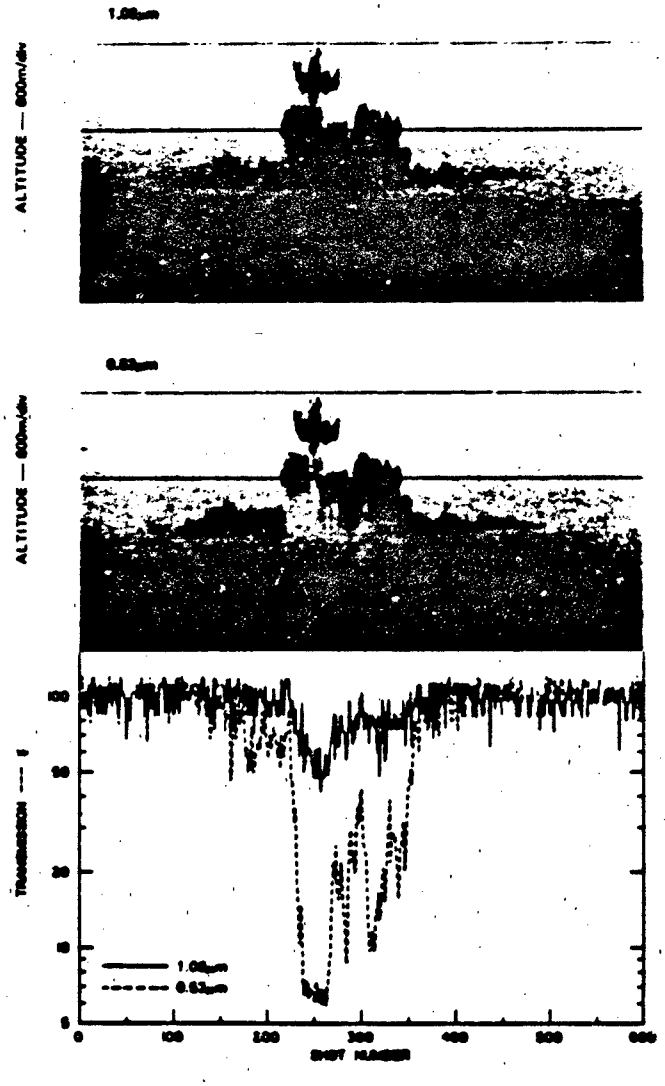

FIGURE 7. (U) CROSS-PLUME STRUCTURE DERIVED FROM ALPHA-1 PLUME BACKSCATTER AND VERTICAL TRANSMISSIONS DERIVED FROM SURFACE RETURNS AT 1.06- 0.53-μm WAVELENGTHS (Aircraft Pass 2).

6. (U) PARTICLE-SIZE DISTRIBUTION PARAMETERS DERIVED FROM MULTIWAVELENGTH DATA

(U) To investigate the use of multi-wavelength data for characterizing particle size distributions, an experiment was conducted using transmissometers operating at 14 different wavelengths, and mounted across a 10-m long aerosol tunnel facility located at SRI International, as shown in Figure 8 (Uthe, 1982). The tunnel was designed with open ends for evaluating lidar techniques. Aerosols consited of particulate material of different size fracitons and single-size fracitons of six other materials. Particle size evaluations were made by multi-stage impactor, and by air permeability analysis

of packed powder. Examples of multiple-wavelength extinction coefficient data is given in Table 1.

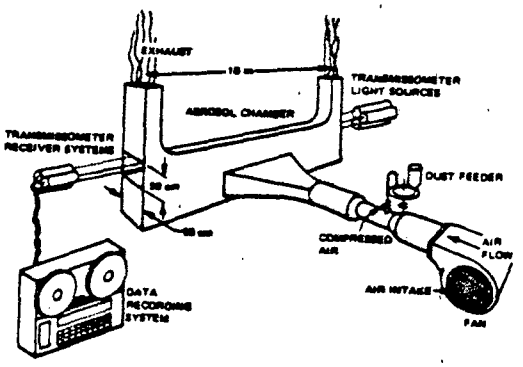

FIGURE 8. (U) DIAGRAM OF EXPERIMENTAL FACILITY

(U) The data base indicates that mean particle size smaller than 1-μm diameter could be estimated usefully from aerosol extinction measurements using a single-laser lidar system operating at 1.06- and 0.53-μm wavelengths (Figure 9). For larger mean particle sizes the extinction ratio is near unity, and longer wavelength systems are required. The data indicate that a two-laser lidar operating at 10.6 and 0.53 μm could provide estimates of mean particle size to diameters of at least 6 μm.

(U) The two-wavelength lidar data collected with ALPHA-1 (Figure 7) can be used with the laboratory results presented in Figure 9 to estimate mean particle size of the smoke plume. Assuming the wavelength difference results entirely from particle size effects, the laboratory data indicate particle diameters of about 0.1 μm, which is consistent with in-situ measurements reported by various investigators in the literature. Inference of particle size is important to evaluate lidar backscatter quantitatively in terms of aerosol extinction and concentration.

TABLE I. (U) EXAMPLES OF MULTI-WAVELENGTH EXTINCTION MEASUREMENTS*

Aerosol Type	Extinction Coefficient (km^{-1}) at Indicated Wavelength (μm)													
	Photopic	0.390	0.450	0.514	0.613	0.670	0.870	0.930	1.045	1.24	1.63	3.39	3.90	10.6
0-10 μm fly ash	83.3	78.2	78.2	78.7	79.6	80.1	83.1	84.7	86.7	90.8	90.6	74.1	71.3	53.2
5-10 μm fly ash	63.5	54.9	56.7	58.3	59.7	60.1	61.6	61.8	62.4	63.5	63.6	67.1	70.3	54.7
2.5-5 μm fly ash	86.6	81.0	81.9	82.7	83.5	83.7	86.8	87.8	89.4	92.8	100.2	94.9	85.6	47.4
0-2.5 μm fly ash	63.5	60.8	60.3	60.5	61.5	62.8	68.6	71.0	75.0	79.7	76.5	29.8	23.9	13.6
Superfine fly ash	98.9	98.1	98.6	98.8	97.8	96.3	89.7	87.5	82.7	72.1	56.7	14.6	13.9	10.1
5 μm silica	90.5	95.7	94.5	92.5	88.9	86.4	78.6	76.1	71.5	65.4	52.3	14.7	11.1	8.3
10 μm silica	71.0	77.7	76.7	71.1	66.8	64.8	58.8	57.2	54.4	50.9	43.0	22.4	20.0	14.8
15 μm silica	95.5	92.8	92.8	92.2	91.0	90.6	86.8	85.7	83.4	81.4	72.3	35.5	39.6	34.1
Iron oxide	117.7	102.7	107.7	113.6	117.7	116.1	102.3	97.4	88.6	74.1	55.2	19.3	17.0	8.2
Ammonium chloride	97.4	134.6	136.9	113.3	90.1	79.0	51.3	45.6	37.2	26.0	16.2	9.5	3.1	0.7
Zinc chloride	76.8	75.2	77.3	77.7	74.8	71.5	58.1	54.1	47.0	35.6	22.0	6.4	3.5	2.2
Titanium dioxide	340.4	268.1	285.1	320.4	347.0	349.3	304.5	282.3	242.3	175.4	101.3	11.10	6.2	4.1
Aluminum	66.4	58.0	59.7	61.4	62.4	62.6	64.0	63.9	63.5	63.6	62.6	58.1	61.3	56.6
Resin	11.0	27.2	19.7	14.3	9.9	8.3	4.9	4.3	3.5	2.3	1.6	—	0.1	—

*ARBITRARY MASS CONCENTRATIONS USED FOR EACH AEROSOL MEASUREMENT.

7. (U) BACKSCATTER PROPERTIES OF NATURAL AND GENERATED OBSCURANTS

(U) As shown above, single-wavelength lidar systems can be used to observe aerosol distributions with high spatial and temporal resolution. However, quantitative evaluation of optical (extinction) or physical (concentration) densities from backscatter records normally require information or assumptions on the size, shape, and composition of the scattering particles. Multiple-wavelength systems may provide sufficient information on particle characteristics for evaluation of aerosol densities from backscatter data. The examples presented below illustrate the sensitivity of lidar signatures to particle characteristics, and suggest analysis techniques for density evaluation.

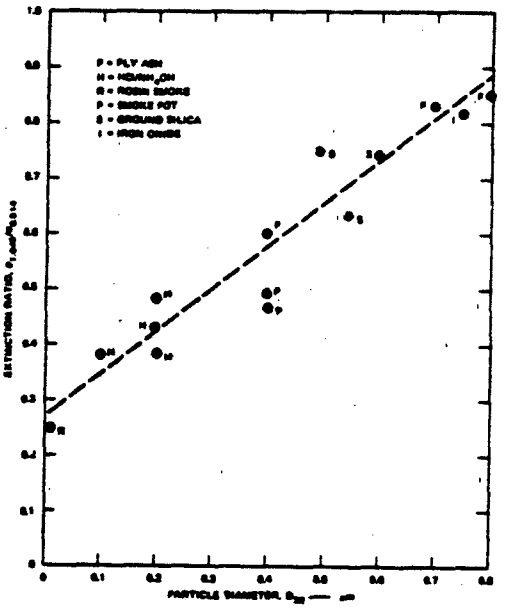

FIGURE 9. (U) RATIO OF EXTINCTION AT 1.046- and 0.514-μm WAVELENGTHS AS A FUNCTION OF MEAN (SAUTER) DIAMETER (IMPACTOR MEASUREMENTS) FOR SUBMICRON PARTICLES OF DIFFERENT COMPOSITIONS.

(U) Figure 10 presents data derived from lidar observations of both black and white smoke generated by using the same technique, but using materials of different chemical composition. As the density of the plume was increased, its opacity was measured by analyzing the clear-air lidar returns observed before and after the plume return; this type of analysis yields a measure of plume opacity that is not affected by uncertainties in plume particle size, shape, and composition. In Figure 10, opacity values derived in this manner are plotted versus simultaneously measured maximum plume backscatter. These data show that for visible-wavelength lidar systems, approximately 5 dB (factor of 3) variation in

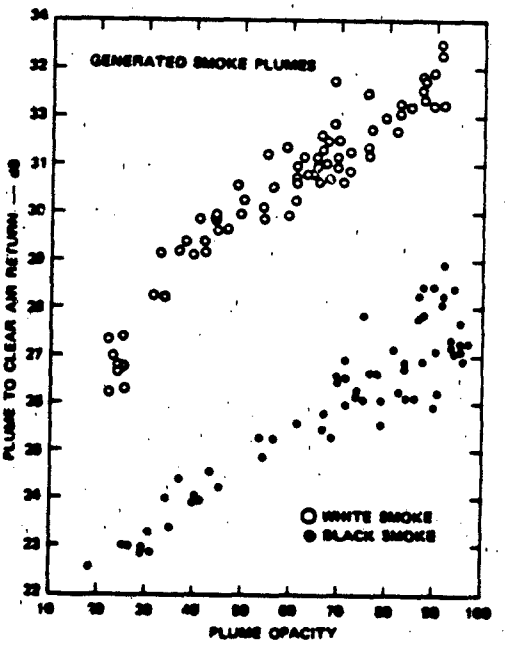

FIGURE 10. (U) PLUME RETURNS PLOTTED AGAINST OPACITIES DERIVED FROM NEAR- AND FAR-SIDE CLEAR AIR RETURNS.

backscatter can occur for a given plume opacity, because of variations in plume micro-characteristics. Clearly, evaluation of extinction coefficients assuming backscatter-to-extinction ratios must consider particle composition (refraction index).

(U) Figure 11 presents lidar backscatter data related to transmissometer derived extinction data for generated aerosols of the same composition (fly ash), but different size distributions. These results show that for a 0.7-μm wavelength lidar system, the backscatter-to-extinction ratio is nearly independent of the particle size. It was also shown, however, that at this wavelength the backscatter-to-mass concentration ratio is greatly dependent on particle size. Results using a 1.06-μm wavelength lidar indicated that the backscatter-to-extinction ratio is more dependent on particle size, but the backscatter-to-mass ratio is less dependent on particle size than at the 0.7-μm wavelength. Later experiments have shown even less dependence on particle size for backscatter-to-mass ratios at 3 to 10 μm wavelengths. Of course, derivation of mass concentration from backscatter data requires knowledge of the particulate specific gravity, and thus, volume concentrations may be more appropriate for lidar measurement.

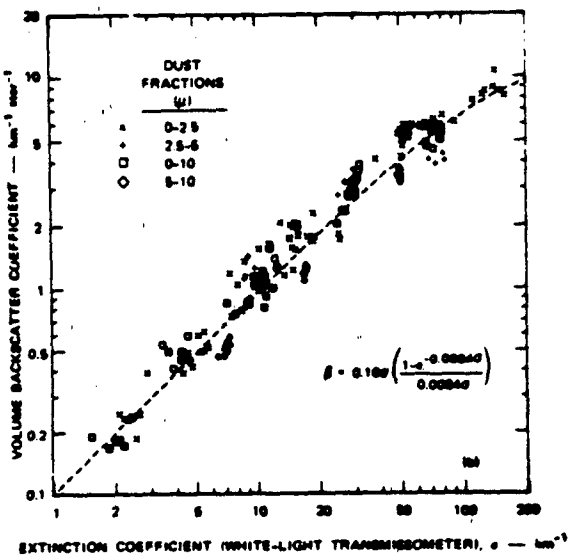

FIGURE 11. (U) VOLUME BACKSCATTER COEFFICIENTS (β) OBSERVED AT A LIDAR WAVELENGTH OF 0.7 μm RELATED TO WHITE-LIGHT VOLUME EXTINCTION COEFFICIENTS. The dashed line represents the best fit to the data of the nonlinear equation indicated.

8. (U) OPTICAL AND PHYSICAL DENSITY INFERENCES FROM SINGLE-ENDED OBSERVATIONS

(U) The data presented in Figure 10 illustrated a single-ended method for evaluating the optical density (opacity) of an aerosol plume. This method has been formally accepted by the U.S. Environmental Protection Agency (Alternate Method 1 to Reference Method 9) for objective measurement of visible emissions from stationary sources. Experiments have been conducted to evaluate the application of backscatter to evaluate optical density (i.e., extinction) as shown by the data presented in Figure 11. Other data relating optical depth to path-integrated backscatter (Figure 12) shows that some information can be obtained, but that dense aerosol clouds can introduce non-linear relationships between

backscatter and extinction; and that wide scatter between these quantities can occur which is probably a result of changing particle characteristics within obscurant clouds. Nevertheless, several experiments have been conducted to evaluate aerosol concentrations.

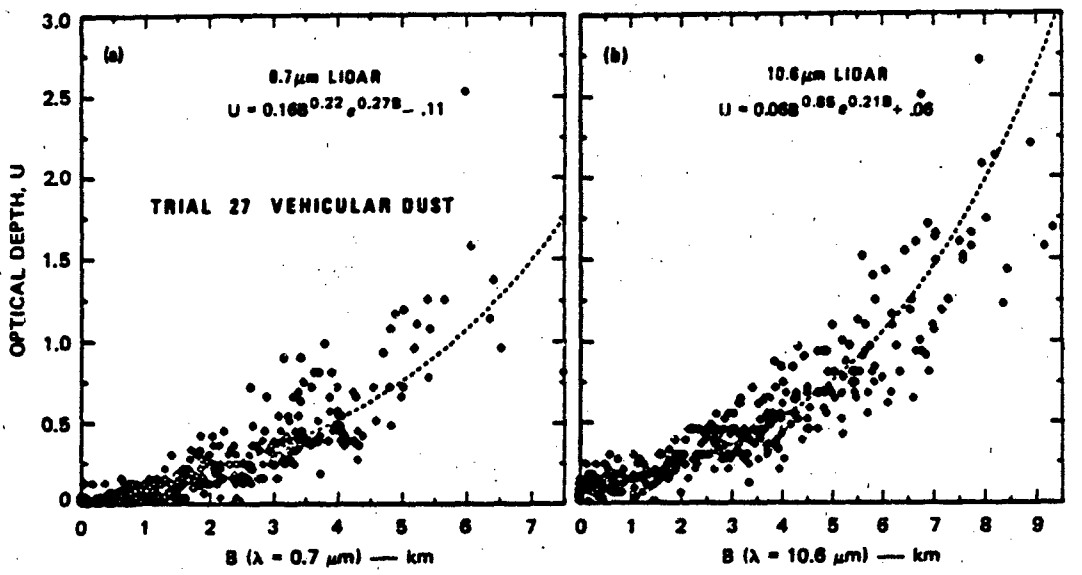

FIGURE 12. (U) LIDAR-DERIVED RELATIONSHIP BETWEEN OPTICAL DEPTH AND PATH INTEGRATED BACKSCATTER FOR A CLOUD OF VEHICULAR DUST.

(U) To investigate the use of lidar for quantitatively evaluating the emission rate of fugitive particulate sources, an experiment was conducted with a controllable particle emission source. A ground-based lidar made cross-plume observations by scanning in elevation at 500 m downwind of the smoke source. In addition to the lidar observations, wind speed and direction were recorded at the lidar site. Cross-plume backscatter values were integrated and adjusted by wind speed and direction to provide an estimate of smoke emission rate. The smoke generator was used at three emission rates, and for each rate 10-20 plume cross sections were recorded. Figure 13 shows that the resulting time-averaged cross-plume backscatter values were linearly related to the source emission rate for the relatively low density plumes. These results indicate the potential of lidar for monitoring smoke plume particle concentrations.

(U) Analytical solutions to the single-scattering lidar equation have been proposed by several investigators as a means to determine range-dependent extinction coefficients from lidar signatures and to correct for attenuation effects in concentration evaluations. For example, Figure 14 presents a

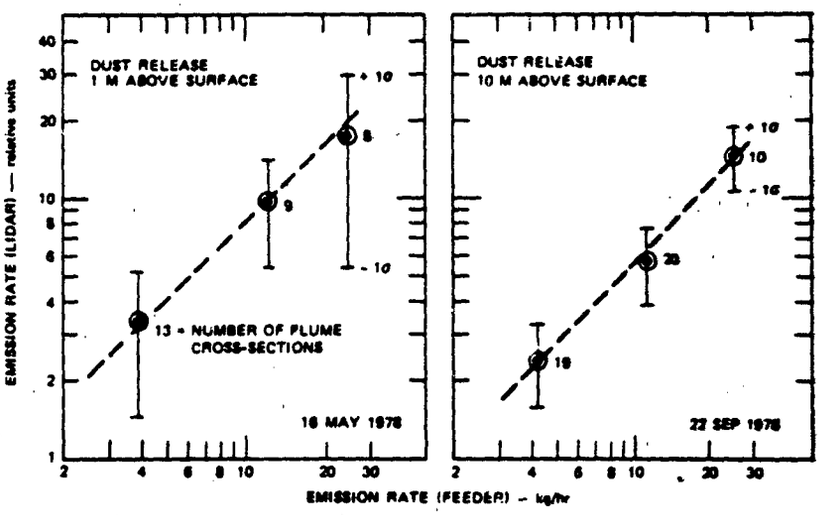

FIGURE 13. (U) PARTICULATE EMISSION RATE EVALUATED FROM LIDAR PLOTTED AS A FUNCTION OF EMISSION RATE EVALUATED FROM PARTICLE FEEDER.

Dashed line is the best-fit linear relation.

cross-plume mass concentration analysis derived from a ground-based elevation scanning lidar system operating at a wavelength of .6943 μm. The mass concentrations were evaluated from the solution form:

$$M(R) = \exp\left[c_1 S(R)\right]\left\{M_o^{-1} - 2\xi_e \int_{R_o}^{R} \exp\left[c_1 S(l)\right] dl\right\}^{-1}$$

where $c_1 = 1/4.34$

$\xi_e = \sigma/M$

σ = extinction coefficient

M_o = clear air concentration

and S = range corrected logrithmic lidar signature as a function of range R.

The parameters M_o and ξ_e were evaluated from independently measured particle size distributions and the Mie scattering theory. The result shows that in this case, attenuation introduced about one order of magnitude (10 dB) decrease in the backscatter from the far side of the plume. For such dense plumes, multiple scattering probably should also be considered in the analytical solution. However, the cross-plume concentration evaluated in the example of Figure 14 agreed well with stack emission data when corrected for observed wind speed at plume height.

9. (U) CONCLUSIONS

(U) The examples presented in this paper primarily were taken from environmental investigations of lidar for quantitative evaluation of pollutant distributions and densities. However, the results illustrate lidar applications for observation and evaluation of obscurant clouds. Ground-based scanning systems can map cloud structure to downwind distances of 1 to 2 km and backscatter data can provide information on cloud optical and physical density. Longer wavelength (10.6 μm) systems are better suited for mapping dense clouds because of less attenuation and multiple scattering effects (depending on particle size distributions). Multiple-wavelength lidar systems can provide information on particle characteristics and thus improve density evaluations.

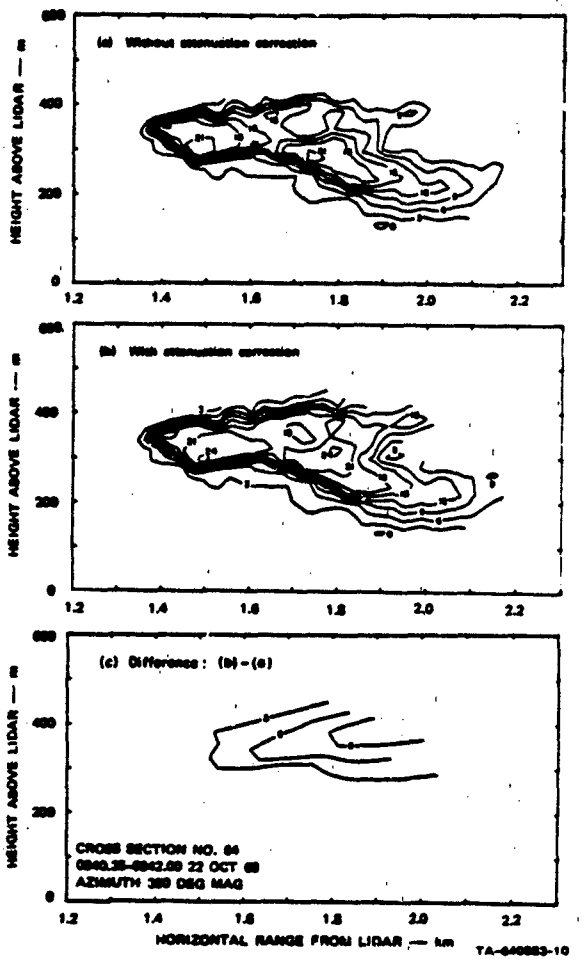

FIGURE 14. (U) EFFECT OF ATTENUATION CORRECTION AND RESULTANT MASS CONCENTRATION DISTRIBUTION (CENTER). THE CONTOURS REPRESENT VALUES OF 10 LOG_{10} (M/M_0), WHERE M IS THE PLUME MASS CONCENTRATION AND M_0 IS THE CLEAR-AIR REFERENCE MASS CONCENTRATION OF 100 $\mu g\ m^{-3}$.

(U) Airborne systems such as ALPHA-1 are particularly well suited for obscurant evaluations especially at distances greater than 1 km downwind of the source. The system can map terrain elevations and surface type and show their effect on cloud transport and diffusion. The terrain also provides a reflective passive target useful for evaluating vertical transmissions of very dense aerosol clouds. The two-wavelength observations provide information on mean particle size to help correct for attenuation and multiple scattering effects, and thus improve density estimates. A new 10.6 μm wavelength airborne lidar system is being constructed that may be the optimum apporach for evaluation of very dense obscurant clouds.

(U) The preparation of this paper was supported by the Army Research Office (ARO), Geosciences Division. The four-wavelength lidar experiments also are funded by ARO. The ALPHA-1 programs were conducted for the Electric Power Research Institute and the aerosol optical data were collected on projects funded by the U.S. Environmental Protection Agency.

REFERENCES

Uthe, E.E., N.B. Nielsen, and W.L. Jimison, 1980: "Airborne Lidar Plume and Haze Analyzer (ALPHA-1)," Bull. Amer. Met. Soc., Vol 61, pp. 1035-1043.

Uthe, E.E., 1981: "Lidar Evaluation of Smoke and Dust Clouds," Applied Optics, Vol. 20, pp. 1503-1510.

Uthe, E.E., 1982: "Particle Size Evaluations Using Multiwavelength Extinction Measurements," Applied Optics, Vol. 21, pp. 454-458.

Uthe, E.E., B.M. Morley, and N.B. Nielsen, 1982: "Airborne Lidar Measurements of Smoke Plume Distribution, Vertical Transmission and Particle Size," Applied Optics, Vol. 21, pp. 460-463.

END

DATE

FILMED

10-85